Personal Verification System Based On Iris Texture Analysis

By

Shrishail Sharad Gajbhar

(2009MIN006)

Submitted in the partial fulfillment of the requirements for the degree of

Master of Technology

in

Instrumentation

(specialization in Computerized Control)

Under the guidance of

Dr.R.S.Holambe

Department of Instrumentation Engineering

Shri Guru Gobind Singhji Institute of Engineering & Technology,

Nanded - 431 606 (M.S)

July 2011

Certificate

This is to certify that dissertation entitled **"Personal Verification System Based On Iris Texture Analysis"** is a bonafide record of project work carried out by **Mr. Gajbhar Shrishail Sharad** under my supervision and guidance. This work is being submitted to the SGGS Institute of Engineering and Technology, Nanded (affiliated to Swami Ramanand Teerth Marathwada University, Nanded) in partial fulfillment of the requirements for the Degree of **Master of Technology in Instrumentation (Specialization in Computerized Control)** during the academic session 2010-2011. The matter contained in this dissertation has not been submitted to any other university or institute for the award of any degree or diploma.

Dr.Raghunath S. Holambe
Guide
Professor, Dept.of Instrumentation Engg.
S.G.G.S.I.E. & T, Nanded

forwarded by

Dr.B.M.Patre
Head, Dept.of Instrumentation Engg.
S.G.G.S.I.E. & T, Nanded

Dr.S.R.Kajale
Director
S.G.G.S.I.E. & T, Nanded

Dissertation Approval Sheet

Dissertation entitled as **"Personal Verification System Based On Iris Texture Analysis"** by **Mr. Gajbhar Shrishail S.** is approved for the degree of *Master of Technology in Instrumentation (Specialization in Computerized Control)* from Shri Guru Gobind Singhji Institute of Engineering and Technology, Nanded (M.S.).

Dr.Raghunath S. Holambe
Guide
Professor, Dept.of Instrumentation Engg.
S.G.G.S.I.E. & T, Nanded

Examiner(s):

1. ----------
2. ----------

Acknowledgements

Behind every successful work, there are efforts of many people, directly or indirectly. I take this opportunity to thank all those who helped me during this endeavor.

First of all, I would like to express my sincere, profound sense of gratitude towards my guide Dr. Raghunath S. Holambe, who was always there with me to show me the way whenever I was in need. I am privileged by being associated with him. His constant support and inspiration gave me the initial thrust required to excel further.

I am thankful to Dr. S. R. Kajale, Director of Shri Guru Gobind Singhji Institute of Engineering and Technology, Nanded for his zealous and encouraging attitude.

I am grateful to Dr. B. M. Patre, Head of the Instrumentation Department, for his all-round support. I would also like to extend my thanks to our respected professors- Dr. S. G. Kahalekar, Dr. L. M. Waghmare, Dr. S. T. Hamde, Dr. V. G. Asutkar, Mr. R. G. Jamkar, Dr. V. R. Thool and Dr. R. V. Sarwadnya for all their valuable inputs given to me over the year.

I thank Mr. Amol Rahulkar, Mr. Pawan Ajmera and Mr. Yogesh Angal whose optimism was a motivation for me. I am grateful to my colleagues Manoj Muley, Jayant Parkhe, Prashant Gaikwad, Ashwin Vatane, Alfiya Ameen for their constant encouragement during this endeavor.

I devote this work to my parents who are behind success of this work. Without their support, this work would have been impossible.

Submitted with regards.

Shrishail Sharad Gajbhar
M.Tech.(Instrumentation)

Abstract

Biometrics has emerged as a reliable person identification method that can overcome some of the limitations of the traditional automatic personal identification methods. A biometric system uses unique and measurable physical, biological, or behavioral traits of people to establish or to verify their identity.

The iris provides one of the most stable biometric signals for use in identification, with a distinctive texture that is formed before birth and remains constant throughout life. Iris recognition is considered to have the highest identification accuracy and commercial iris recognition systems have been deployed in many applications, like passports and border control.

In this thesis, we have followed the general framework of Daugman's algorithm comprising of four stages namely Segmentation, Normalization, Feature Encoding and Matching. Pupil is segmented using thresholding and morphological operations, iris boundary is found by using two techniques Daugman's integro-differential operator and circular hough transform. Daugman's rubbersheet algorithm is used for normalization. Gabor filters and Log-Gabor filters are used for feature extraction and binary template is created by quantizing phase into four quadrants. Hamming distance is used for pattern matching.

The system was tested on three iris databases namely CASIA v1, Multimedia University (MMU) and IIT Delhi with all possible intra-class and inter-class comparisons with respective classes taken.

Keywords*:* iris recognition; automatic segmentation; Gabor filter; hamming distance; inter/intra class distribution; iris template; match score.

Contents

List of Figures

List of Tables

Nomenclature

Abbreviations

CHT	Circular Hough Transform
IDO	Integro Differential Operator
FNMR	False Non Match Rate
FMR	False Match Rate
FAR	False Acceptance Rate
GAR	Genuine Acceptance Rate
FRR	False Rejection Rate
FTE	Failure To Enroll Rate
FTA	Failure To Acquire Rate
DET	Detection Error Trade-off
ROC	Receiver Operating Characteristics
EER	Equal Error Rate
IR	Infrared
ID	Identification
HD	Hamming Distance
WT	Wavelet Transform
BATH	University of Bath
CASIA	Chinese Academy of Sciences Institute of Automation
IITD	Indian Institute of Technology, Delhi
ICE	Iris Challenge Evaluation
WED	Weighted Euclidean Distance

Chapter 1

Introduction

Personal identity refers to a set of attributes (e.g., name, social security number, etc.) that are associated with a person. Establishing (determining or verifying) the identity of a person is called person recognition or authentication and it is a critical task in any identity management system. Identity management is the process of creating, maintaining and destroying identities of individuals in a population. To combat the epidemic growth in identity theft and to meet the increased security requirements in a variety of applications ranging from international border crossing to accessing personal information in various applications such as sharing networked computer resources, performing remote financial transactions, web-based services (e.g., online banking) and the deployment of decentralized customer service centers (e.g., credit cards) have further underscored the need for reliable identity management systems that can accommodate a large number of individuals [3].

The three basic ways to establish the identity of a person are "something you know" (e.g., password, personal identification number), "something you carry" (e.g., physical key, ID card) and "something you are" (e.g., face, voice). Traditional methods of establishing a persons identity include knowledge based (e.g., passwords) and token-based (e.g., ID cards) mechanisms can be easily misplaced, shared or stolen. Moreover, passwords and ID cards cannot provide vital authentication functions like non-repudiation and detecting multiple enrollments. For example, users can easily deny using a service by claiming that their password has been stolen or guessed. Individuals can also conceal their true identity by presenting forged or duplicate identification documents. Therefore, it is becoming increasingly apparent that knowledge-based and token-based mechanisms alone are not sufficient for reliable identity determination and stronger authentication schemes based on something you are, namely biometrics, are needed.

1.1 Biometrics

Biometrics is the science of establishing the identity of an individual based on the physical, chemical or behavioral attributes of the person. The term biometrics comes from the ancient Greek bios = "life" and metron = "measure". Notions of *biological*, *measuring* and *recognition* are common to any biometric definition. Until the late 1800s the automatic recognition of individuals was largely done using photographic memory. In 1883, the French police and anthropologist Alphonse Bertillon developed an anthropometric system, known as Bertillonage [4], to fix the problem of identification of convicted criminals. As illustrated by figure 1.1.

This was a quite complex procedure that could take up to twenty minutes and is considered the first scientific system widely used to identify criminals. Its basis was the measurement of certain lengths and widths of the head and body and the recording of individual markings, such as tattoos and scars. However this systems faded when it was discovered that some people share the same measures and several people could be treated as one. The failure of Bertillonage motivated the use of fingerprinting, which is presently almost standardized worldwide. In 1880, the British scientific journal Nature published an article by Henry Faulds and William James describing the uniqueness and permanence of fingerprints. This motivated the design of the first elementary fingerprint recognition system by Sir Francis Galton and improved by Sir Edward R. Henry. Having quickly disseminated, the first fingerprint system in the United States was inaugurated by the New York State Prison Department in 1903 and the first known convicted due to fingerprint evidences was reported in 1911 [5]

Figure 1.1: Anthropometric system by Alphonse Bertillon

1.1.1 Modes of Functioning

Independently of the used trait, the biometric applications follow the procedure illustrated in figure 1.2 The process begins by the data capturing, where the biometric sample is acquired. Next, through the feature extraction a biometric signature is created, that is further compared with a specific or several biometric signatures registered in the database. These are commonly designated as biometric templates and were collected during the enrollment process and correspond to a verified subject identity. If the comparison between biometric signatures has enough similarity, it is assumed that both of these were extracted from the same person, otherwise, they must have been extracted from different persons.

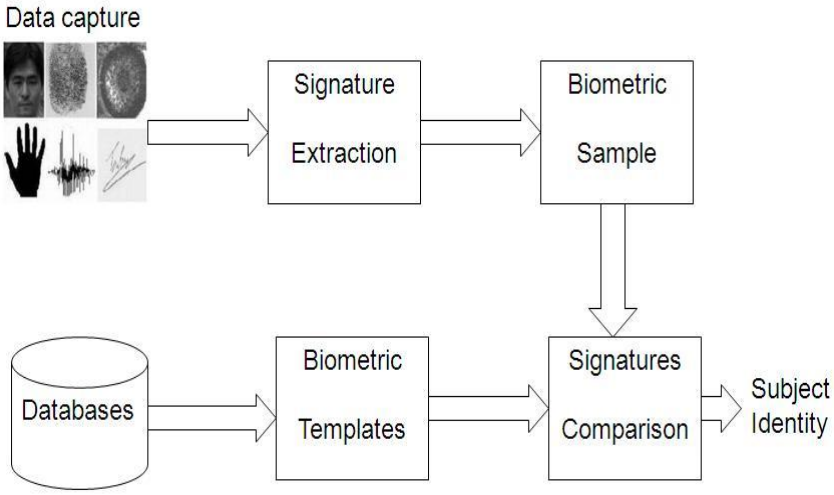

Figure 1.2: Typical stages of biometric recognition process

The number of comparisons between the biometric sample and templates determines a basic distinctions among the two modes of performing biometric recognition: verification and identification.

In the verification mode, also named as positive recognition, the system verifies the authenticity of a claimed enrolled identity, trying to answer the question: is this person who he/she claims to be? This requires that, together with the biometric sample, the subjects ID must be given to the recognition algorithm. Further, the comparison between the biometric template correspondent to that identity and the sample is performed. If the similarity is high enough, the claimed identity is accepted, meaning that both biometric signatures were extracted from the same person. Otherwise, the identity is denied, meaning that the enrolled and the sample signatures were extracted from different subjects.

The identification mode, often named as negative recognition, tries to answer the question: who is this person?, or sometimes: is this person in the database? After acquiring the required data and extracting the biometric sample, a comparison is made with the N enrolled identities, in order to find the identity from which the sample was collected. In this mode, it is usual to output a list of the k most probable identities of a biometric sample.

1.1.2 A Classification of Biometric Systems

Biometric systems can be classified according to six perspectives:

Overt / covert If the user is aware about the acquisition of his biometric data, the application is defined as overt; otherwise, is defined as covert. This is clearly one of the most concerning characteristics of a biometric system, regarding the privacy issue.

Habituated / non-habituated When the majority of the people that interacts with the biometric system are every-day users, the recognition is performed in the habituated mode. If the average frequency of use from each user is low, the recognition is performed in the non-habituated mode. This is relevant to the degree of cooperation and training demanded from the users.

Attended / non-attended If the user is observed and guided by supervisors during the process, the biometric recognition is performed attended; if not, the use is considered non-attended. Obviously, the easy-of-use of the recognition system is much more relevant in the non-attended mode.

Standard / non-standard environment When all the conditions can be controlled and the recognition takes place indoors within constrained conditions, it is considered that the recognition is performed within a standard environment; if not, the use is called in non-standard environment.

Public / private If the users are not employees of the organization that owns the recognition system, the application is public; if the users are employees, the application is called private.

Open / closed If the system uses completely proprietary formats, the application is considered closed. Otherwise, when the system is able to exchange data with others, it is called open and, once again, privacy and legal issues should be addressed.

1.1.3 Biometric Traits

Biometric systems use a variety of physical or behavioral characteristics 1.3, including fingerprint, face, hand/finger geometry, iris, retina, signature, gait, palmprint, voice pattern, ear, hand vein, odor or the DNA information of an individual to establish identity [3]. In the biometric literature, these characteristics are referred to as traits, indicators, identifiers or modalities. While biometric systems have their own limitations they have an edge over traditional security methods in that they cannot be easily stolen or shared. Besides bolstering security, biometric systems also enhance user convenience by alleviating the need to design and remember passwords.

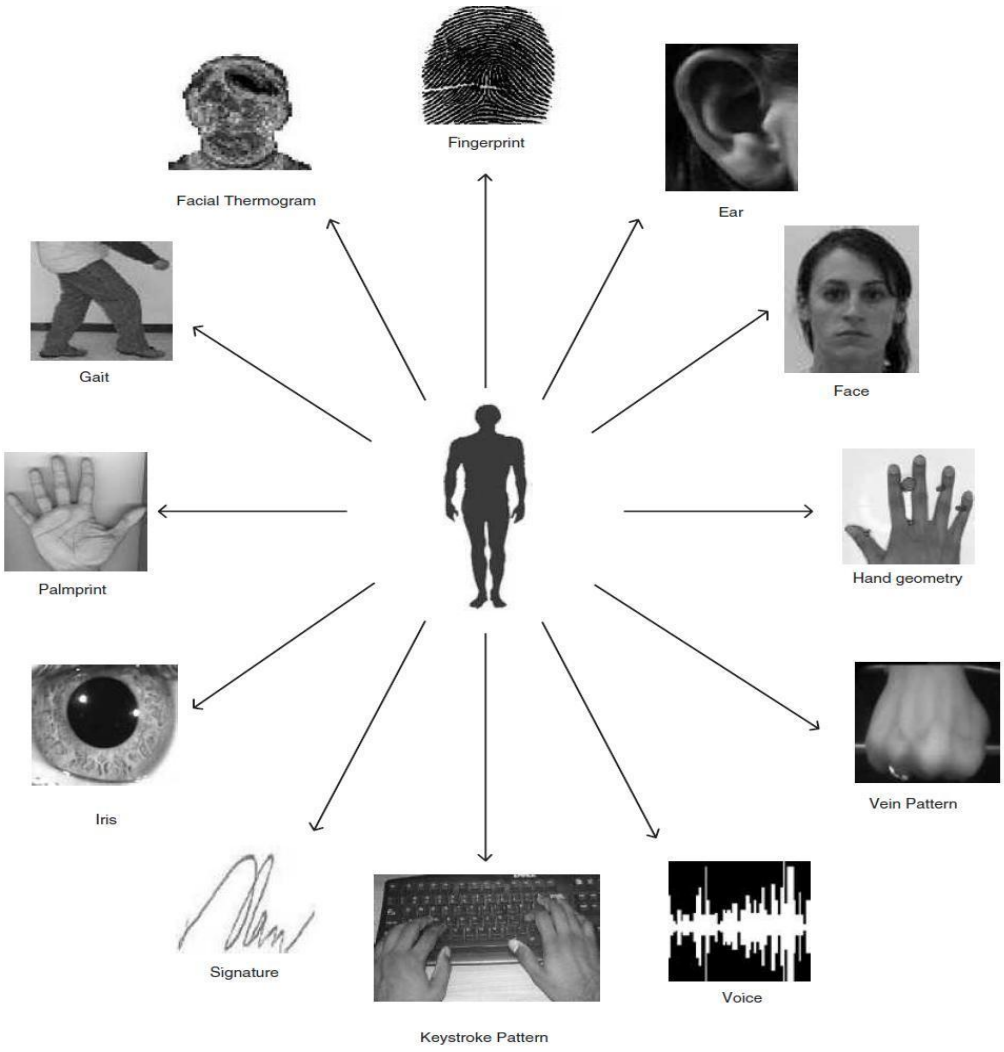

Figure 1.3: Examples of biometric traits that can be used for authenticating an individual.

Physiological Traits

Physiological biometrics measure a specific part of the structure or shape of a portion of a subjects body. The types of physiological biometrics include:

Fingerprint: A fingerprint is a pattern of ridges and furrows located on the tip of each finger. Fingerprints were used for personal identification for many centuries and the matching accuracy is acceptable. In the past, patterns were extracted by creating an inked impression of the fingertip on paper. Today, compact sensors provide digital images of these patterns.

The main advantages for the use of fingerprints are the higher levels of acceptability and their easy of use, while it is considered vulnerable to noise and distortion brought on by dirt and twists.

Hand: The geometry of an entire human hand is quite unique, almost as much as fingerprints themselves. Usually a hand scan does not measure the fingerprint-like patterns in the fingers and palms, but instead relies on the lengths and angles of fingers, the geometry of the entire collection of 27 bones, plus muscles, ligaments, and other tissues.

The hand geometry-based biometric systems are easy to use and inexpensive. The main disadvantage is its relative low discriminating capacity, also the relative large dimensions of the subjects hands and the requirement of contact to perform recognition makes it unappropriate for certain applications (e.g., laptop computers access).

DNA: The deoxyribonucleic acid (DNA) is represented through a one-dimensional code, unique for each person. Humans have 23 pairs of chromosomes containing their DNA blueprint. This method is considered to have some drawbacks, as the easy contamination and sensitivity, the impossibility to perform real-time recognition and severe privacy issues, due to the fact of the DNA can reveal susceptibility to some diseases.

Iris: The iris begins to form in the third month of gestation and the structures creating its pattern are largely complete by the eighth month. It is the annular region of the eye bounded by the pupil and the sclera (white part of the eye) on either side. Its complex pattern can contain many distinctive features such as arching ligaments, furrows, ridges, crypts, rings, corona, freckles and a zigzag collarette.

The available results of both accuracy and speed of iris-based identification are highly encouraging and point to the feasibility of large-scale recognition using iris information.

Retina: The retina is the surface at the rear of the interior of the eye. Retinal scan measures the blood vessel patterns in the back of the eye. Digital images of

retinal patterns can be acquired by projecting a low intensity beam of visual or infrared light into the eye and capturing an image of the retina.

Since it is protected in the eye itself, and is not easy to change or replicate the retinal vasculature, this is considered as one of the most secure biometric traits. Retina based systems are used for high security applications, such as access to prisons.

Face: The importance of facial features for human recognition cannot be overstated. Facial images are the most common biometric characteristic used by humans to perform personal recognition. This is a non intrusive and suitable trait to perform covert recognition.

Although performance of commercially available systems is reasonable, there is still significant room for improvement, since false rejection rate is about 10% and the false accept rate is about 1%. These systems face strong difficulties when the faces are captured under different angles and uncontrolled ambient illumination.

Ear: Using ears for the recognition of individuals has been interesting for the research community for, at least, 100 years. During crime scene investigation, ear marks are often used for identification in the absence of valid fingerprints.

Commonly, there are at least three methods for ear recognition: taking a photo of an ear, taking earmarks by pushing ear against a flat surface and taking thermogram pictures of the ear. The requirement of users cooperation is needed, in order to acquire acceptable ear images. Apart from this, rotation, even small, is a common problem.

Facial Thermogram: It is possible to capture the pattern of heat radiated by the human body with an infrared camera. That pattern is considered to be unique for each person, enabling its potential use for biometric purposes. It was observed that the capturing of face images through an infra-red camera produces a unique facial signature when heat passes through the facial tissue and is emitted from the skin. These facial signatures are often called facial thermograms. It is claimed that a face thermogram is unique to each individual and is less vulnerable to disguises. Face thermograms may depend heavily on a number of factors such as the emotional state of the subjects, or body temperature, and like face recognition, face thermogram recognition is view-dependent [6].

Hand Vein: It is believed that the pattern of blood veins is unique to every individual, even among identical twins. Moreover, palms have a broad and complicated vascular pattern that has minor variations over lifetime and is not considered intrusive. As veins are internal and have a wealth of differentiating features, attempts to forge an identity are extremely difficult, thereby enabling a high level of

security. Among the disadvantages, the high level of cooperation required and the fact that it demands physical contact between the subject and some part of the system.

Palmprint: Similarly to the widely used fingerprints, the palms of the human hands contain unique patterns of ridges and valleys. Since a palm is larger then a finger, a palmprint is expected to be even more distinguishable than a fingerprint. Palmprint recognition offers promising future for medium-security access control system, although it is not as stabilized and matured as the fingerprint technology. Compared to other biometric traits, the facts that a higher level of cooperation is demanded to users and the required physical contact between the users and the capturing device can be regarded as disadvantages.

Behavioral Traits

Behavioral biometrics are more concerned with how you do something, rather than just a static measurement of a specific body part. Some of the behavioral biometrics in use include these:

Signature: Signature can be regarded as unique and results from both behavioral and hand geometry variations associated to each subject. The way a person signs his or her name is known to be characteristic of that individual since centuries, although the analysis of the signature dynamics is recent.

There are two major strategies to perform signature recognition: image-based and dynamics analysis. The first approach is the most classical and is based on the visual appearance of the signature. The latter analyzes both speed, direction and pressure of writing, stroke order and its major weak point results of the specific hardware dependence.

Keystroke dynamics: It is believed that each person types on a keyboard in a distinguishable way, such that the analysis of the different rhythms that a subject types in the keyboard can be used for its recognition.

This technology examines either dynamics as speed and pressure, the length of time each key is held down, the time elapsed between hitting certain keys and the tendencies to switch between a numeric keypad and keyboard numbers. The main advantage of the use of keystroke-based biometrics is its potential for continuous monitoring.

Voice: Oppositely to the majority of the biometric traits, that are image-based, voice possesses the singularity of dealing with acoustic information. The most relevant features of a subjects vocal pattern are determined by physical characteristics as the vocal tracts, mouth, nasal cavities and lips shape. These are low varying fea-

tures over adult lifetime, although the individual behavior and social environments can highly influence the subjects voice.

Speech-based authentication is currently restricted to low-security applications because of the high variability in an individuals voice and poor accuracy performance of typical speech-based authentication systems.

Gait: The human gait is a periodic activity with each gait cycle covering two strides: the left foot forward and right foot forward strides. Each stride spans the double-support stance to the legs-together stance as the legs swing past each other and back to the double-support stance. Potential information in the basis of gait biometrics can derive from two aspects: shape and dynamics.

Gait-based biometric systems tend to present high false rejection rates due to to changes in the walking surface, walking speed. Also, since video-sequence is used to capture the required data, it is considered as one of the most computationally expensive methods.

1.1.4 Comparison Between the Most Common Biometrics Traits

Biometric systems can be evaluated regarding seven parameters: universality, uniqueness, permanence, collectability, performance, acceptability and circumvention [7]. These parameters are also called as seven pillars of biometric wisdom.

- Universality: All human beings are endowed with the same physical characteristics - such as fingers, iris, face, DNA which can be used for identification.
- Uniqueness: For each person these characteristics are unique, and thus constitute a distinguishing feature.
- Permanence: These characteristics remain largely unchanged throughout a person's life.
- Collectability: A person's unique physical characteristics need to be collected in a reasonably easy way for quick identification.
- Performance: The degree of accuracy of identification must be quite high before the system can be operational.
- Acceptability: Applications will not be successful if the public offers strong and continuous resistance to biometrics.

- Circumvention: In order to provide added security, a system needs to be harder to circumvent than existing identity management systems.

Table 1.1 shows comparison of most common biometric traits depending upon above parameters.

Trait	Unique-ness	Univer-sality	Perman-ence	Collect-ability	Perform-ance	Accept-ability	Circum-vention
DNA	87 %	95 %	94 %	19 %	19 %	15 %	55 %
Ear	46 %	58 %	85 %	50 %	53 %	100 %	50 %
Face	44 %	92 %	50 %	84 %	25 %	99 %	37 %
Fingerprint	78 %	47 %	91 %	62 %	98 %	49 %	71 %
Gait	25 %	50 %	25 %	100 %	21 %	100 %	50 %
Hand	54 %	57 %	54 %	78 %	50 %	67 %	59 %
Iris	96 %	93 %	97 %	62 %	98 %	50 %	95 %
Keystroke	17 %	23 %	28 %	56 %	25 %	67 %	50 %
Retina	94 %	86 %	66 %	29 %	98 %	23 %	100 %
Signature	35 %	39 %	34 %	83 %	23 %	97 %	33 %
Voice	39 %	49 %	31 %	59 %	23 %	99 %	33 %

Table 1.1: Comparison between the most common biometric traits.

1.1.5 Factors that Influence the Biometric Traits

Every biometric system depends on the features, whether genotypic or randotypic or behavioral. Genotypic refers to the traits that are defined by the genetic makeup of the individual and do not change over time. Phenotypic refers to the actual expression of a feature, through the interaction of genotype, its development and surrounding environment.behavioral traits are those aspects that a subject develops through training or repeated learning. Table 1.2 shows the comparison of various biometric system based on these factors.The origin of the biometric traits is relevant due to its influence on the system's error rates. For instance, the dynamics of the behavioral features over time strongly increases the false rejection rates.

Trait	Genotypic	Randotypic	Behavioral
DNA	48 %	48 %	4 %
Ear	40 %	40 %	20 %
Face	40 %	40 %	20 %
Fingerprint	25 %	62.5 %	12.5 %
Gait	30 %	10 %	60 %
Hand Geometry	25 %	62.5 %	12.5 %
Iris	1 %	98 %	1 %
Keystroke	1 %	1 %	98 %
Retina	1 %	98 %	1 %
Signature	1 %	1 %	98 %
Voice	42 %	29 %	29 %

Table 1.2: Factors of influence of the biometric traits.

1.1.6 Biometric Functionalities

The functionalities provided by a biometric system can be categorized as verification and identification. Figure 1.4 shows the enrollment and authentication stages of a biometric system operating in the verification and identification modes.

In verification, the user claims an identity and the system verifies whether the claim is genuine, i.e., the system answers the question "Are you who you say you are?". In this scenario, the query is compared only to the template corresponding to the claimed identity. If the users input and the template of the claimed identity have a high degree of similarity, then the claim is accepted as "genuine". Otherwise, the claim is rejected and the user is considered an "impostor". Verification is typically used for positive recognition, where the aim is to prevent multiple people from using the same identity.

Identification functionality can be classified into positive and negative identification. In positive identification, the user attempts to positively identify himself to the system without explicitly claiming an identity. A positive identification system answers the question "Are you someone who is known to the system?" by determining the identity of the user from a known set of identities. In contrast, the user in a negative identification application is considered to be concealing his true identity from the system. Negative identification is also known as screening and

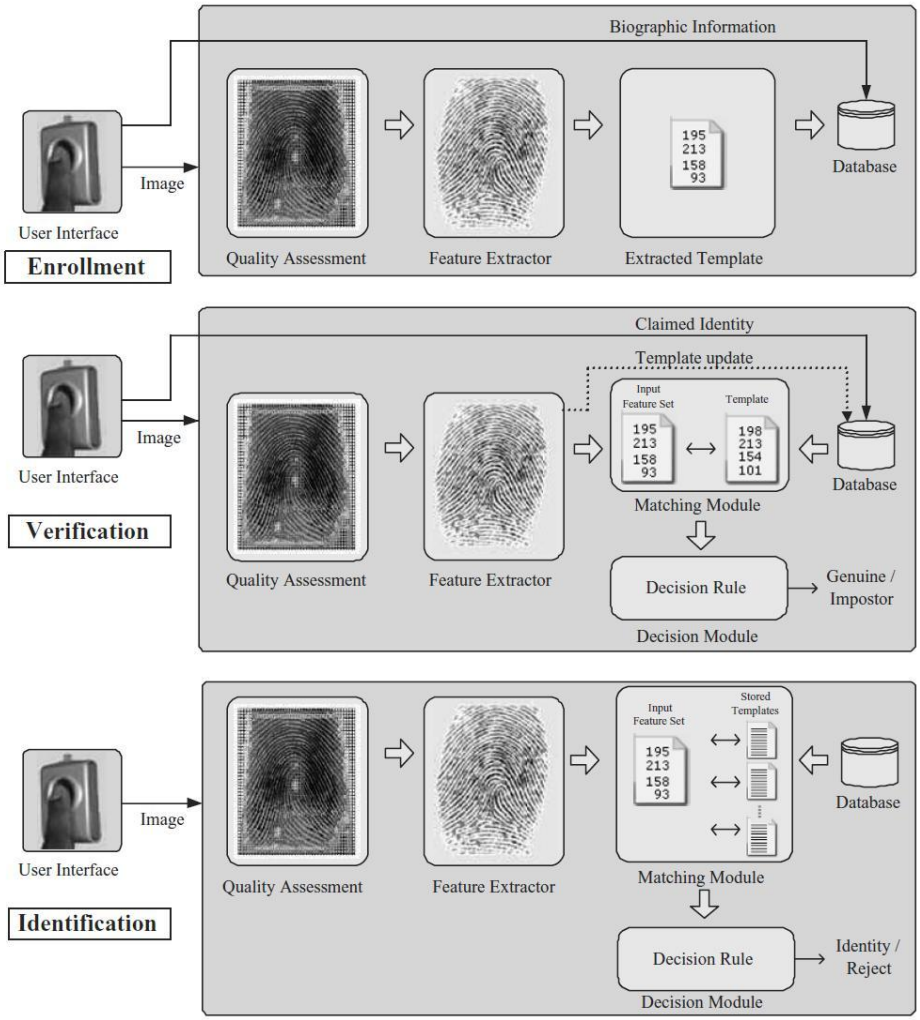

Figure 1.4: Enrollment and recognition (verification and identification) stages of a biometric system..

the objective of such systems is to find out "Are you who you say you are not?". Screening is often used at airports to verify whether a passengers identity matches with any person on a "watch-list". Screening can also be used to prevent the issue of multiple credential records (e.g., drivers licence, passport) to the same person. Negative identification is also critical in applications such as welfare disbursement to prevent a person from claiming multiple benefits under different names. In both positive and negative identification, the users biometric input is compared with the templates of all the persons enrolled in the database and the system outputs either the identity of the person whose template has the highest degree of similarity with the users input or a decision indicating that the user presenting the input is not an enrolled user.

1.1.7 Performance of a Biometric System

Unlike password-based systems, where a perfect match between two alphanumeric strings is necessary in order to validate a users identity, a biometric system seldom encounters two samples of a users biometric trait that result in exactly the same feature set. This is due to imperfect sensing conditions (e.g., noisy fingerprint due to sensor malfunction), alterations in the users biometric characteristic (e.g., respiratory ailments impacting speaker recognition), changes in ambient conditions (e.g., inconsistent illumination levels in face recognition) and variations in the users interaction with the sensor (e.g., occluded iris or partial fingerprints). Thus, seldom do two feature sets originating from the same biometric trait of a user look exactly the same, fact, a perfect match between two feature sets might indicate the possibility that a replay attack is being launched against the system. The variability observed in the biometric feature set of an individual is referred to as intra-class variation, and the variability between feature sets originating from two different individuals is known as inter-class variation. A useful feature set exhibits small intra-class variation and large inter-class variation.

The degree of similarity between two biometric feature sets is indicated by a similarity score. A similarity match score is known as a genuine or authentic score if it is a result of matching two samples of the same biometric trait of a user. It is known as an impostor score if it involves comparing two biometric samples originating from different users. An impostor score that exceeds the threshold η results in a false accept (or, a false match), while a genuine score that falls below the threshold η results in a false reject (or, a false non-match). The False Accept Rate (FAR) (or, the False Match Rate (FMR)) of a biometric system can therefore be defined as the fraction of impostor scores exceeding the threshold η. Similarly, the False Reject Rate (FRR) (or, the False Nonmatch Rate (FNMR)) of a system may be defined as the fraction of genuine scores falling below the threshold η. The Genuine Accept Rate (GAR) is the fraction of genuine scores exceeding the threshold η. Therefore, GAR = 1 - FRR Regulating the value of η changes the FRR and the FAR values, but for a given biometric system, it is not possible to decrease both these errors simultaneously.

The FAR and FRR at various values of η can be summarized using a Detection Error Tradeoff (DET) curve that plots the FRR against the FAR at various thresholds on a normal deviate scale and interpolates between these points (Figure 6.2)). When a linear, logarithmic or semi-logarithmic scale is used to plot these error rates, then the resulting graph is known as a Receiver Operating Characteristic (ROC)

curve . In many instances, the ROC curve plots the GAR (rather than the FRR) against the FAR.

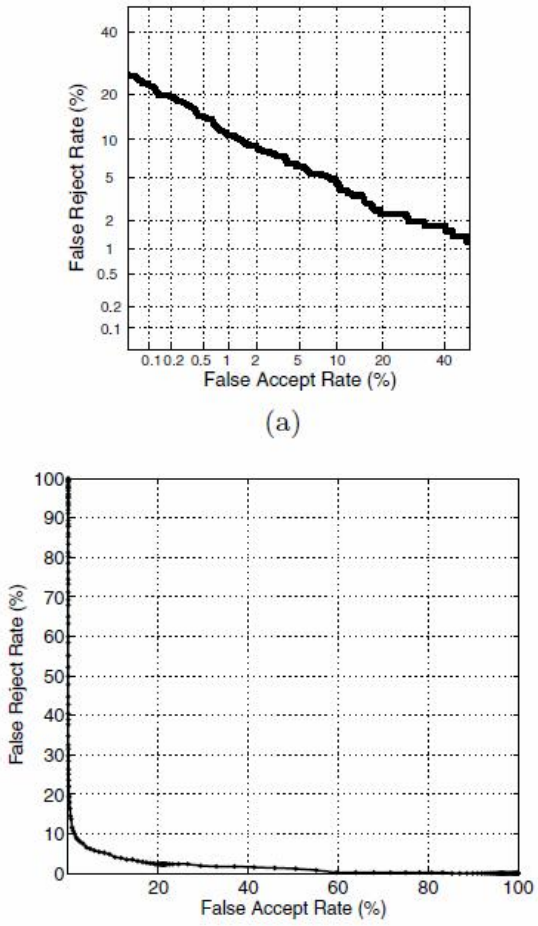

Figure 1.5: The graph in (a) shows a DET curve that plots FRR against FAR in the normal deviate scale. In (b) a ROC curve plots FRR against FAR in the linear scale.

The performance of a biometric system may also be summarized using other single-valued measures such as the Equal Error Rate (EER) and the d-prime value. The EER refers to that point in a DET curve where the FAR equals the FRR; a lower EER value, therefore, indicates better performance. The d-prime value (d') measures the separation between the means of the genuine and impostor probability distributions in standard deviation units and is defined as, $d' = \frac{(mean1 - mean2)}{\sqrt{(\frac{std1^2 + std2^2}{2})}}$ where the mean1, mean2 and std1, std2 are the means and standard deviations, respectively, of the genuine and impostor distributions. A higher d-prime value indicates better performance.

1.2 Iris Recognition

This section is totally related with the utilization of the iris for biometric purposes. We start by an overall description of the eyes anatomy followed by the identification of the most important regions of the human iris. Further, we identify the most typical stages of common iris recognition proposals and describe the most relevant approaches to each of these stages.

1.2.1 Eye and Iris Anatomy

In this sub-section we start with the description of the human eye anatomy, followed by a highly detailed description of the iris, which is the most relevant part of the eye.

Eye Anatomy

A schematic drawing of the human eye is shown in Fig 1.6 [8] The anterior portion of the eye consists of the cornea, iris, pupil, and crystalline lens. The pupil serves as an aperture which is adjusted by the surrounding iris, acting as a diaphragm that regulates the amount of light entering the eye. Both the iris and the pupil are covered by the convex transparent cornea. Together with the crystalline lens, the cornea is responsible for the formation of the optical image on the retina.

Ciliary muscle actions cause the zonular fibers to relax or tighten and thus provide accommodation, the active function of the crystalline lens. This ability to change its curvature, allowing objects at various distances to be brought into sharp focus on the retinal surface. The aqueous humor fills the anterior chamber between the cornea and iris, and also fills the posterior chamber that is situated between the iris and the zonular fibers and crystalline lens. The aqueous humor is responsible for maintaining the intraocular pressure and thereby helps the eyeball maintain its shape. Moreover, this clear watery fluid nourishes the cornea and crystalline lens. Taken all together, with its refracting constituents, self-adjusting aperture, and finally, its detecting segment, the eye is very similar to a photographic camera. The film of this optical system is the retina, the multilayered sensory tissue of the posterior eyeball onto which the light entering the eye is focused, forming a reversed and inverted image. External to the retina is the choroid, the layer that lies between retina and sclera. The choroid is primarily composed of small arteries and veins. As it consists of numerous blood vessels and thus contains many blood cells, the choroid supplies most of the back of the eye with necessary oxygen and nutrients.

The sclera is the external fibrous covering of the eye. Iris is described in more detail in the following section due to their major role in biometric applications.

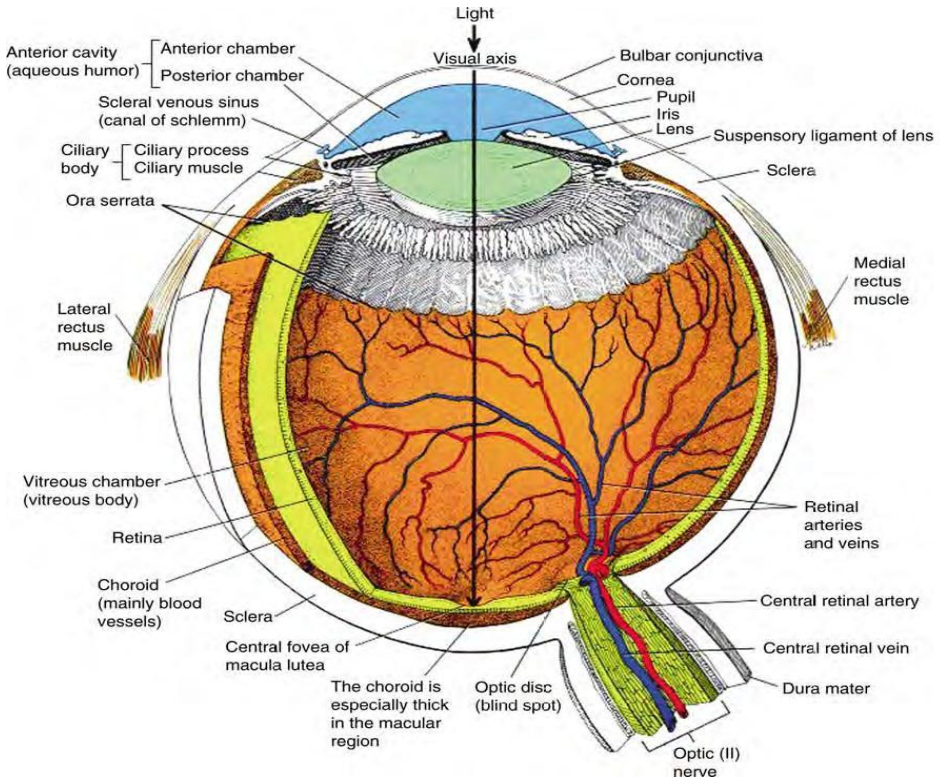

Figure 1.6: Schematic drawing of the human eye.

Iris Anatomy

Illustrated by figure 1.7 the iris consists of two major regions: the pupillary and the ciliary zone. The pupillary zone is the inner portion of the iris whose edges form the pupillary iris border. The ciliary zone is the outer portion of the iris, which extends itself into the iris origin in the ciliary body. The region that separates the pupillary and scleric portions is designated as the collarette. Two muscles, the dilator and the sphincter muscles, control the size of the iris to adjust the amount of light entering the pupil.

The iris begins to form during the third month of gestation and the structure is complete by the eight month, although pigmentation continues into the first year after birth. The visible features of the iris arise in the trabeculum, which is a meshwork of connective tissues with arching ligaments, crypts, contraction furrows, a corona and pupillary frill, coloration and freckles. Although the anterior layer covering the trabecular framework creates the predominant iris texture seen with

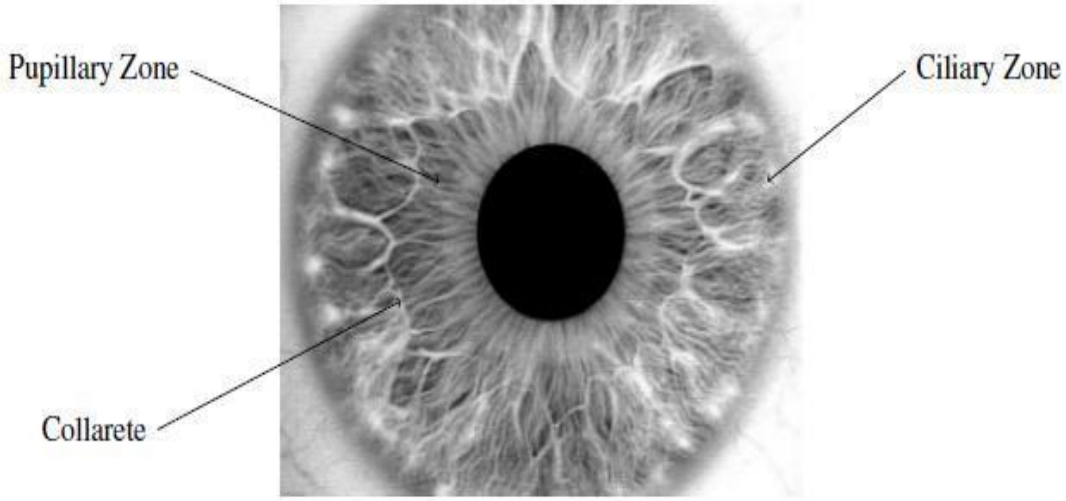

Figure 1.7: Morphology of the human iris.

visible light, additional discriminating information can be given by the location of all of these sources of radial and angular variation. Together, as mentioned by [9], they provide a distinguishable and unique signal.

The texture and minutia of the iris is believed to have high random morphogenesis and no genetic penetrance in its expression. Past studies about the iris texture concluded that the inter-subject variability of its pattern spans about 250 degrees-of-freedom and have an entropy of about 3.2 bits per square-millimeter [9].

These biological characteristics of the iris patterns turned it as one of the most suitable traits for biometric purposes. As discussed in the comparison between the most common traits, iris is generally accepted as one of the most promising biometric traits and is the subject for the development and proposal of many biometric recognition algorithms. In the following section, we detail the typical iris recognition stages with emphasis to the almost standard Daugmans recognition method that, apart from being the first proposed, is the basis for the large majority of the deployed and commercial iris recognition systems.

1.2.2 Typical Stages of Iris Recognition

Figure 1.8 illustrates the typical stages of iris recognition systems. The initial stage deals with iris segmentation. This process consists in localizing the iris inner (pupillary) and outer (scleric) borders, assuming either circular or elliptical shapes for both of the borders.

In order to compensate the variations in the pupil size and in the image capturing distances, it is common to translate the segmented iris region into a fixed length and dimensionless polar coordinate system. This stage is usually accomplished through the method proposed by Daugman [2].

Regarding feature extraction, iris recognition approaches can be divided into three major categories: phase-based methods (e.g., [2]), zero-crossing methods (e.g., [10]) and texture analysis based methods (e.g., [11]).

Finally, the comparison between iris signatures is made, producing a numeric dissimilarity value. If this value is higher than a threshold, the system outputs a non-match, meaning that each signature belongs to different irises. Otherwise, the system outputs a match, meaning that both signatures were extracted from the same iris.

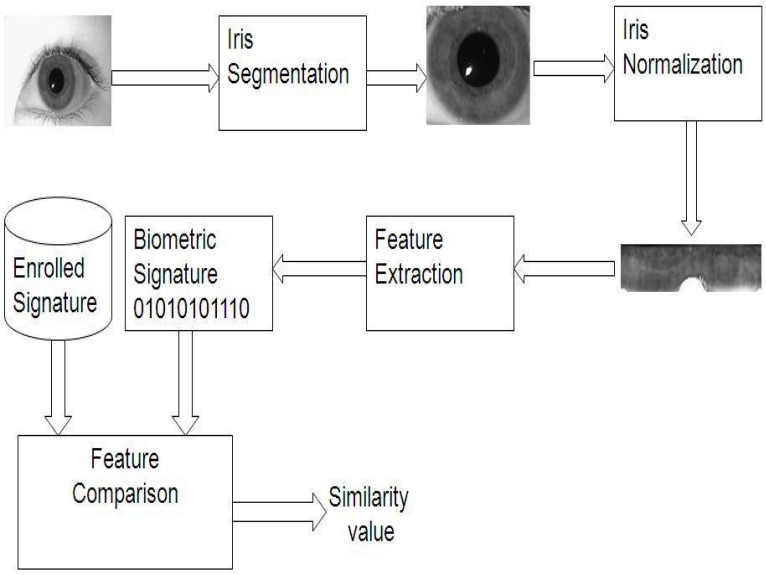

Figure 1.8: Typical stages of the iris recognition.

1.2.3 Iris Segmentation

In 1993, J. Daugman [2] presented one of the most relevant methods, constituting the basis of the majority of the functioning systems. Regarding the segmentation stage, this author introduced an integro-differential operator to find both the iris inner and outer borders. This operator remains actual and was proposed in 2004 with minor differences by Nishino and Nayar [12].

Similarly, Camus and Wildes [13] and Martin-Roche et al. [14] proposed integro-differential operators that search the N^3 space, with the objective of maximizing

the equations that identify the iris borders.

Wildes [11] proposed iris segmentation through a gradient based binary edge-map construction followed by circular Hough transform. This is the most common method, that has been proposed with minor variants by Cui et al. [15], Huang et al. [16], Kong and Zhang [17], Ma et al. [18], [19] and [20].

Morphologic operators were applied by Mira and Mayer [21] to obtain iris borders. They detected the pupillary and scleric borders by applying thresholding, image opening and closing.

1.2.4 Iris Normalization

Due to the varying size of the pupil and of the distance and angle of the image capturing framework, the size of the captured irises can have high variations, increasing the complexity of the recognition task. Robust representations for pattern recognition must be invariant to changes in the size, position, and orientation of the patterns. In the iris recognition compass, this requires a representation of the iris data invariant to the dimension of the captured image. This is influenced by the distance between the eye and the capturing device, by the camera optical magnification factor and by the iris orientation, caused by torsional eye rotation and camera angles. As described in [1], the invariance to all of these factors can be achieved through the translation of the captured data into a double dimensionless polar coordinate system. As figure 1.9 illustrates, this translation process is based both in polar (θ) and radial (r) variables.

The rubber sheet model assigns to each point on the iris, regardless of its size and pupillary dilation, a pair of real coordinates (r, θ), where r is on the unit interval [0, 1] and θ is an angle in [0, 2π]. The remapping of the iris image I(x, y) from raw cartesian coordinates (x, y) to the dimensionless non concentric polar coordinate system (r, θ) can be represented as:

$$I(x(r,\theta), y(r,\theta)) \rightarrow I(r,\theta) \tag{1.1}$$

where x(r, θ) and y(r, θ) are defined as linear combinations of both the set of pupillary boundary points $(x_p(\theta), y_p(\theta))$ and the set of limbus boundary points along the outer perimeter of the iris $(x_s(\theta), y_s(\theta))$ bordering the sclera, which are detected in the iris segmentation stage, as:

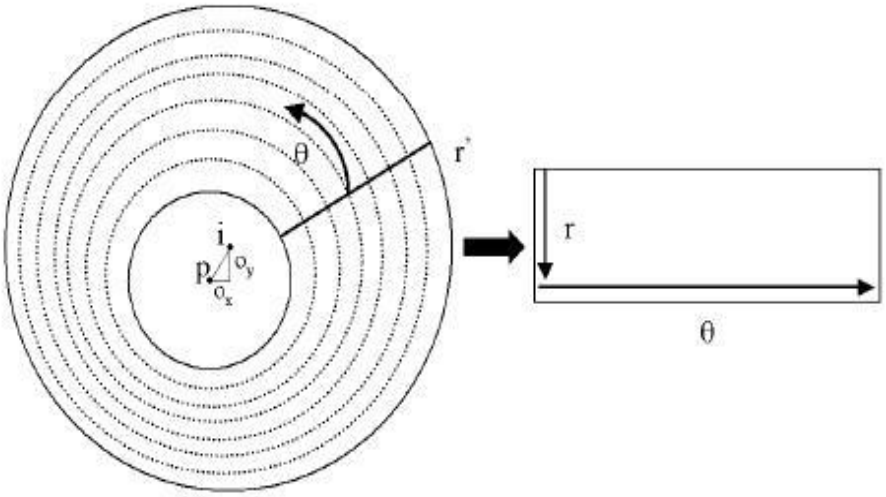

Figure 1.9: Normalization of the iris image through the Daugman rubber sheet.

$$x(r,\theta) = (1-r) * x_p(\theta) + (1-r) * x_s(\theta) \tag{1.2}$$

$$y(r,\theta) = (1-r) * y_p(\theta) + (1-r) * y_s(\theta) \tag{1.3}$$

1.2.5 Feature Extraction

As stated above, from the viewpoint of feature extraction, recognition approaches can be divided into three major categories: phase-based methods (e.g., Daugman [2]), zero-crossing methods (e.g., Boles and Boashash [10] and Roche et al. [14]) and texture analysis based methods (e.g., Wildes [11], and Ma et al. [22]).

Daugman [2] uses multiscale quadrature wavelets to extract texture phase information and obtain an iris signature with 2048 binary components. Once again, this proposal acted as basis for others with minor differences, as Ma et al. [22].

To characterize the iris texture, Boles and Boashash [10] computed the zero-crossing representation of a 1D wavelet at different resolutions of concentric circles. Wildes [11] proposed the characterization of the iris texture through a Laplacian pyramid with 4 different levels (scales).

One of the most common approaches consist in the dyadic wavelet decomposition either using Haar, Mallat or other mother wavelets. This can be found in several proposals, among which are Ali and Hassanien [23], Ma et al. [19].

1.2.6 Feature Comparison

Although the method chosen to compare between iris signature is highly conditioned by the feature extraction strategy, the feature comparison is generally performed through the use of distance metrics: Hamming (e.g., Daugman [18], Tisse et al. [24]), Euclidean (e.g., Huang et al. [25]), Weighted Euclidean (e.g., Zhu et al. [26] and Ma et al. [18]) or methods based on signal correlation (Wildes [11]).

1.2.7 Some Relevant Iris Recognition System

1.2.8 Daugman's Method

Iris segmentation: The author describes an integro-differential operator that searches for the maximal difference between the average intensity of circumferences with consecutive radius values.This operator is described in section

Normalization: After the segmentation of both iris borders, to compensate the variations in the size of the pupil, we translated the images to dimensionless polar coordinate system through a process known as the Daugman Rubber Sheet [2], which is described in section

Feature Extraction: The iris data encoding was accomplished through the use of two dimensional Gabor filters. These spatial filters have the form:

$$G(x,y) = e^{-\pi[(x-x_0)^2/\alpha^2+(y-y_0)^2/\beta^2]} e^{-2\pi \mathrm{i}[u_0(x-x_0)+v_0(y-y_0)]} \tag{1.4}$$

where (x_0,y_0) defines the position in the image (α,β) is the filter width and length and (u_0,v_0) specify the modulation, with spatial frequency $w_0 = \sqrt[2]{u_0^2 + v_0^2}$ and direction $\theta_0 = \arctan(\frac{v_0}{u_0})$ The real parts of the 2-D Gabor filters are truncated to be zero volume and achieve illumination invariance. For each resulting bit the sign of the real and imaginary parts from quadrature image projections is analyzed and, through quantization, assigned binary values: 1 and 0 respectively for positive and negative projection values.

Feature Comparison: The feature extraction binarization process allows the utilization of the Hamming distance as the similarity measure for two iris signatures. Given two binary sets with N bits : $A = \{a_1, a_2, ...a_N\}$ and $B = \{b_1, b_2, ...b_N\}$ the Hamming distance is:

$$HD(A,B) = \frac{1}{N} * \sum_{i=1}^{N} a_i \bigotimes b_i \tag{1.5}$$

being $a \bigotimes b$ the logical XOR operation. Thus, for two completely equal and different

signatures, the value of the Hamming distance will be respectively 0 and 1.

1.2.9 Wilde's Method

Wildes system [11] is also a patented iris recognition system. It uses the gradient-based Hough transform to decide the two circular boundaries of an iris. It includes two steps. First a binary edge map is generated by using a Gaussian filter. Then, votes in a circular Hough space are analyzed to estimate the three parameters of one circle (x_0, y_0, r). A Hough space is defined as

$$H(x_0, y_0, r) = \sum_i h(x_i, y_i, x_0, y_0, r) \tag{1.6}$$

where (x_i, y_i) is an edge pixel and

$$h(x_i, y_i, x_0, y_0, r) = \begin{cases} 1 & if\ (x_i, y_i)\ is\ on\ circle\ (x_0, y_0, r) \\ 0 & otherwise \end{cases}$$

The location (x_0, y_0, r) with the maximum value of H(x_0, y_0, r) is chosen as the parameter vector for the strongest circular boundary.

Wildes system models the eyelids as parabolic arcs. The upper and lower eyelids are detected by using a Hough transform based approach similar to that described above. The only difference is that it votes for parabolic arcs instead of circles. Wildes system utilizes a Laplacian pyramid decomposition to encode the iris texture patterns. It uses normalized correlation to determine the similarity of two iris codes. The final decision is obtained from a Fisher linear discriminant based on the strength of match of each frequency band. A 100% verification accuracy was claimed when testing on 600 iris images (60 different irises). The testing iris dataset is not publicly available.

1.2.10 Other Methods

The algorithm of Boles and Boashash [10] extracts a set of one dimensional signals from the iris image using the intensity values on a set of circular contours centered at the pupil center, which is located using edge detection techniques. Then the set of one dimensional signals is further encoded by using a zero crossing transformation at different resolution levels. When calculating the overall dissimilarity between two iris codes, it uses the average of the dissimilarity at each resolution level. A 100% verification and identification accuracy was reported with the experiments conducted on 11 iris images. The source of the testing iris images was not indicated.

In an algorithm proposed by Ma et al. [19], the iris images are projected to the vertical and horizontal directions to estimate the center of the pupil. This saves time in searching for the iris boundaries. After normalizing the located iris patterns, the image contrast is enhanced by subtracting estimated background illumination. When extracting the iris patterns, a filter modulated by a circularly symmetric sinusoidal function is employed. Instead of using the whole iris image, their region of interest is constrained to the area close to the pupil because in this area the pupil texture is claimed to be more abundant. By doing this, they avoid the eyelid and eyelash noise. Their representation of the iris is a feature vector of length 1,536 bits. A Fisher linear discriminant is used to reduce the dimension of the feature vector. The minimum distance classifier is utilized in classification. The algorithm was tested on the CASIA version 1 dataset [27]. The reported identification rate is 99.43%, and the FAR is 0.001% while the FRR is 1.29%.

Table 1.3 shows comparison of some few iris recognition techniques

Year	Author	Localization	Feature Extraction	Matching
1993	Daugman [2]	Integro differential operator (IDO)	2D Gabor transform	Hamming distance (HD)
1997	Wildes [11]	Circular Hough Transform (CHT)	LOG filters	Fisher discriminant analysis
1998	Boles [10]	Edge and contour detection	Zero crossings of WT	Dissimilarity function
2002	Tisse [24]	IDO	Hilbert transform	HD
2002	Li Ma [22]	Hough Transform	Multiple Gabor filters and wavelet transform	Weighted Euclidean distance
2003	Li Ma [19]	HT	Even symmetric gabor filters	Similarity measures
2003	Masek [28]	Edge detection and HT	1D log-Gabor filters	HD
2004	Li Ma [20]	Edge detection and HT	Key local varitions using WT	Exclusive OR operation
2006	Proenca [4]	Canny edge detector and HT	Fuzzy clustering	Multiple signatures
2006	Abhyankar [29]	Active shape models	Biorthogonal WT	HD
2007	Monro [30]	HT	DCT	HD

Table 1.3: Summary of Iris recognition techniques.

Chapter 2

Iris Image Databases

In this chapter we describe the main characteristics of the public and freely available iris image databases for biometrics purposes.

2.1 Public and Free Databases

The biometrics research and development demands the analysis of human data. Obviously, it is unrealistic to perform the test of algorithms in data captured on-the-fly, due to the enormous uneasiness that this would imply. Moreover, the fair comparison between recognition methods demands similar input data to valorize and contextualize their results. Therefore, when it comes to the test of recognition methods, standard biometric databases assume high relevance and become indispensable to the development process.

2.1.1 BATH Database

The University of Bath (BATH) iris image database is constantly growing and at present contains over 16000 iris images taken from 800 eyes of 400 subjects. It results of a project which aims to build an "high quality iris image resource" [31]. The majority of the database comprises images taken from students and staff of the University of Bath Images from the BATH database contain almost exclusively noise factors related with iris obstructions (due to eyelids and eyelashes), as shown in figure 2.1

2.1.2 CASIA Database

Iris recognition has been an active research topic of the Institute of Automation from the Chinese Academy of Sciences [27]. Having concluded about a lack of iris

Figure 2.1: Examples of iris images from the BATH database.

data for algorithm testing, they developed the CASIA image database. Apart from being the oldest, this database is clearly the most known and widely used by the majority of the researchers.

CASIA iris image database [27] (version 1,2,3) the CASIA v.1 database includes 756 iris images from 108 eyes, hence 108 classes. For each eye, 7 images are captured in two sessions, where three samples are collected in the first and four in the second session. Similarly to the above described database, its images were captured within an highly constrained capturing environment, which conditioned the characteristics of the resultant images. They present very close and homogeneous characteristics and their noise factors are exclusively related with iris obstructions by eyelids and eyelashes. Moreover, the postprocess of the images filled the pupil regions with black pixels, which some authors used to facilitate the segmentation task. From our viewpoint, this significantly decreased the utility of the database in the evaluation of robust iris recognition methods. fig 2.2 shows some images from CASIA database.

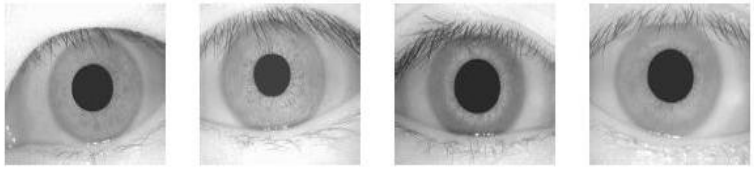

Figure 2.2: Examples of iris images from the CASIA database.

2.1.3 ICE Database

The Iris Challenge Evaluation (ICE) is a contest designed to measure the accuracy of the underlying technology that makes iris recognition possible. Its goals are to promote the development and advancement of iris recognition and assess the technologys current level of performance. The ICE [32] database is comprised of 2954 images, with a variable number of images per subject. Similarly to the remaining public iris databases, its images were captured having quality as the main concern

and clearly simulate the users cooperation in the image capturing.fig 2.3 shows some images from ICE database.

Figure 2.3: Examples of iris images from the ICE database.

2.1.4 MMU Database

The Multimedia University3 has developed a small data set of 450 iris images (MMU) [33]. They were captured through one of the most common iris recognition cameras presently functioning (LG IrisAccess R 2200). This is a semi-automated camera that operates at the range of 7-25 cm. Further, a new data set (MMU2) comprised of 995 iris images has been released and another common iris recognition camera (Panasonic BM-ET100US Authenticam) was used. The iris images are from 100 volunteers with different ages and nationalities. They come from Asia, Middle East, Africa and Europe and each of them contributed with five iris images from each eye. Obviously, the images are highly homogeneous and their noise factors are exclusively related with small iris obstructions by eyelids and eyelashes. fig 2.4 shows some images from MMU database.

Figure 2.4: Examples of iris images from the MMU database.

2.1.5 UPOL Database

The UPOL [34] iris image database was built within the University of Palackeho and Olomouc 4. Its images have the singularity of being captured through an optometric framework (TOPCON TRC50IA) and, due to this, are of extremely high quality and suitable for the evaluation of iris recognition in completely noise-free environments.

The database contains 384 images extracted from both eyes of 64 subjects (three images per eye). As can be seen in figure 3.5, its images have maximum homogeneity and inclusively the iris segmentation is facilitated by the dark circle that surrounds the region corresponding to the iris. Obviously, these characteristics make this database the less appropriate for the non-cooperative iris recognition research. fig 2.5 shows some images from UPOL database.

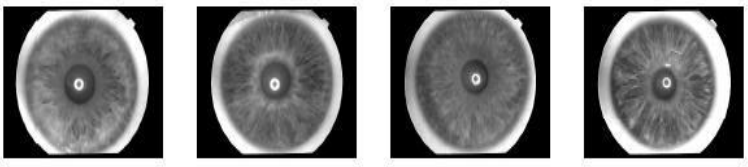

Figure 2.5: Examples of iris images from the UPOL database.

2.1.6 IITD Database

This iris image database mainly consists of the iris images collected from the students and staff at IIT Delhi, India. This database has been acquired in the Biometrics Research Laboratory during January - July 2007 using JIRIS, JPC1000, digital CMOS camera. The acquired images were saved in bitmap format. The database of 2240 images is acquired from 224 different users and made available freely to the researchers. All the subjects in the database are in the age group 14-55 years comprising of 176 males and 48 females. The resolution of these images is 320 x 240 pixels and all these images were acquired in the indoor environment.fig 2.6 shows some images from IIT,Delhi database.

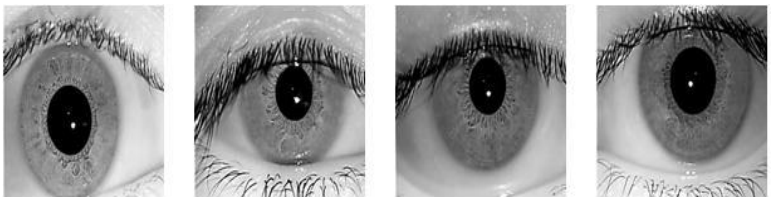

Figure 2.6: Examples of iris images from the IITD database.

2.1.7 Publicly Available Iris Image Databases Information

Table 2.1 shows the information about publicly available iris image Databases. For performance evaluation of our iris recognition system we have performed experimentation mainly on three databases **CASIA v1, MMU, IITD**.

Database	Number of irises	Number of images	Camera used	How to obtain
CASIAv1	108	756	CASIA camera	www.cbsr.ia.ac.cn/Databases.htm
CASIAv3	1500	22051	CASIA OKI irispass-h	www.cbsr.ia.ac.cn/Databases.htm
ICE2005	244	2953	LG2200	Email -ice@nist.gov
ICE2006	480	60000	LG2200	Email -ice@nist.gov
MMU1	90	450	LG IrisAccess	pesona.mmu.edu.
MMU2	199	995	Panasonic BM-ET100	ccteo@mmu.edu.my
UBIRIS	241	1877	Nikon E5700	iris.di.ubi.pt
Univ of Bath	800	16000	ISG LightWise	Fax to www.bath.ac.uk
UPOL	128	384	SONY DXC	www.inf.upol.cz/iris
WVU	488	3099	OKI irispass-h	arun.ross@mail.wvu.ed
IITD	224	2240	JIRIS, CMOS	http://web.iitd.ac.in

Table 2.1: Publicly available iris image Databases Information.

2.1.8 Attributes of Iris Images from Available Databases

Table 2.2 shows attributes of images from publicly available iris image Databases i.e size, iris radius, noise etc.

Iris Database	Image Size,pix	Iris Radius,pix	Pupil radius,pix	Noise%
BATH	1280×960	232	101	6.29
CASIA	320×280	102	37	12.72
ICE	640×480	119	54	6.70
MMU	320×240	57	21	7.83
UPOL	768×576	286	74	1.03
UBIRIS	800×600	206	45	27.62
WVU	800×600	204	54	16.10

Table 2.2: Attributes of iris images from available databases.

Chapter 3

Iris Segmentation

Iris segmentation accomplish the job of determining the specific iris region from an eye image, mainly the iris boundary, the pupil boundary, the upper eyelid and lower eyelids. The artifacts could exist commonly within the iris images, such as the eyelash occlusion, the eyelid occlusion and the image noise. A successful removal of these artifacts generates the clean iris region for the subsequent recognition. An iris is normally segmented by detecting its inner (pupil) and outer (limbus) boundaries. Well-known methods such as the Integro-differential, Hough transform and active contour models have been successful techniques in detecting the boundaries. In the following, these methods are described and some of their weaknesses are pointed out.

3.1 Daugman's Integro-differential Operator

In order to localize an iris, Daugman proposed the Integro-differential operator [2]. The operator assumes that pupil and limbus are circular contours and performs as a circular edge detector. Detecting the upper and lower eyelids are also performed using the Integro- differential operator by adjusting the contour search from circular to a designed arcuate [1]. The Integro-differential is defined as:

$$max(r, x_0, y_0) \left| G_\sigma(r) * \frac{\partial}{\partial r} \int_{r,x_0,y_0} \frac{I(x,y)}{2\pi r} ds \right| \tag{3.1}$$

The operator pixel-wise searches throughout the raw input image, I(x,y), and obtains the blurred partial derivative of the integral over normalized circular contours in different radii. The pupil and limbus boundaries are expected to maximize the contour integral derivative, where the intensity values over the circular borders would make a sudden change. Path of the normalized contour integral is along a circular arc

ds of radius r and center coordinates (x_0,y_0). The symbol $*$ denotes convolution and $G_\sigma(r)$ is a smoothing function such as a Gaussian of scale σ. The complete operator behaves as a circular edge detector, blurred at a scale set by σ , searching iteratively for the maximal contour integral derivative at successively finer scales of analysis through the three parameter space of center coordinates and radius (x_0,y_0,r) defining a path of contour integration. The path of contour integration in above equation is changed from circular to arcuate, with spline parameters fitted by statistical estimation methods to model each eyelid boundary.

3.2 Circular Hough Transform

Hough transform is a standard image analysis tool for finding curves that can be defined in a parametrical form such as lines, polynomials and circles. The recognition of a global pattern is achieved using the local patterns. For instance, recognition of a circle can be achieved by considering the strong edges in an image as the local patterns and searching for the maximum value of a circular Hough transform.

Wildes et al. [11], Kong and Zhang [17], Tisse et al. [24] and Ma et al. [18] use Hough transform to localize irises. The localization method, similar to Daugman's method, is also based on the first derivative of the image. In the proposed method by Wildes, an edge map of the image is first obtained by thresholding the magnitude of the image intensity gradient:

$$|\nabla G(x,y) * I(x,y)| \tag{3.2}$$

$\nabla \equiv (\frac{\partial}{\partial x}, \frac{\partial}{\partial y})$ and

$$G(x,y) = \frac{1}{2\pi\sigma^2} e^{-\frac{(x-x_0)^2+(y-y_0)^2}{2\sigma^2}} \tag{3.3}$$

G(x,y) is a Gaussian smoothing function with scaling parameter σ to select the proper scale of edge analysis. The edge map is then used in a voting process to maximize the defined Hough transform for the desired contour. Considering the obtained edge points as ,(x_i, y_i) j=1,2,.....n a Hough transform can be written as:

$$H(x_0,y_0,r) = \sum_i h(x_i,y_i,x_0,y_0,r) \tag{3.4}$$

where

$$h(x_i,y_i,x_0,y_0,r) = \begin{cases} 1 & if\ (x_i,y_i)\ is\ on\ circle\ (x_0,y_0,r) \\ 0 & otherwise \end{cases}$$

The limbus and pupil are both modeled as circles and the parametric function g is

defined as:

$$g(x_i, y_i, x_0, y_0, r) = (x_i - x_0)^2 + (y_i - y_0)^2 - r^2 \tag{3.5}$$

Assuming a circle with the center (x_0,y_0) and radius r, the edge points that are located over the circle result in a zero value of the function. The value of g is then transformed to 1 by the h function, which represents the local pattern of the contour. The local patterns are then used in a voting procedure using the Hough transform H, in order to locate the proper pupil and limbus boundaries. In order to detect limbus, only vertical edge information is used. The upper and lower parts, which have the horizontal edge information, are usually covered by the two eyelids. The horizontal edge information is used for detecting the upper and lower eyelids, which are modeled as parabolic arcs.

3.3 Discrete Active Contours

Ritter et al. [35] make use of active contour models for localising the pupil in eye images. Active contours respond to pre-set internal and external forces by deforming internally or moving across an image until equilibrium is reached. The contour contains a number of vertices, whose positions are changed by two opposing forces, an internal force, which is dependent on the desired characteristics, and an external force, which is dependent on the image. Each vertex is moved between time t and t + 1 by

$$v_i(t+1) = v_i(t) + G_i(t) + F_i(t) \tag{3.6}$$

where $F_i(t)$ is the internal force, Gi is the external force and $G_i(t)$ is the position of vertex i. For localisation of the pupil region, the internal forces are calibrated so that the contour forms a globally expanding discrete circle. The external forces are usually found using the edge information. In order to improve accuracy Ritter et al. use the variance image, rather than the edge image.

A point interior to the pupil is located from a variance image and then a discrete circular active contour (DCAC) is created with this point as its centre. The DCAC is then moved under the influence of internal and external forces until it reaches equilibrium, and the pupil is localised.

3.4 Implementation

For iris segmentation we followed the following strategy:

1. Pupil boundary detection: using binary morphology and "center of mass" technique

2. Iris boundary detection: We used two techniques 1)Daugman's integro-differential operator [2] 2)Circular hough transform [11]

3. Eyelid detection: integro-differential operator with spline interpolation. [1]

3.4.1 Pupil Boundary Detection

In an iris image, the pupil typically appears as a large dark mass, the largest homogeneous region of dark pixels in the image. Our algorithm takes advantage of this fact by isolating the darker regions of the image to create a binary image, and then performing binary morphology in order to determine which region is actually the pupil. We remark that no assumptions are made as to where the pupil lies within the image. Also, since all of the images we consider are orthogonal (meaning the eye peers straight into the camera, we assume for convenience that pupils (and later, irises also) are circular. The process to detect the pupil is as follows.

In some cases, because of the illumination conditions or for other reasons, the iris may appear darker than expected so that the boundary between pupil and iris is not very sharp. To sharpen it, we perform adaptive histogram equalization on the image before any segmentation processing begins. Next we use a grayscale threshold to binarize the image; values below the threshold (we use a value of 50 for MMU, and Casia v1 and 42 for IITD) are changed to 1, those above the threshold become 0. Then we apply binary morphology: (1) a fill, to fill in holes in the masses; (2) an erosion, to get rid of most or all of the noise; and (3) a dilation to restore the mass(es) after erosion. This process is displayed in Fig 3.1 If one mass remains, this is the pupil. When two or more masses remain, which can result from a dark eyebrow or shadow in the original image, component labeling technique is used, the component with maximum number of pixels is preserved which is pupil portion since most of the noise is removed in erosion.Once the pupil is determined, we compute its "center of mass," and its radius. (If the pupil is not circular, the radius corresponds to the radius of the smallest circle which encloses it.) We pass the location of the center to the iris boundary detection algorithm. For reducing the computational complexity we have assumed that pupil and iris are cocentric but very often the pupil center is nasal, and inferior, to the iris center [1].

figure shows the pupil boundary detection on test images from the databases used i.e MMU,CASIA v1,and IITD.

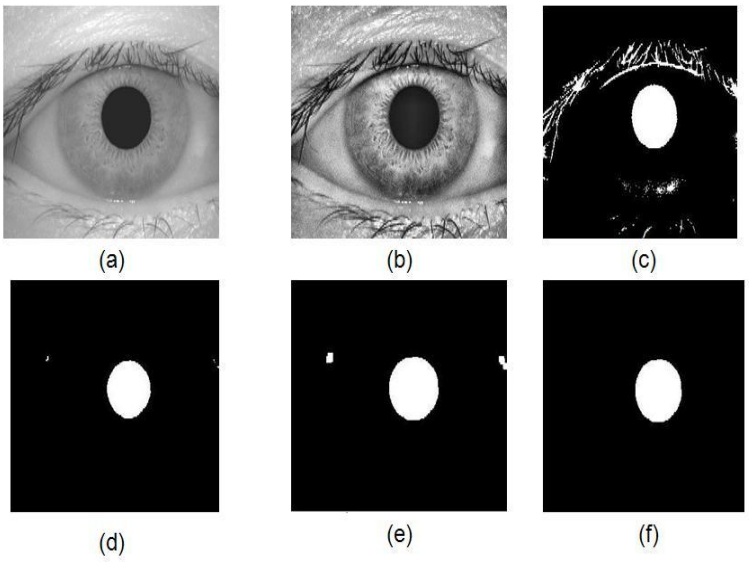

Figure 3.1: The pupil segmentation process (a)original image (b)adaptive histogram equlized image (c)thresholded image (d)erosion (e)dilation (f)segmented pupil

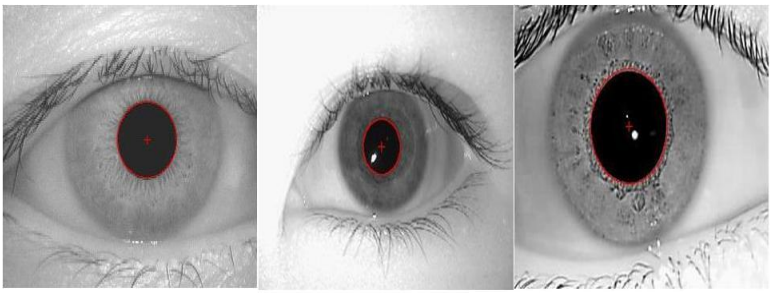

Figure 3.2: The pupil boundary detection on test images form CASIA(left), MMU(middle) and IITD(right).

The pupil segmentation was correct in about 98% of images with a round pupil on all databases; in the rest of those images, the size of the pupil was overestimated by varying amounts for all three databases. As compared to use of IDO or CHT for pupil segmentation is computationally intensive while this approach is simple and computationally efficient.

3.4.2 Iris Boundary Detection

For detecting iris boundary we implemented two widely used techniques

1. Integro-differential operator
2. Circular hough transform

While implementing Daugman's integro differential operator given by equation 3.1 for iris(limbic) boundary detection we have to make two modifications due to 1)upper and lower eyelid occlusion and 2)generally unequal left and right limbic distances the method is restricted to just two arcs along horizontal meridian each subtending $\pi/4$ radians (45 degrees) i.e angular arc of contour integration `ds` is restricted in range to two opposing 90° cones centered on horizontal meridian since eyelids generally obscure the upper and lower limbus of the iris. So "exploding pie wedges" [36] search for finding maximum in the rate of change of integrated luminance convolved with the smoothed gaussian blur as the radius of expansion increases, the maximum in this derivative with respect to radius invariably corresponds to correct left and right boundaries of the iris. fig 3.3 shows the selection of `ds` for contour integration for locating the outer iris boundary.

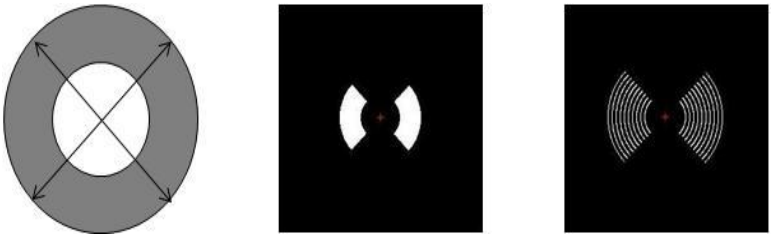

Figure 3.3: Angular arc of contour integration `ds` for detection of iris boundary.

The gray scale values under the `ds` is summed for each increment in radius and radius is found at which we get maximum difference in line integral value. fig 3.4 shows the iris boundary detection for test images.

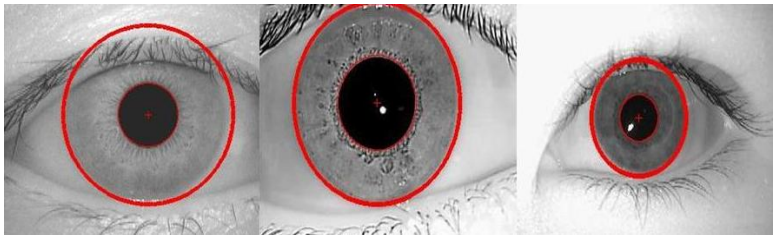

Figure 3.4: Iris boundary detection using integro-differential operator.

Detecting Circles by Circular Hough Transform

The Hough transform is a mapping from the image plane onto the parameter space. The parameter space is quantized into an accumulator array, and each accumulator stands for the curve specified by the coordinates of the accumulator. For each edge point on the image plane, the curves passing through the point are computed, and the accumulators corresponding to these curves are incremented by 1. After the

transform, the accumulator with a peak value indicates the existence of a curve, which is specified by the coordinates of the accumulator, on the image plane.The circle with center `(a,b)` and radius `r` is specified by the parameters (x_0, y_0, r_0) in the equation

$$(x - a) + (y - b) = r^2 \tag{3.7}$$

The parametric representation of the circle is

$$x = a + rcos(\theta)\ y = b + rsin(\theta) \tag{3.8}$$

Thus the parameter space for a circle will belong to R^3 whereas the line only belonged to R^2. As the number of parameters needed to describe the shape increases as well as the dimension of the parameter space increases so do the complexity of the Hough transform.

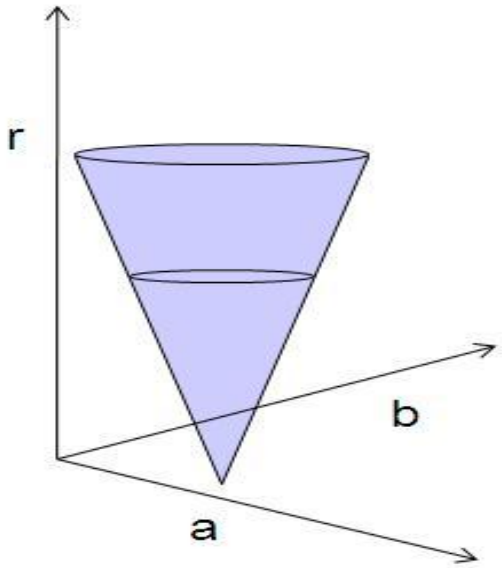

Figure 3.5: The parameter space used for CHT, which is voted by an edge point.

Choosing (a,b,r) as the parameters of the Hough transform, the locus of the accumulators, in the parameter space, incremented by an edge point on the image plane is a right circular cone (see Fig. 3.5). If there is a circle on the image plane, all the right circular cones incremented by the edge points of the circle will intersect at a common accumulator in the parameter space. The coordinates of this common accumulator are the parameters of the equation for the circle on the image plane. i.e The locus of (a, b) points in the parameter space fall on a circle of radius R centered at (x, y). The true center point will be common to all parameter circles, and can be found with a Hough accumulation array.

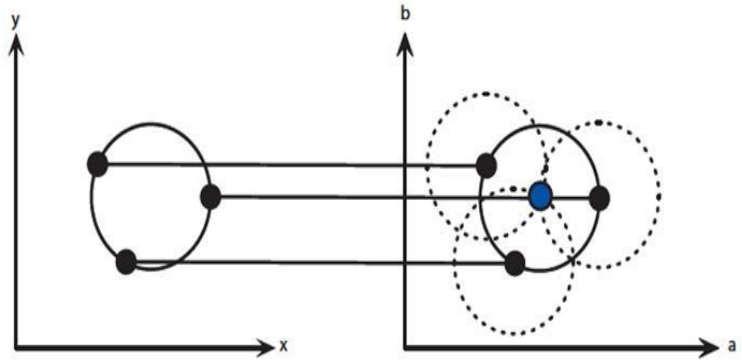

Figure 3.6: Each point in geometric space (left) generates a circle in parameter space (right). The circles in parameter space intersect at the (a, b) that is the center in geometric space..

Most of the time the radius is unknown so we must know the range of radius to search for.Our accumulator is 3D i.e for radius of range $(r_1, r_2, ...r_n)$ our accumulator will be $HA(:, :, r_i)$ where i=1,...n. the radius for which we get the maximum votes is the radius of the circle and the location of that point is nothing but the center point in the image space. Figure 3.7 shows the circle detection using CHT. the Algorithm can be summarized as follows:

1. Load Image.
2. Detect edges.
3. For each edge point
   - For each value of r
     (a) Draw a circle with centre in the edge point and radius r.
     (b) Increment all points that the circle passes through
4. Find one or several maxima in the accumulator.

For drawing circle in discrete space, we have assumed circle to be consisting of polygon of n no of sides preferably 600. Then using the parametric equations of circle given by equation 3.8 we can find points on the circumference of circle, assigning 1 to all these points draws circle on discrete space.

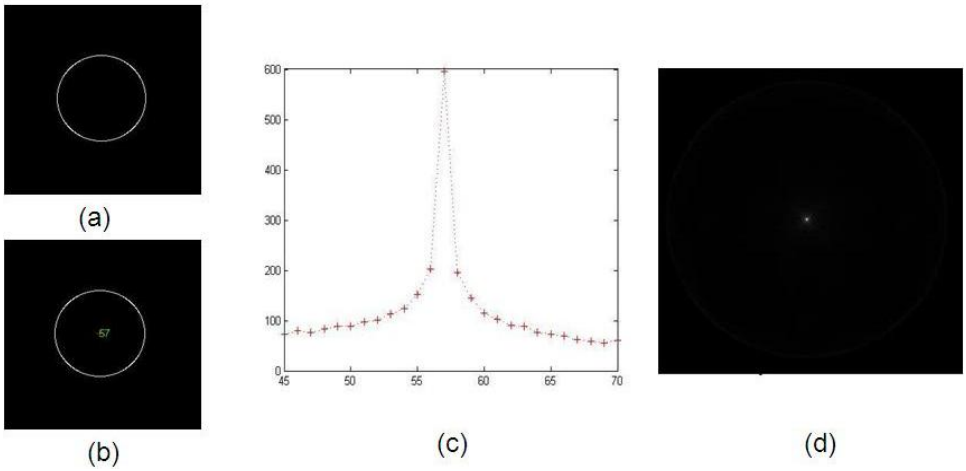

Figure 3.7: Circle detection using circular hough transform (a)Image with the unknown circle (b)Detected circle (c)Plot of Accumulator votes and radius (d)Hough Accumulator for detected radius.

The above example of circle detection can be generalized for detecting iris boundary the edge image is found by canny edge detection. The range of iris radius is provided same as that was for IDO.

Fig 3.8 shows use of CHT for iris boundary detection for iris database image.

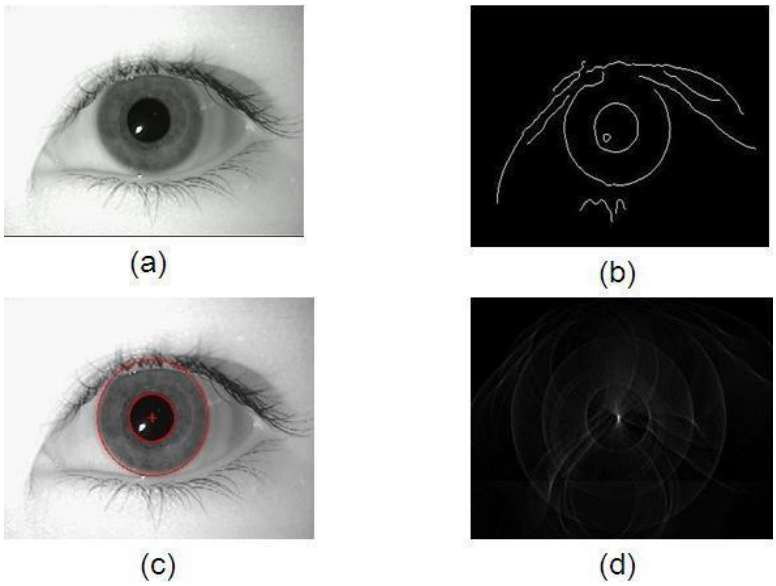

Figure 3.8: Iris boundary detection using Circular Hough Transform (a)aeval1.jpg (MMU) (b)Edge image (c)Iris boundary detection (d)Hough accumulator for detected radius..

3.4.3 Upper and Lower Eyelid Detection

For upper and lower eyelid detection we followed Daugman's approach in his paper "How iris recognition works" [1] as shown in figure 3.9

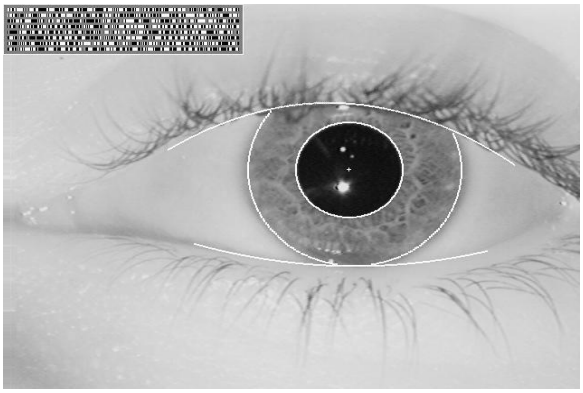

Figure 3.9: Figure from Daugman's paper [1] representing iris segmentation with detected pupil, iris and eyelid boundaries.

Daugman used integro-differential operator given by equation 3.1 in which `ds` is changed from circular to arcuate for detection of upper and lower eyelids and spline interpolation with parameters fitted by standard statistical estimation [1].

Figure 3.10 and figure 3.11 shows our implementation of upper and lower eyelid detection by using integro-differential operator. We separately detected upper and lower eyelids, the path of contour integration used is as shown in figure. The procedure is similar to finding pupil or iris boundary by IDO except the `ds` used. After detection of presence of eyelid we have chosen two points heuristically from eyelid corners and one point from the area `ds` preferably the midpoint and applied spline interpolation [37].

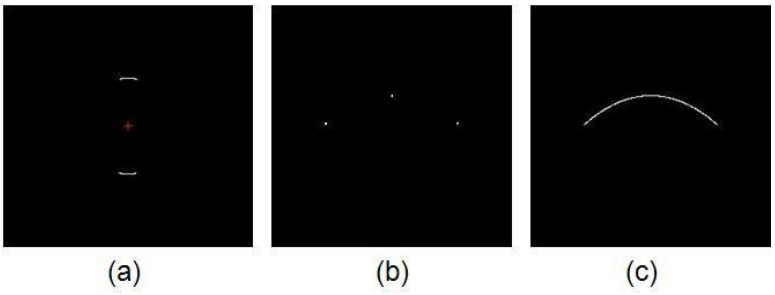

Figure 3.10: Procedure for eyelid drawing (a)area `ds` used for contour integration (b) Points for spline interpolation (c) Eyelid shape.

figure 3.12 shows the overall segmentation results similar to as that shown in figure 3.9 on test images from the databases used.

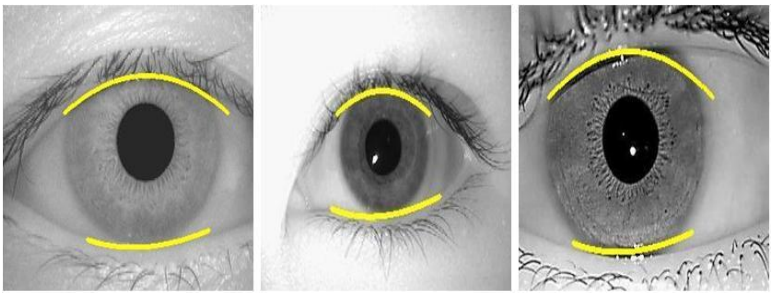

Figure 3.11: Detection of upper and lower eyelids for images from CASIA,MMU, and IITD databases.

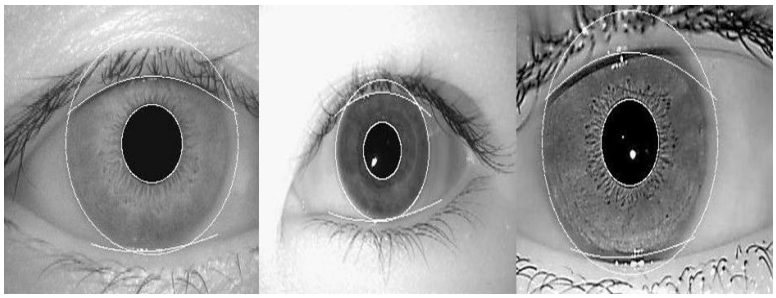

Figure 3.12: Overall segmentation results on test images from CASIA,MMU, and IITD databases.

3.4.4 Noise Removal

With the available segmentation data it better to remove unnecessary region prior to normalization figure 3.13 shows noise removed images Here we have cropped the segmented iris images so that pupil center becomes geometric center of image. The noisy regions are assigned NaN values.

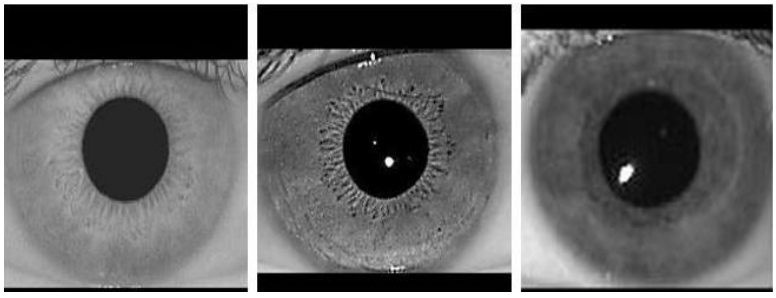

Figure 3.13: Noise removed images i.e images with only iris portion.

3.4.5 Results

The automatic segmentation model is proven to be successful. The CASIA and MMU databases provided good segmentation, since those eye images had been taken specifically for iris recognition research and boundaries of iris pupil and sclera were clearly distinguished. But on IIT, Delhi database this is not the case because the images are cropped such that iris portion is either close or outside the image boundaries.

The major problem faced in pupil-iris boundary is pupil deformation. Due to simple thresholding and binary morphology the computation task is reduced drastically the only problem is when image is severely occluded by eyelids and eyelashes.

One problem faced with the implementation was that it required different parameters to be set for each database. These parameters were the radius of iris and pupil to search for, and threshold values for creating edge maps. However, for installations of iris recognition systems, these parameters would only need to be set once, since the camera hardware, imaging distance, and lighting conditions would usually remain the same.

The eyelid detection system also proved quite successful, and managed to isolate most occluding eyelid regions. One problem was that it would sometimes isolate too much of the iris region, which could make the recognition process less accurate, since there is less iris information. However, this is preferred over including too much of the iris region, if there is a high chance it would also include undetected eyelash and eyelid regions.

Tables 3.1, 3.3, 3.2 shows the overall segmentation results for CASIA, MMU and IITD databases respectively:

Segmented Area	Images	Successful Segmentation	Partial(failed) Segmentation	Successful Segmentation percentage
Pupil-center finding	350	350	0	100%
Pupil-Iris Boundary	350	343	7	98%
Iris-Sclera Boundary	350	333	17	95.14%
Eyelid Boundary	350	330	20	94.28%

Table 3.1: Overall Segmentation results for CASIA.

Segmented Area	Images	Successful Segmentation	Partial(failed) Segmentation	Successful Segmentation percentage
Pupil-center finding	175	175	0	100%
Pupil-Iris Boundary	175	170	5	97.14%
Iris-Sclera Boundary	175	168	7	96%
Eyelid Boundary	175	163	12	93.14%

Table 3.2: Overall Segmentation results for MMU.

Segmented Area	Images	Successful Segmentation	Partial(failed) Segmentation	Successful Segmentation percentage
Pupil-center finding	625	625	0	100%
Pupil-Iris Boundary	625	620	5	99.20%
Iris-Sclera Boundary	625	576	49	92.15%
Eyelid Boundary	625	564	61	90.25%

Table 3.3: Overall Segmentation results for IITD.

In the above results integro differential operator is used for iris boundary detection, it is clear from the above results that the integro differential operator is best for segmenting iris images.the only constraint is that image should have good contrast. Although we successfully implemented circular hough transform for iris boundary detection but our implementation takes more time and is computationally inefficient, though we can reduce reduce the time and computation. Segmentation results for CASIA using CHT are less due to low contrast iris-scelera boundary. For MMU and IITD results are good.

Chapter 4

Iris Normalization

Normalization refers to preparing a segmented iris image for the feature extraction process. Once the iris region is successfully segmented from an eye image, the next stage is to transform the iris region so that it has fixed dimensions in order to allow comparisons. The dimensional inconsistencies between eye images are mainly due to the stretching of the iris caused by pupil dilation from varying levels of illumination. Other sources of inconsistency include, varying imaging distance, rotation of the camera, head tilt, and rotation of the eye within the eye socket. The normalization process will produce iris regions, which have the same constant dimensions, so that two photographs of the same iris under different conditions will have characteristic features at the same spatial location.

For normalization we have assumed the pupil region and iris region are concentric i.e pupil and iris center are concentric but practically pupil region is slightly nasal to iris region.

4.1 Iris Normalization Techniques

4.1.1 Daugman's Rubber Sheet Model

Daugman's normalization method transforms a localized iris texture from Cartesian to polar coordinates. The proposed method is capable of compensating the unwanted variations due to distance of eye from camera (scale) and its position with respect to the camera (translation). The Cartesian to polar transformation is defined as:

The process is inherently dimensionless in the angular direction. In the radial direction, the texture is assumed to change linearly, which is known as the rubber sheet model. The rubber sheet model linearly maps the iris texture in the radial

direction from pupil border to limbus border into the interval [0 1] and creates a dimensionless transformation in the radial direction as well. The homogenous rubber sheet model as shown in figure 4.1 devised by Daugman [1] remaps each point within the iris region to a pair of polar coordinates (r,θ) where r is on the interval [0,1] and θ is angle [0,2π].

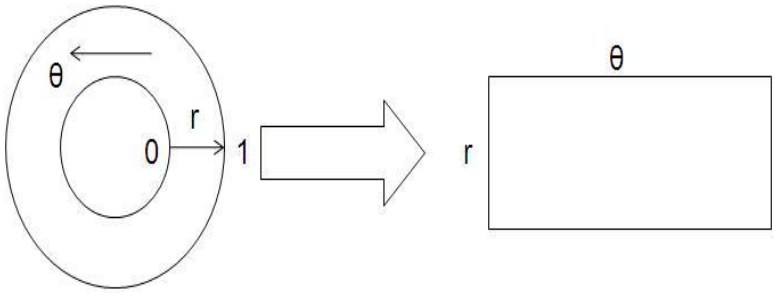

Figure 4.1: Daugmans rubber sheet model.

The remapping of the iris region from (x,y) Cartesian coordinates to the normalized non-concentric polar representation is modelled as-

$$I(x(r,\theta), y(r,\theta)) \rightarrow I(r,\theta) \tag{4.1}$$

$$x(r,\theta) = (1-r) \times x_p(\theta) + (1-r) \times x_i(\theta);$$
$$y(r,\theta) = (1-r) \times y_p(\theta) + (1-r) \times y_i(\theta);$$

where, where I(x,y) is the iris region image, (x,y) are the original Cartesian coordinates, (r,θ) are the corresponding normalized polar coordinates.(x_p, y_p) and $(x_i, y_i)$are the coordinates of the pupil and iris boundaries along the θ direction. The rubber sheet model takes into account pupil dilation and size inconsistencies in order to produce a normalized representation with constant dimensions. In this way the iris region is modelled as a flexible rubber sheet anchored at the iris boundary with the pupil center as the reference point.

Although the normalization method compensates variations due to scale, translation and pupil dilation, it is not inherently invariant to the rotation of iris. Rotation of an iris in the Cartesian coordinates is equivalent to a shift in the polar coordinates. In order to compensate the rotation of iris textures, a best of n test of agreement technique is proposed by Daugman in the matching process. In this method, iris templates are shifted and compared in n different directions to compensate the rotational effects.

4.1.2 Wildes Image Registration

Wildes has proposed an image registration technique for normalizing iris textures. In this method, a newly acquired image, $I_a(u, v)$ would be aligned with an image in the database, $I_d(u, v)$, that the comparison is performed. The alignment process is a transformation using a choice of mapping function, (U(x,y); V (x,y)) that would minimize the function:

$$\int_x \int_y (I_d(x, y) - I_a(x - u, y - v))^2 dxdy \tag{4.2}$$

The alignment process compensates the rotation and scale variations. The mapping function is constrained to capture a similarity transformation of image coordinates (x,y) to $(x^{'}, y^{'})$,i.e.,

$$\begin{pmatrix} x^{'} \\ y^{'} \end{pmatrix} = \begin{pmatrix} x \\ y \end{pmatrix} - sR(\phi) \begin{pmatrix} x \\ y \end{pmatrix} \tag{4.3}$$

with s as the scaling factor and R(ϕ) a matrix representing rotation by ϕ. The para- meters s and ϕ are recovered by an iterative minimization procedure.

Wildes normalization process is based on a different approach compared to Daugman's method. In this method, normalization is performed in the matching time. Comparing to Daugman's approach, the normalization method would be time consuming in identification applications. However, for verication purposes the method is capable of compensating unwanted factors such as variations in rotation and scale.

4.1.3 Other Normalization Techniques

Lim et al. uses a method very similar to the pseudo polar transform of Daugman. In this method, after finding the center of pupil and the inner and outer boundaries of iris, the texture is transformed into polar coordinates with a fixed resolution. In the radial direction, the texture is normalized from the inner boundary to the outer boundary into 60 pixels which is fixed throughout all iris images. The angular resolution is also fixed to a 0.8 degree over the 360 degree which produces 450 pixels in the angular direction. Bole's normalization technique is also similar to Daugman's method with the difference that it is performed at the time of matching. The method is based on the diameter of the two matching irises. The ratio of the diameters are calculated and the diameter of irises are adjusted to have the same diameters. The number of samples is also fixed and it is set to a power-of-two integer in order to be suitable for the dyadic wavelet transform.

4.2 Implementation

For normalization of iris regions a technique based on Daugmans rubber sheet model was employed. The center of the pupil was considered as the reference point, a number of data points are selected along each radial line and this is defined as the radial resolution. The number of radial lines going around the iris region is defined as the angular resolution. For simplicity we have assumed cocentric pupil and iris center. The normalized pattern is created simply by transforming noise removed iris images as shown in fig 4.2 from cartesian to polar coordinate system. We have normalized images from CASIA database and IITD database to fixed 64×512 size since their iris radius is well above 100, while for MMU database image are normalized to 30×360 size. Another 2D array was created for marking reflections, eyelashes, and eyelids detected in the segmentation stage. In order to prevent non-iris region data from corrupting the normalized representation, data points which occur along the pupil border or the iris border are discarded. As in Daugmans rubber sheet model, removing rotational inconsistencies is performed at the matching stage and will be discussed in the next chapter.

4.3 Results

The normalization process proved to be successful and some results are shown in Figure 4.2

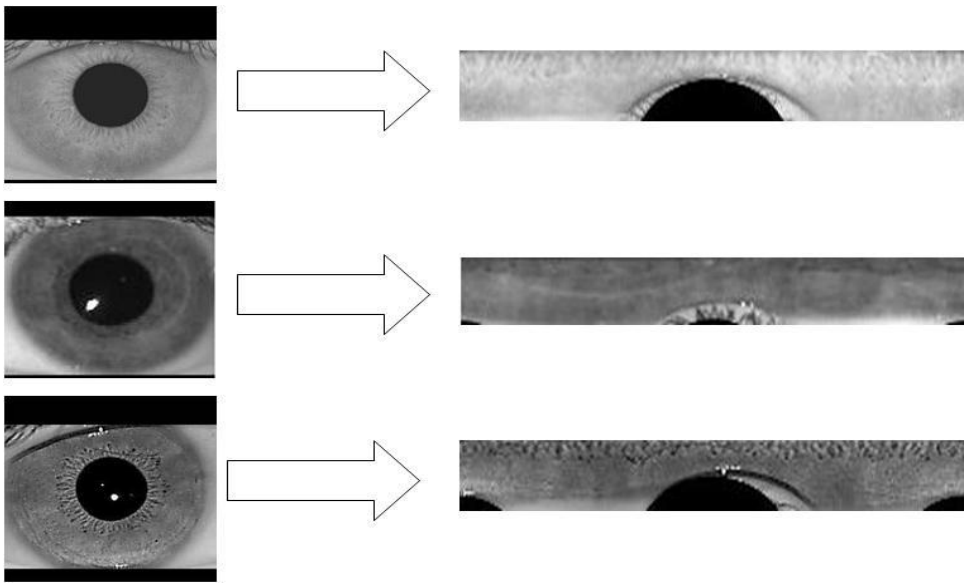

Figure 4.2: Normalized images of test images from databases.

4.4 Image Enhancement

The normalized iris image has low contrast and may have nonuniform brightness caused by the position of light sources. All these may affect the subsequent processing in feature extraction and matching. In order to obtain a more well-distributed texture image, we first approximate intensity variations across the whole image. The mean of each 16×16 small block constitutes a coarse estimate of the background illumination. This estimate is further expanded to the same size as the normalized image by bicubic interpolation. The estimated background illumination as shown in Fig. 4.3(b) is subtracted from the normalized image to compensate for a variety of lighting conditions. Then, we enhance the lighting corrected image by means of histogram equalization in each 32×32 region. Such processing compensates for the nonuniform illumination, as well as improves the contrast of the image. Fig. 4.3 shows the preprocessing result of an iris image, from which we can see that finer texture characteristics of the iris become clearer

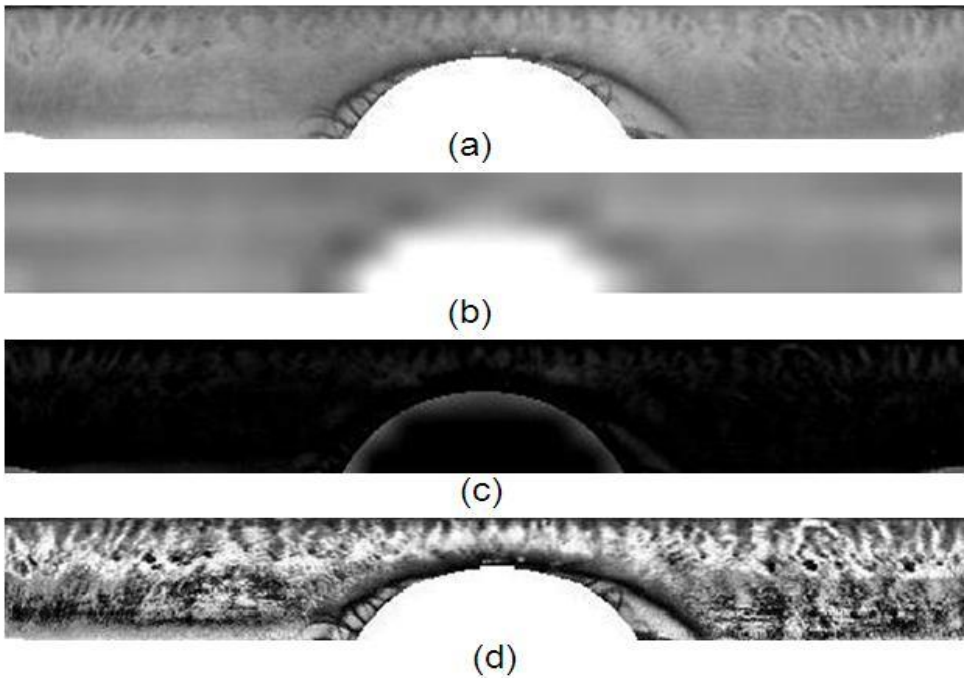

Figure 4.3: Image preprocessing. (a)Normalized image.(b) Estimated background illumination. (d)Image after background substraction. (e)Normalized image after enhancement

Chapter 5

Feature Extraction and Matching

5.1 Feature Extraction Techniques

The iris has an interesting structure and presents plentiful texture information. So, it is attractive to search representation methods which can capture local crucial information in an iris. The uniqueness and variability are the key to successful personal identifications, in order to distinguish between templates.

5.1.1 2D Gabor Filters

The Daugman system applies a series of 2D Gabor wavelets to the isolated iris region in the normalized polar coordinates (r,θ). The Gabor filter could be seen as a Gaussian envelope multiplexed by a series of sinusoidal waves with different scales and rotations. Here the Daugman system uses the same function to explore the local intensity correlation of iris images in the space and frequency domains [1]. The filter wavelet is specified as:

$$H(r,\theta) = e^{-i\omega(\theta-\theta_0)}e^{-(r-r_0)/\alpha^2}e^{-(\theta-\theta_0)/\beta^2} \tag{5.1}$$

in which α and β are used to specify the multi-scale 2D wavelet size. ω represents the wavelet frequency, which is inversely proportional to α and β. (r_0, θ_0) represents the center location of the frequency selective filter bank.A collection of feature points are sampled from the original iris image in the Cartesian coordinates. These feature points are mapped, or in other words, unwrapped into a matrix representation in the normalized polar coordinates according to the Daugman rubber sheet model. Then the set of Gabor filter banks are applied to this matrix template and the template

is decomposed into a set of complex coefficients h at each location (r_0, θ_0):

$$h = \int_r \int_\theta I(r,\theta) e^{-i\omega(\theta-\theta_0)} e^{-(r-r_0)/\alpha^2} e^{-(\theta-\theta_0)/\beta^2} \tag{5.2}$$

in which r and θ represent, respectively, the dimensions along the radial and circumferential directions in the normalized polar coordinates. The complex domain is divided into four phases, and each phase is represented by two binary bits. After the Gabor feature extraction, a complex feature matrix is generated from the image. For each complex feature value h, two binary bits $(h_R; h_I)$ are used to represent phase information at the pixel location. And the binary phase pairs from the entire image are combined into a binary feature template for pattern comparison and decision making. The Hamming distance is calculated between two binary feature templates to evaluate their closeness of match.

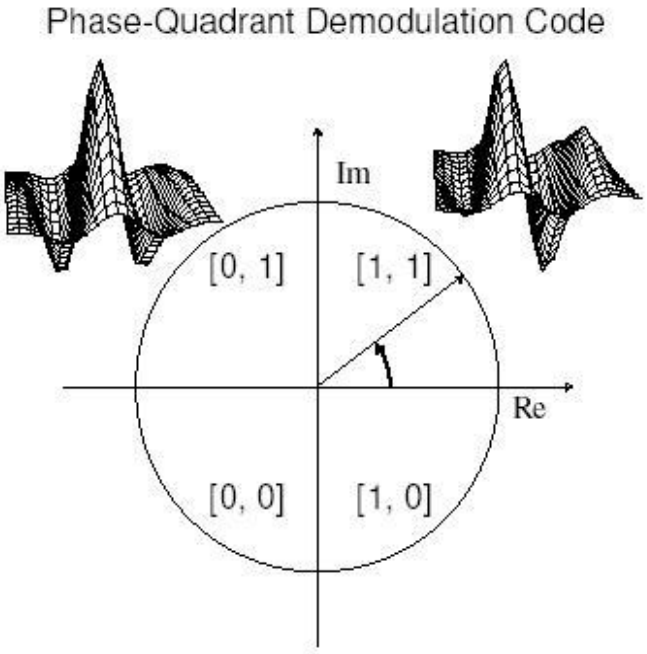

Figure 5.1: Gabor phase feature representation [1].

With different parameters selected for the Gabor decomposition, the phase encoding and feature extraction repeatedly process the iris region. One set of Gabor filter bank will extract one pair of complex phasors over each feature point. With k sets of Gabor filter banks applied to an unwrapped image template of $M \times N$ matrix, a binary phase feature matrix of $2kM \times 2kN$ would be extracted as the binary iris template for the Hamming distance calculation.

5.1.2 Laplacian of Gaussian Filter

Compared to the Gabor filter wavelets used by the Daugman system, the Wildes system employs a Laplacian of Gaussian filter G to extract the features from the iris image [11]. The filter G is defined as:

$$G = \frac{1}{\pi\sigma^4}\left(1 - \frac{\rho^2}{2\sigma^2}\right) \tag{5.3}$$

in which ρ is the distance from the Gaussian center to the image point along the radius, and σ is the standard deviation of the Gaussian filter. The segmented image I in the Cartesian coordinates is filtered with the Gaussian filter G to construct a Laplacian pyramid. First the image I is convolved with the filter G, and then down-sampled by 2 to generate the first filtered image $g1$. Subsequently, each filtered image g_k is generated by convolving the previous one g_{k-1} with filter G, then down-sampled by 2, as shown in Equation 5.4

$$g_k = (G * g_{k-1})_{\uparrow 2} \tag{5.4}$$

Each level of the Laplacian pyramid is generated according to Equation 5.5.

$$l_k = g_k - 4G * (g_{k+1})_{\uparrow 2} \tag{5.5}$$

in which l_k is the k^{th} level of the Laplacian pyramid [38]. In the Wildes system, these different levels of Laplacian pyramids are combined into the feature templates of the iris images. During the pattern comparison, the normalized correlation is used to compare two iris feature templates to calculate the closeness of match and thus make the decision of classification.

5.1.3 Log-Gabor Filter

Field presented a model to explore the effectiveness in coding the information in natural images [39]. The use of the Log-Gabor filter is examined to encode the spatial, frequency and orientation information in an image. He pointed out that Daugman system uses the Gabor filter for feature extraction, which is mostly efficient in the Cartesian coordinates.

However, the unwrapping process maps the iris pixel intensities from the Cartesian coordinates to the normalized polar coordinates. This transfer changes the relative spatial distribution among iris pixels, and therefore partially destroys some of the ability of the Gabor filter in extracting and compacting the spatial and fre-

quency information. Field proposed the Log-Gabor function to counterbalance the effect produced by the polar-mapping. The frequency response of the Log-Gabor function is:

$$G(f) = e^{-[log(f/f0)]^2/2[log(\sigma/f_0)]^2} \tag{5.6}$$

in which f_0 represents the center frequency and σ represents the bandwidth of filter. With an unwrapped iris matrix representation, each row of pixel intensities corresponds to a ring of pixels centered at the pupil center. The Log-Gabor filter is applied to the 1D image vectors to extract the phase feature templates. Since the normalization process is warping the iris region from the circular shape to the rectangular matrix, or from the Cartesian coordinates to the normalized polar coordinates, the spatial relationship along the concentric sampling rings is different from the spatial relationship along the radius. As a result, 2D Gabor filter feature extraction mechanism mixes the relative spatial relationship when it multiplexes over the normalized polar scale. In other words, 2D Gabor filter applies a symmetric Gaussian envelope to the normalized polar image representation which is not supposed to be treated evenly between radial and circumferential directions. On the other hand, the 1D Log-Gabor filter extracts the feature vector from each row of the normalized matrix representation, which avoids mixing the relative position information between the radial and the circumferential directions.

5.1.4 Zero Crossings of Wavelet Transform

In the Boles and Boashash system, the dyadic wavelet transform is applied to preprocess the image intensity vectors, and uses the zero-crossings from the decomposed signals as the feature vectors for pattern matching [10].

A series of virtual circles are sampled from the gray-scale intensity iris images. Each circle is centered at the centroid of the pupil and represented with a 1-dimension signal vector $f(n)$. The iris signal vector $f(n)$ is sampled with a resolution of N. N is chosen to be an integer square as $N = 2^j$, to make it convenient for the subsequent dyadic wavelet decomposition. Then, the 1-dimension image vector f(n) is decomposed with a set of dyadic wavelets at different resolutions. The locations of the zero-crossing points are used as the feature vectors. The dyadic wavelet transform of signal f(n) is defined as:

$$W_{a,b}f(n) = \sum_{-N}^{N} f(n)\frac{1}{a}\psi\left(\frac{n-b}{a}\right) \tag{5.7}$$

$\psi\left(\frac{n-b}{a}\right)$ represents the dyadic wavelet function. a is a scalar, and b is a translation parameter to specify the size and position of the mother wavelet. The dyadic wavelet is defined as the second derivative of smoothing function $\theta(n)$, which is not specified in the reference.

5.2 Matching Algorithms

With various feature extraction schemes, an iris image is transformed into a unique representation within the feature space. In order to make the decision of acceptance or refusal, a distance is calculated to measure the closeness of match. In iris recognition systems, such distance measures include the Hamming distance (HD), the normalized correlation (NC) and the weighted Euclidean distance (WED).

5.2.1 Hamming Distance

The Daugman algorithm [1] calculates the difference between individual patterns as a measure of statistical independence. With the encoded binary phase feature vectors, the Hamming distance between any two iris templates is defined in Equation 5.8

$$HD = \frac{\|(template_A \otimes template_B) \cap mask_A \cap mask_B\|}{mask_A \cap mask_B} \tag{5.8}$$

in which $template_A$ and $template_B$ represent the two encoded iris feature matrices. $mask_A$ and $mask_B$ are two binary masks, with the locations of the identified noise pixels marked with binary '0' and the rest of the mask with binary '1'. $\otimes$ is the logical XOR operator comparing bit by bit, and $\cap$ is the logical AND operator taking the common area of the valid iris regions. Therefore, the Hamming distance calculates the pattern difference with a bit-by-bit comparison. For iris templates from the same eye, their statistical independence and the Hamming distance tend to approach zero, while two different iris templates tend to have a Hamming distance of 0.5. As a result, by setting a threshold on the Hamming distance between iris templates, a decision could be made about whether they come from the same eye or not, thus achieving the personal identification.

5.2.2 Normalized Correlation

The Wildes system employs the normalized correlation between two encoded iris images to measure their closeness of match. The normalized correlation is defined

as:

$$NC = \frac{\sum_{i=1}^{n}\sum_{j=1}^{m}(p_1[i,j] - u_1)p_2[i,j] - u_2)}{nm\sigma_1\sigma_2} \tag{5.9}$$

in which p_1 and p_2 are the two encoded iris templates of size $n \times m$, u_1 and u_2 are the means of the images p_1 and p_2, and σ_1 and σ_2 are the standard deviations of the images p_1 and p_2.

5.2.3 Weighted Euclidean Distance

The Euclidean distance is one way of dening the closeness of match between two iris feature templates. It is calculated by measuring the norm between two vectors. For the weighted Euclidean distance, another factor is taken into consideration because the percentage of decision-making varies in different dimensions. Y. Zhu et al. [26] tried to use the weighted Euclidean distance to evaluate the closeness of an unknown iris template to a template in the existing database, defined as:

$$WED = \sum_{i=1}^{N} \frac{(f_i - g_i)^2}{\delta_i^2} \tag{5.10}$$

in which f is the unknown iris template to be matched and g is the iris template in the existing database to be compared with. i is used to denote the index of features in the templates, and is the standard deviation of the i^{th} feature in template g. Similar to the Hamming distance, the weighted Euclidean distance is another distance metric within a biometric system. In a complete system, the designer would have to interpret the metric to achieve identification or verification. In the Wildes algorithm, the iris template g with a minimum WED to the template f is identified to be from the same subject.

5.3 Implementation

5.3.1 Feature Extraction

The iris has a particularly interesting structure and provides abundant texture information. So, it is desirable to explore representation method which can capture local underlying information in an iris. From the viewpoint of texture analysis, local spatial patterns in an iris mainly involve frequency and orientation information.

For feature extraction we have used special Gabor filter bank proposed by B.S.Manjunath [40]. A two dimensional Gabor function g(x, y) and its Fourier

transform G(u, v) can be written as:

$$g(x,y) = \frac{1}{2\pi\sigma_x\sigma_y} exp\left[-\frac{1}{2}\left(\frac{x^2}{\sigma_x^2} + \frac{y^2}{\sigma_y^2}\right) + 2\pi\jmath Wx\right] \tag{5.11}$$

$$G(u,v) = exp\left\{-\frac{1}{2}\left(\frac{(u-W)^2}{\sigma_u^2} + \frac{v^2}{\sigma_v^2}\right)\right\} \tag{5.12}$$

where $\sigma_u = 1/2\pi\sigma_x$ and $\sigma_v = 1/2\pi\sigma_y$ Gabor functions form a complete but nonorthogonal basis set. Expanding a signal using this basis provides a localized frequency description. A class of self-similar functions, referred to as Gabor wavelets in the following discussion, is now considered. Let g(x, y) be the mother Gabor wavelet, then this self-similar filter dictionary can be obtained by appropriate dilations and rotations of g(x, y) through the generating function:

$$g_{mn}(x,y) = a^{-m} g(x',y') \quad a > 1 \quad \text{m,n =integer}$$

$$x' = a^{-m}(xcos\theta + ysin\theta), \ and \ y' = a^{-m}(-xsin\theta + ycos\theta), \tag{5.13}$$

where $\theta = n\pi/K$ and K is the total number of orientations. The scale factor a^{-m} in 5.13 is meant to ensure that the energy is independent of m.

The nonorthogonality of the Gabor wavelets implies that there is redundant information in the filtered images, and the following strategy is used to reduce this redundancy. Let U_l, and U_h, denote the lower and upper center frequencies of interest. Let K be the number of orientations and S be the number of scales in the multiresolution decomposition. Then the design strategy is to ensure that the half-peak magnitude support of the filter responses in the frequency spectrum touch each other as shown in Fig. . This results in the following formulas for computing the filter parameters σ_u, and σ_v, (and thus σ_x and σ_y).

$$a = (U_h/U_l)^{1/s-1}, \ \ \sigma_u = \frac{(a-1)U_h}{(a+1)\sqrt{2ln2}},$$

$$\sigma_v = tan\left(\frac{\pi}{2k}\right)\left[U_h - 2ln\left(\frac{2\sigma_u^2}{U_h}\right)\right]\left[2ln2 - \frac{(2ln2)^2\sigma_u^2}{U_h^2}\right]^{\frac{-1}{2}} \tag{5.14}$$

where $W = U_h$, and m = 0, 1, ..., S - 1. In order to eliminate sensitivity of the filter response to absolute intensity values, the real (even) components of the 2D Gabor filters are biased by adding a constant to make them zero mean (This can also be done by setting G(0,0) in 5.12 to zero).

Figure 5.2 shows gabor filter dictionary dictionary design.

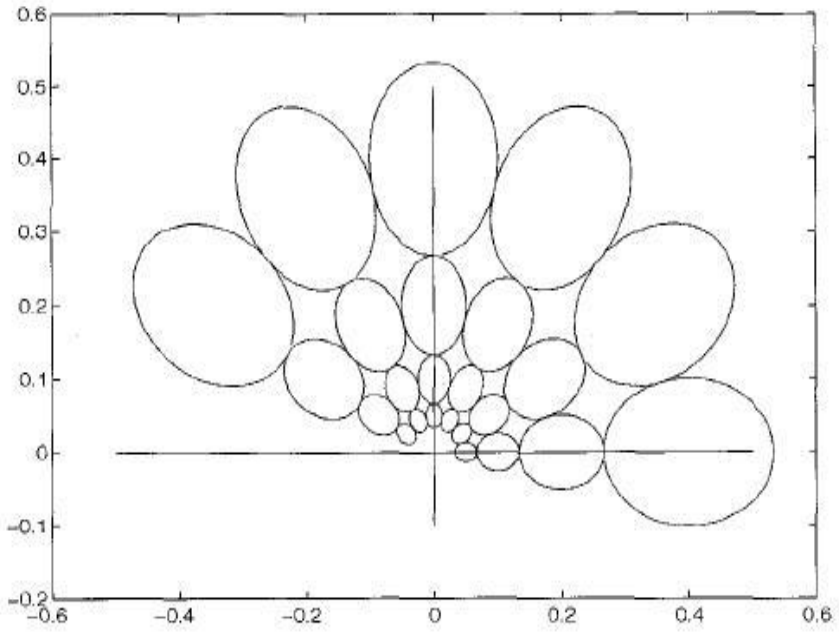

Figure 5.2: The contours indicate the half-peak magnitude of the filter responses in the Gabor filter bank. With filter parameters $U_h = 0.4$, $U_l = 0.05$, K=6,and S=4..

Figure 5.3 shows 3D view of gabor filters in spatial domain.

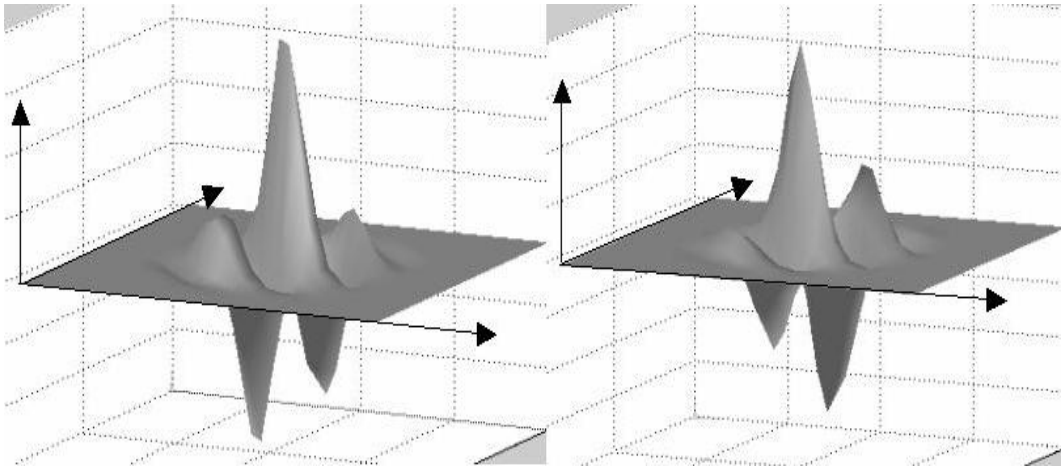

Figure 5.3: A quadrature pair of 2D Gabor filters left) real component or even symmetric filter characterized by a cosine modulated by a Gaussian right) imaginary component or odd symmetric filter characterized by a sine modulated by a Gaussian.

Following figures shows scale and frequency orientations of gabor filters.

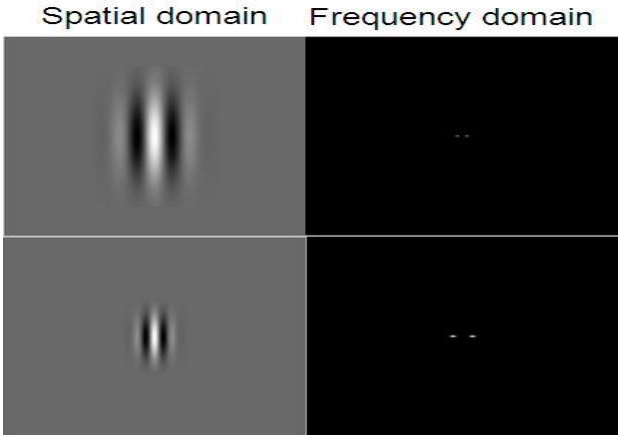

Figure 5.4: Preferred spatial frequency and size of gabor filters at various scales can be obtained figure shows gabor filters at two different scales in space and frequency domain.

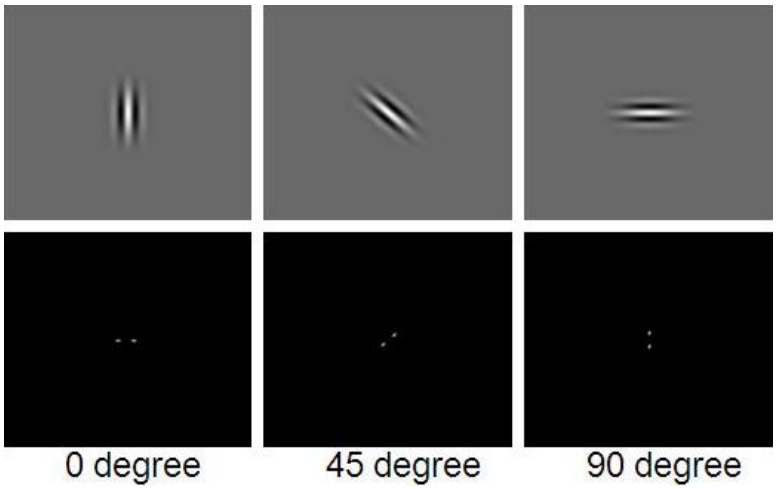

Figure 5.5: 2D Gabor filter in space and frequency domain and at various orientations (0,45,90).

Gabor filtering is done by convolution of a image with set of Gabor kernels designed to detect certain frequencies and certain orientations. Generally the Gabor filter bank is often composed of kernels detecting 4 different wavelengths/frequencies at 8 different orientations from 0° to 180°. The reason the orientations are only for a half circle is, that the absolute response would be the same, and the phase would just be rotated by 180°. The response to each filter in the filterbank is stored and used as part of the basis for comparison. For 4 wavelengths and 8 orientations, 32

filter responses have to be calculated. Figure 5.6 shows response of gabor filters for input image with 1 scale and 4 orientations.

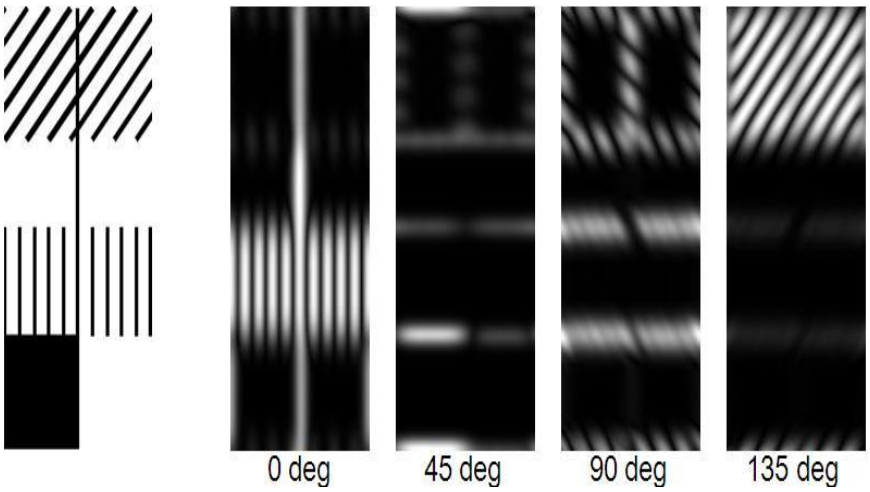

Figure 5.6: Gabor outputs for input image at four orientations and one scale (frequency).

Convolution of an image with the kernel gives a response that is proportional to how well the local feature in the image matches the kernel. This property of convolution is general for signal processing.

While encoding the extracted features from the gabor filter banks we tried to address following issues for the proof of some important facts that affect performance of iris recognition system :

1. The iris details are spread along the radial direction in the original image corresponding to the vertical direction in the normalized image so information density in the angular direction corresponding to the horizontal direction in the normalized image is higher than that in other directions As a result, the differences of orientation information among irises seem to be not significant [19].

2. Frequency information should account for the major differences of irises from differentpeople. In general, the majority of useful information of the iris is in a frequency band of about three octaves [19].

3. It is desirable to obtain an iris representation invariant to translation, scale, and rotation .

4. Dimensionality reduction has very small impact on recognition accuracy. i.e the size of feature vector does not the affect iris recognition accuracy [19].

As stated above, for the proof above statements we modified our feature template as follows:

1. To ensure the first fact we used four orientations 0°,45°,90°,135° and created four templates in each orientation 0° vector corresponds to radial components that is vertically oriented patterns, while ,90° corresponds to angular information.

2. To check the effect of frequency selectivity, first we used only one scale selecting only one particular frequency and increasing number of scales for evaluating its significance on recognition performance.

3. To obtain an iris representation invariant to translation, scale, and rotation we have created binary phase code which is shifted while matching for accounting rotation invariance.

4. The output of filtering is then phase quantized to four levels using the Daugman method [1], with each filter producing two bits of data for each phasor. The size of feature vectors are CASIA(64×1024), MMU(30×720), IITD(64×1024)

The feature encoding process is illustrated in Figure 5.7,

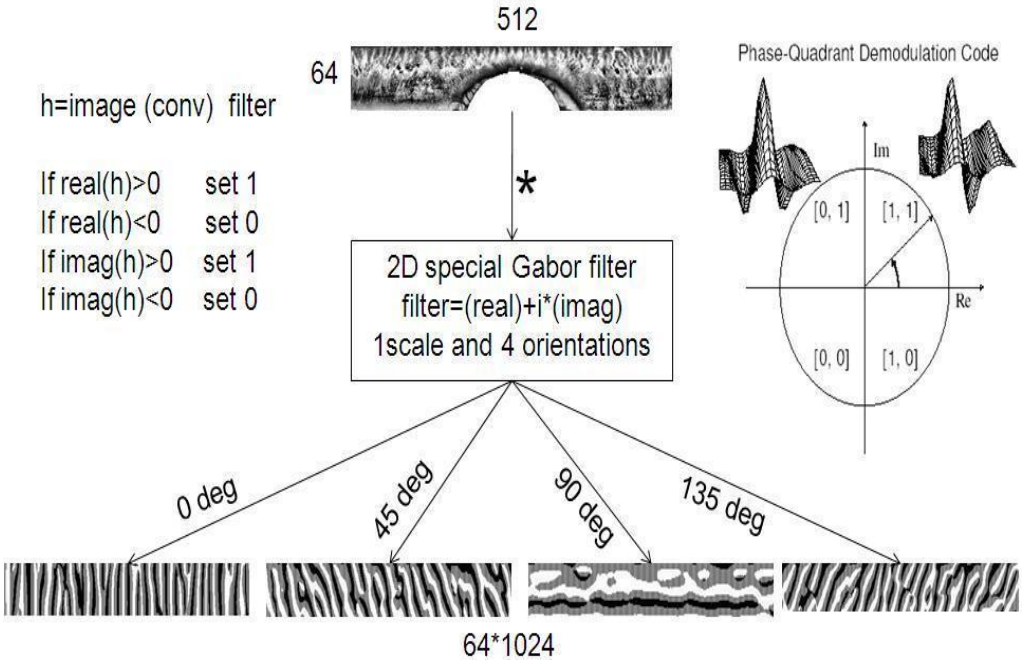

Figure 5.7: An illustration of the feature encoding process.

Local regions of an iris are projected onto quadrature 2D Gabor wavelets, generating complex-valued coefficients whose real and imaginary parts specify the coordinates of a phasor in the complex plane.The angle of each phasor is quantized to one of the four quadrants, setting two bits of phase information. This process is repeated all across the iris.

As shown in figure 5.7, we have created four feature vectors for each scale with orientation selectivity of 0°, 45°, 90°, 135° respectively. These feature vectors are compared individually at the time of matching and their average mean is taken as resulting hamming distance.

For comparison purpose we also tested our system using Log-Gabor filters for feature extraction used by Masek [28], originally proposed by Field [39]. Field suggests that that natural images are better coded by filters that have Gaussian transfer functions when viewed on logarithmic frequency scale (Gabor functions have Gaussian transfer functions when viewed on linear frequency scale). There are two important characteristics to note, Firstly, Log-gabor filters always have no DC component, and secondly, the transfer function an extended tail at the high frequency end. Ordinary Gabor functions over represents low frequency components and under represents high frequency components as shown in fig 5.8.

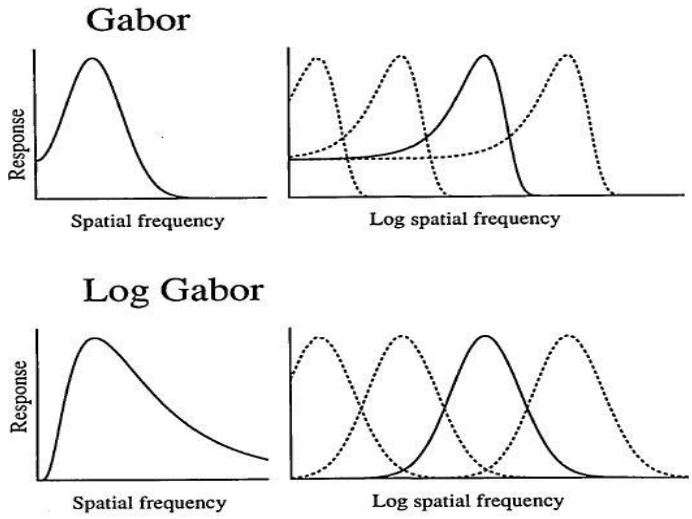

Figure 5.8: Gabor and Log-Gabor functions on logarithmic axis.

Due to singularity in the log function at the origin one cannot construct an analytic expression for the shape of the log Gabor function in the spatial domain.

The equation of Log-Gabor filter is $G(f) = e^{-[log(f/f_0)]^2/2[log(\sigma/f_0)]^2}$
wo is the filter's centre frequency, σ/f_0) value of .74 will result in a filter bandwidth

of approximately one octave, .55 will result in two octaves, and .41 will produce three octaves, so we can construct filters of arbitrary bandwidths. Figure 5.9 illustrates the ability of the Log Gabor function to capture broad spectral information with a compact spatial filter.

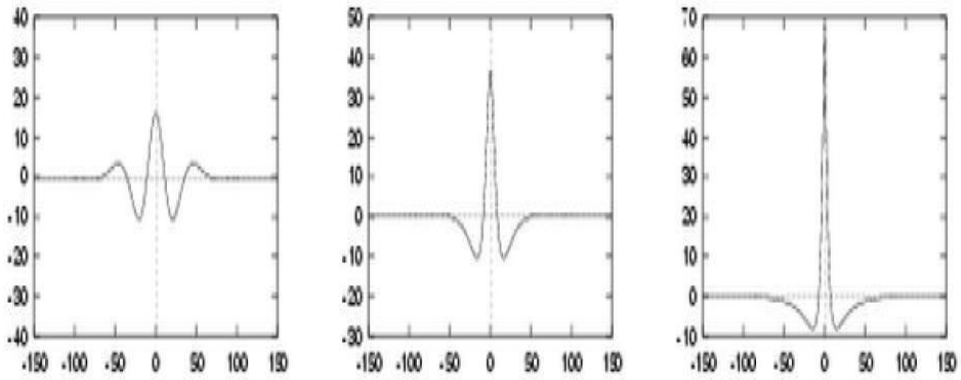

Figure 5.9: Log Gabor wavelets all tuned to the same frequency, but having bandwidths of 1, 2 and 3 octaves respectively..

For bandwidths of less than 1 octave, both Gabor and Log Gabor functions have same shape and produce similar results [39].

5.3.2 Matching

For matching, the Hamming distance was chosen as a metric for recognition, since bit-wise comparisons were necessary. The Hamming distance algorithm employed also incorporates noise masking, so that only significant bits are used in calculating the Hamming distance between two iris templates. Now when taking the Hamming distance, only those bits in the iris pattern that correspond to '0' bits in noise masks of both iris patterns will be used in the calculation. The Hamming distance will be calculated using only the bits generated from the true iris region, and this modified Hamming distance formula is given as :

$$HD = \frac{\sum_{j=1}^{N} \|(X_j \otimes Y_j) \cap Xn'_j \cap Yn'_j\|}{N - \sum_{k=1}^{N} Xn_k \cap Yn_k} \tag{5.15}$$

where X_j and Y_j are the two bit-wise templates to compare, Xn_j and Yn_j are the corresponding noise masks for X_j and Y_j, and N is the number of bits represented by each template.

Although, in theory, two iris templates generated from the same iris will have a Hamming distance of 0.0, in practice this will not occur. Normalization is not

perfect, and also there will be some noise that goes undetected, so some variation will be present when comparing two intra-class iris templates.

In order to account for rotational inconsistencies, when the Hamming distance of two templates is calculated, one template is shifted left and right bit-wise and a number of Hamming distance values are calculated from successive shifts. This bit-wise shifting in the horizontal direction corresponds to rotation of the original iris region by an angle given by the angular resolution used. If an angular resolution of 180 is used, each shift will correspond to a rotation of 2 degrees in the iris region. This method is suggested by Daugman [1], and corrects for misalignments in the normalized iris pattern caused by rotational differences during imaging. From the calculated Hamming distance values, only the lowest is taken, since this corresponds to the best match between two templates.

The number of bits moved during each shift is given by two times the number of filters used, since each filter will generate two bits of information from one pixel of the normalized region. The actual number of shifts required to normalize rotational inconsistencies will be determined by the maximum angle difference between two images of the same eye, and one shift is defined as one shift to the left, followed by one shift to the right. The shifting process for one shift is illustrated in Figure 5.10

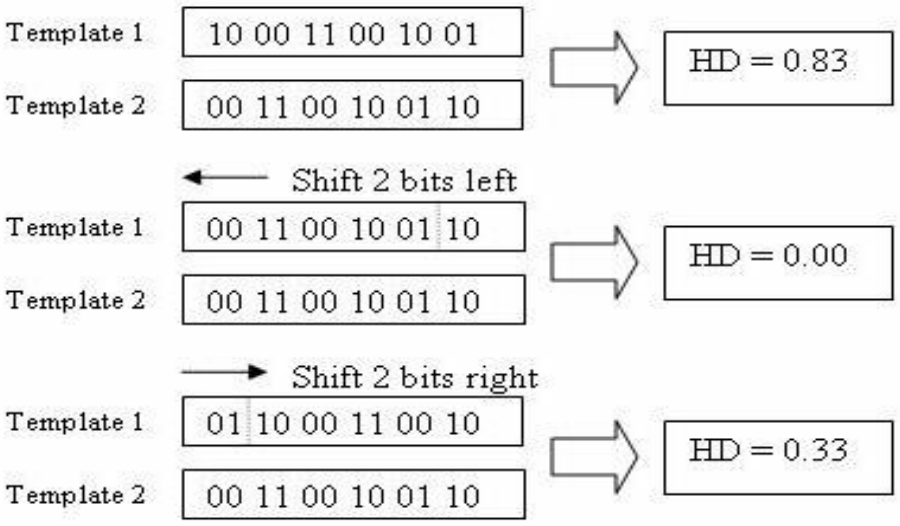

Figure 5.10: shifting process.

Chapter 6

Experimental Results

6.1 Overview

In this chapter, the performance of the iris recognition system as a whole is examined. We have tried to verify some important facts that affect the performance of iris recognition accuracy. For comparison purpose we have also tested our system using LOG gabor filters for feature extraction that is widely used by researchers.

6.2 Performance Evaluation

Performance evaluation assesses accuracy and usability of biometric algorithms or systems. Performance measures are computed for verification, identification, in order to either discover the state-of-the-art of biometric technologies or quantify how well a biometric system meets the requirements of specific applications.

For most biometric technologies, there are two main tasks when applying them in practice, i.e. verification and identification. The former needs to answer "Is he who he says he is?, while the latter cares about who is he?. According to whether the unidentified end-user is enrolled in the system, identification is further categorized into two types: closed-set identification and open-set identification. We have tested our system in verification mode.

6.2.1 Performance Measures

Performance measures in biometrics define quantifiable assessments of the processing speed, recognition accuracy, and other functional characteristics of a biometric algorithm or system.

Fundamental Performance Measures

The following measures are considered to be fundamental because they can be employed regardless of the types of applications of biometric systems. The failure-to-enroll and failure-to-acquire rates measure the performance of the feature extracting component, while the false match and false nonmatch rates measure that of the matching component.

- *FTE (failure-to-enroll rate)* is the proportion of the population for whom the system fails to complete the enrollment process. The failure-to-enroll occurs when the user cannot present the required biometric characteristic, or when the submitted biometric sample is of unacceptably bad quality.
- *FTA (failure-to-acquire rate)* is the proportion of verification or identification attempts for which the system fails to capture or locate biometric samples of sufficient quality.
- *FNMR (false nonmatch rate)* is the proportion of genuine attempt samples falsely declared not to match the template of the same characteristic from the same user submitting the sample.
- *FMR (false match rate)* is the proportion of zeroeffort impostor attempt samples falsely declared to match the compared nonself template.

Performance Measures for Verification System

Verification is one of the two major applications of biometrics, where the user makes a positive claim to an identity, features extracted from the submitted biometric sample are compared with the enrolled templates for the claimed identity, and an accept- or reject decision regarding the identity claim is returned. In evaluating the performance of biometric systems, the unit operation is a transaction, which can be a single attempt but mostly consists of multiple attempts. In this aspect, the fundamental measures, FMR and FNMR, cannot be directly applied to the overall performance evaluation of a biometric system, and the following metrics are designed for more general measures.

FAR is the proportion of verification transactions with truthful claims of identity that are incorrectly denied.

$$FAR(percent) = 100 \times \frac{(\text{Number of false acceptance})}{(\text{Total no of acceptance by system})}$$

FAR (false accept rate) is the proportion of verification transactions with zero-effort wrongful claims of identity that are incorrectly confirmed.

$$FRR(percent) = 100 \times \frac{(\text{Number of false rejections})}{(\text{Total no of rejections by system})}$$

Other Performance Measures

Genuine score distribution and Impostor score distribution are computed and graphically reported to show how the algorithm separates the two classes.

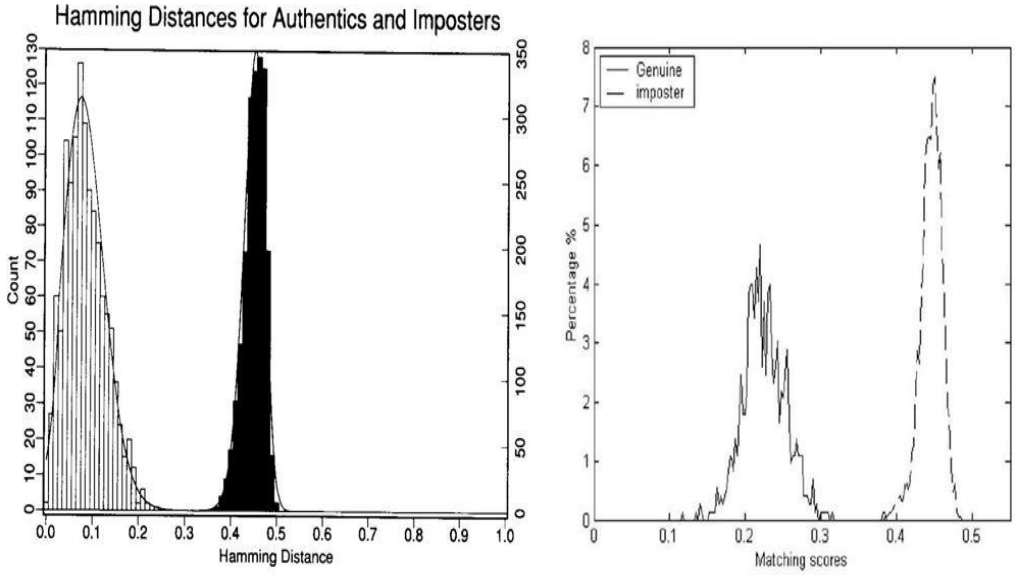

Figure 6.1: Genuine and imposter distribution examples left figure taken from Daugman's paper [2] and right from A.K.Jain's book [3].

the d' prime value is used to discriminate between intraclass and interclass.

$$d' = \frac{|\mu_1 - \mu_2|}{\sqrt{(\sigma_1^2 + \sigma_2^2)/2}}$$

where the μ's and σ's are the means and standard deviations, respectively, of the genuine and impostor distributions. A higher d-prime value indicates better performance.

EER (equal error rate) is computed as the point where FNMR=FMR. In practice, the matching score distributions are not continuous and a crossover point might not exist. The strength of the EER is that it gives a comparison of different biometric systems. That is, since biometric systems in general do not always offer the same threshold settings, it would be difficult to compare apples to apples. Thus, in comparing a normalized statistic like the EER, we can try to get some relative comparison of two biometric systems.

Graphic Performance Measures

When presenting test results, the matching or decision-making performance of biometric systems are graphically represented using Detection Error Trade-off (DET), Receiver Operating Characteristics (ROC), or Cumulative Match Characteristic (CMC) curves. ROC curves are a traditional method for summarizing the performance of imperfect diagnostic, detection, and pattern-matching systems. ROC curves are threshold independent, allowing performance comparison of different systems under similar conditions, or of a single system under differing conditions. ROC curves may be used to plot matching algorithm performance (1-FNMR against FMR), end-to-end verification system performance (1-FRR against FAR).

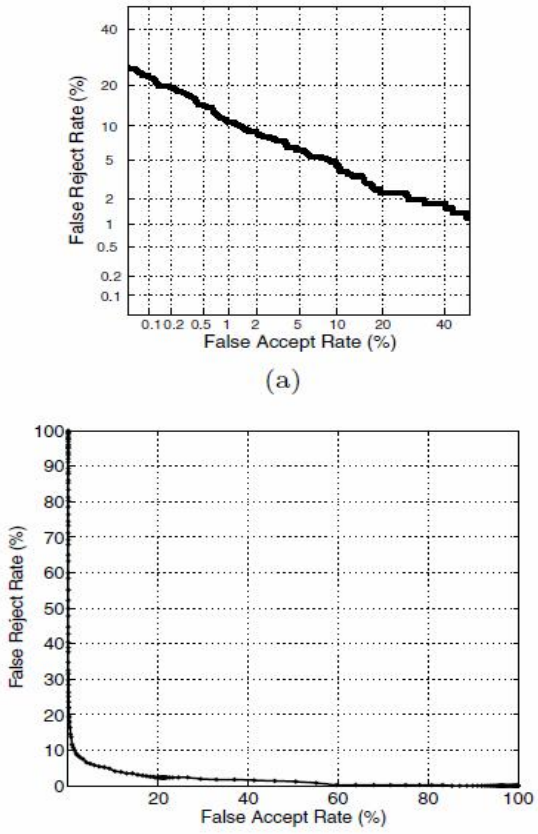

Figure 6.2: The graph in (a) shows a DET curve (b) a ROC curve taken from [3].

The FAR and FRR at various values of thresholds can be summarized using a Detection Error Tradeoff (DET) curve [41] that plots the FRR against the FAR at various thresholds on a normal deviate scale and interpolates between these points.

6.3 Databases for Evaluation

Performance measures are generally obtained by testing the biometric systems on some database. Pure recognition of 100 percent means nothing if database is not mentioned clearly. The database is divided into Registered(Training) and Testing database. As stated earlier we have used CASIA v1,MMU, and IITD databse. Except CASIA we have used 2 images for registration and 3 images for testing, for CASIA we have used 3 images for registration and 4 images for testing.
Total comparisons = no of images from registered database × no of images from testing database.
Genuine vector = no of images for registration from one class × no of images for testing from one class × no of classes.
Table 6.1 shows the other details.

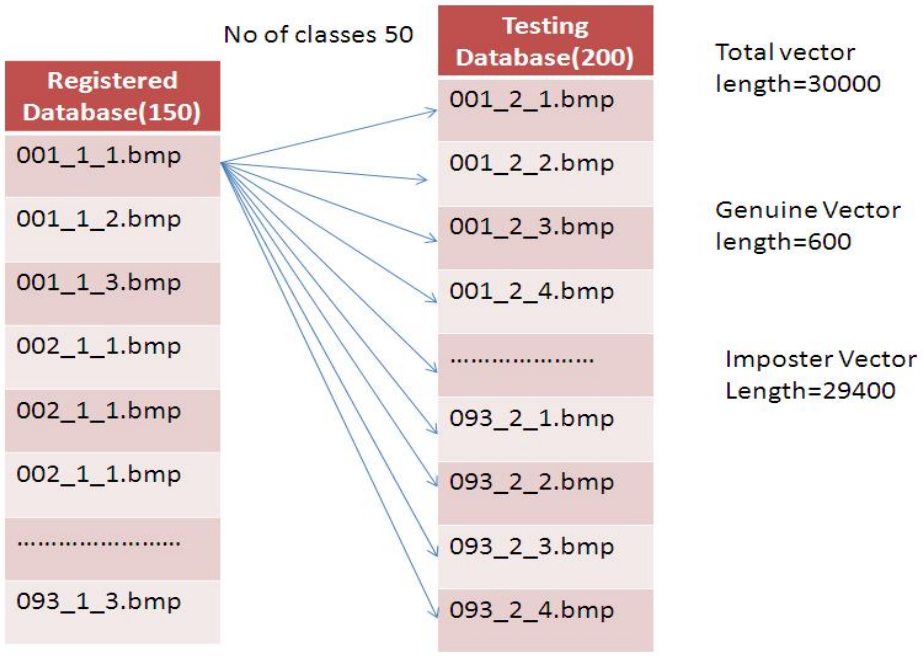

Figure 6.3: Samples taken from CASIA database for performance evaluation .

Database	Classes	Registered	Testing	Comparisons	Genuine Vector
CASIA	50	150	200	30000	600
MMU	35	70	105	7140	210
IITD	125	250	375	93000	750

Table 6.1: Databases information for performance evaluation.

6.4 Experiments

While evaluating the performance of iris recognition system many factors affect the accuracy of system such as iris image quality, segmentation of iris, feature extraction techniques for analyzing the iris texture.

Since we have used the public iris image databases which are specially designed for research having iris images of sufficient quality acquired under the strict imaging conditions. We have successfully segmented the iris images from the above databases. So, to evaluate the performance of our system we have concentrated on feature extraction and matching stage.

Our experimentation strategy is as follows:

- First we have analyzed the effect of increasing number of scales of gabor filters, as per literature using multiscale gabor filters provides better recognition. Our gabor filter bank have maximum 4 scales and 6 orientations. For each scale we have created four templates with orientation selectivity of 0°, 45°, 90°, 135° respectively. These feature vectors are compared individually at the time of matching and their average mean is taken as resulting hamming distance. So for 4th scale we have 16 feature vectors per image which increases the size of template. Our aim is to find the scale at which optimum results are obtained.

- For comparison we have tested our system using Log-gabor filters for feature extraction with filter parameters selected to give filter bandwidth of about two octave.

- We have analyzed the effect of number of shifts of template bits which accounts the rotational inconsistencies, on iris recognition performance. The optimum number of shifts can be determined by examining the mean and standard deviation of the intra-class distribution. Without template shifting the intra-class Hamming distance distribution will be more randomly distributed, since templates, which are not properly aligned, will produce Hamming distance values equivalent to comparing inter-class templates. As the number of shifts increases, the mean of the intra-class distribution will converge to a constant value, since all rotational inconsistencies would have been accounted for.

6.5 Results for Performance Analysis using Special Gabor Filters with One Scale.

6.5.1 For CASIA

Genuine and Imposter Distribution

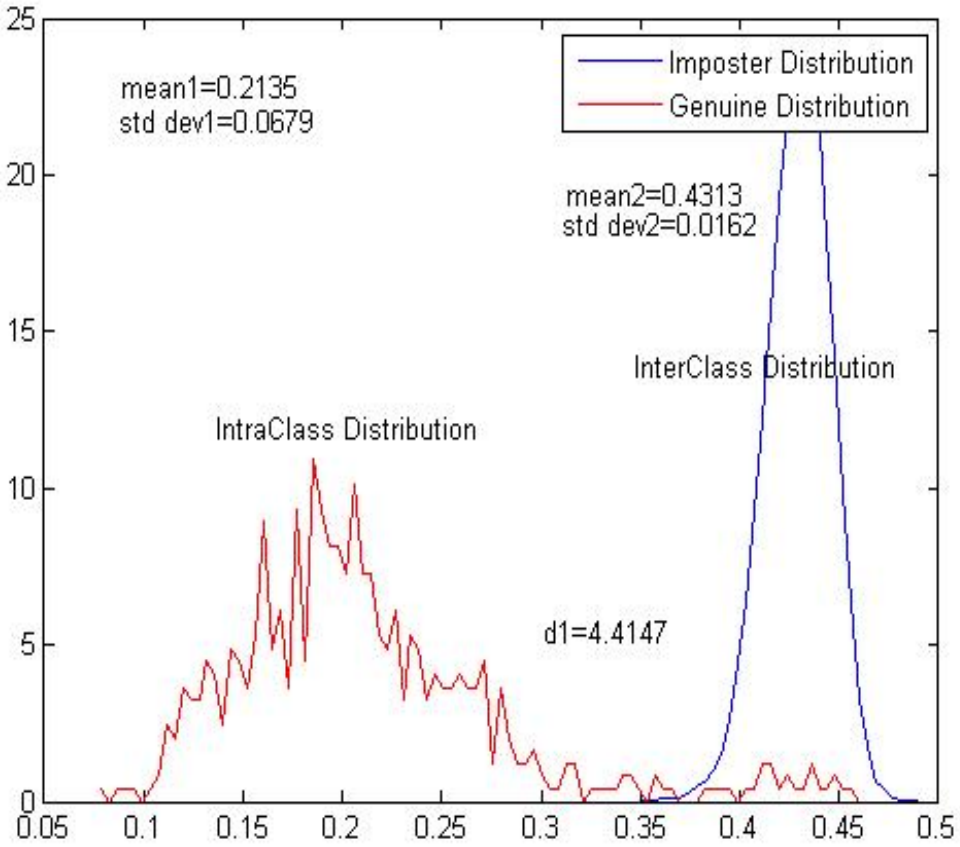

Figure 6.4: Genuine and imposter distribution using special gabor filter bank.

ROC and DET Curves

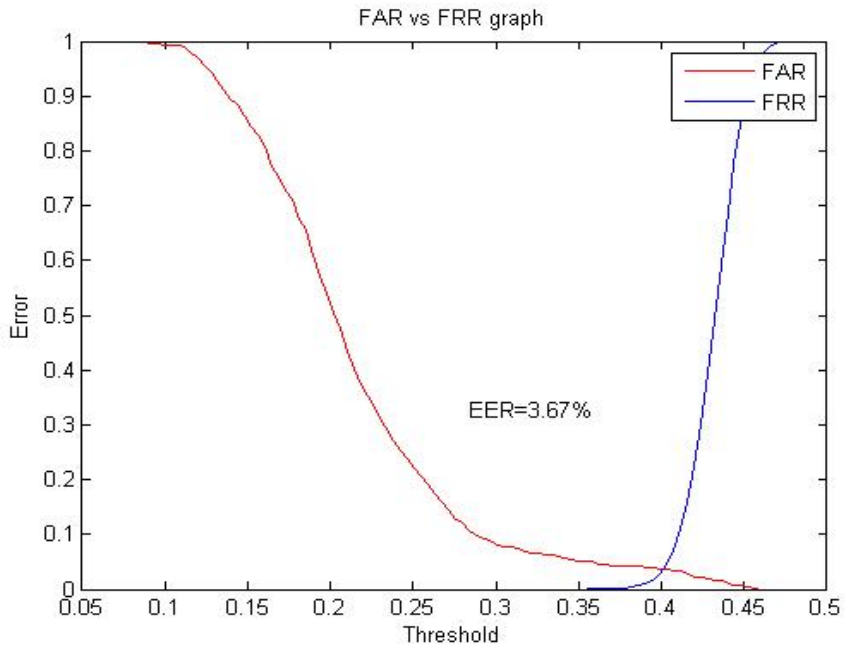

Figure 6.5: Plot of FAR versus FRR for CASIA.

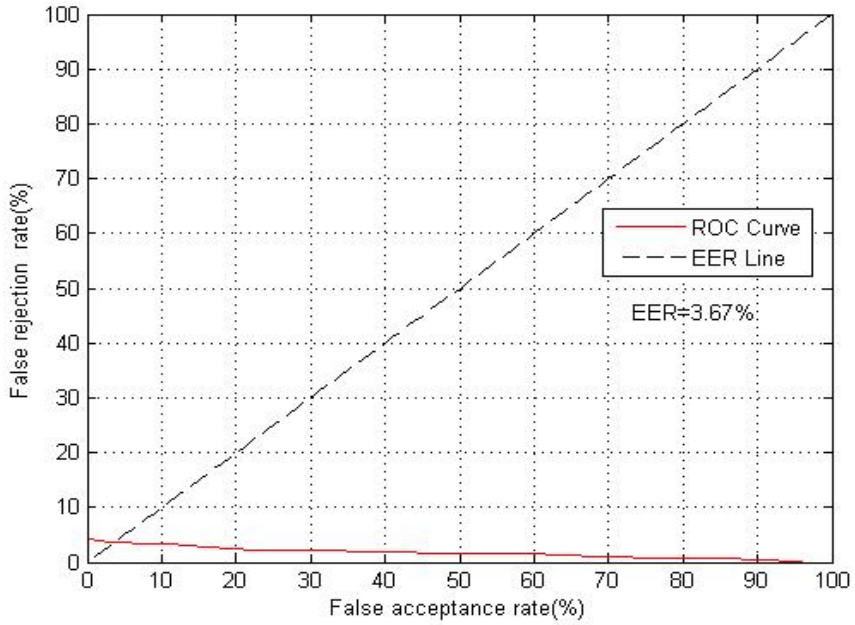

Figure 6.6: Plot of Receiver Operating Characteristic curve for CASIA.

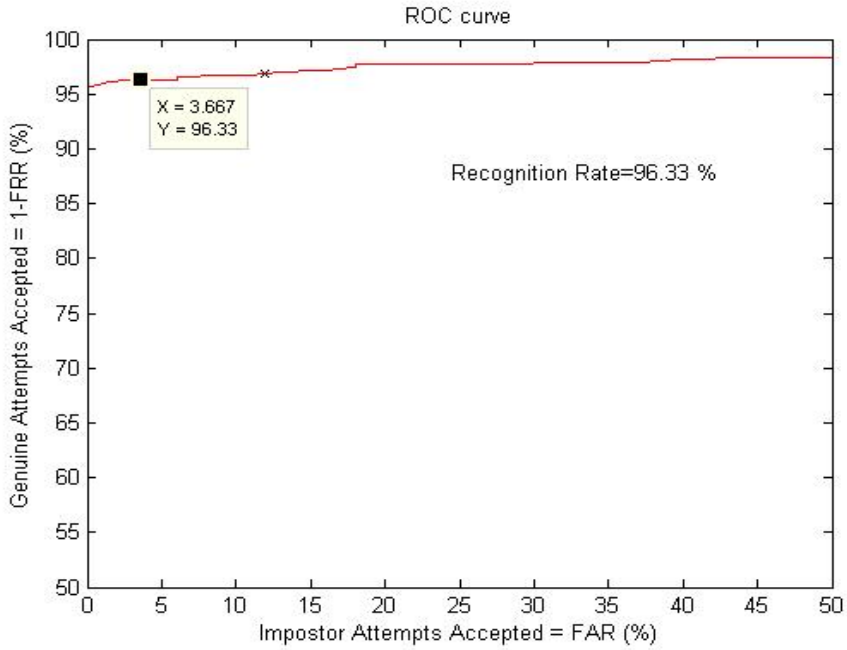

Figure 6.7: Plot of FAR versus GAR for CASIA.

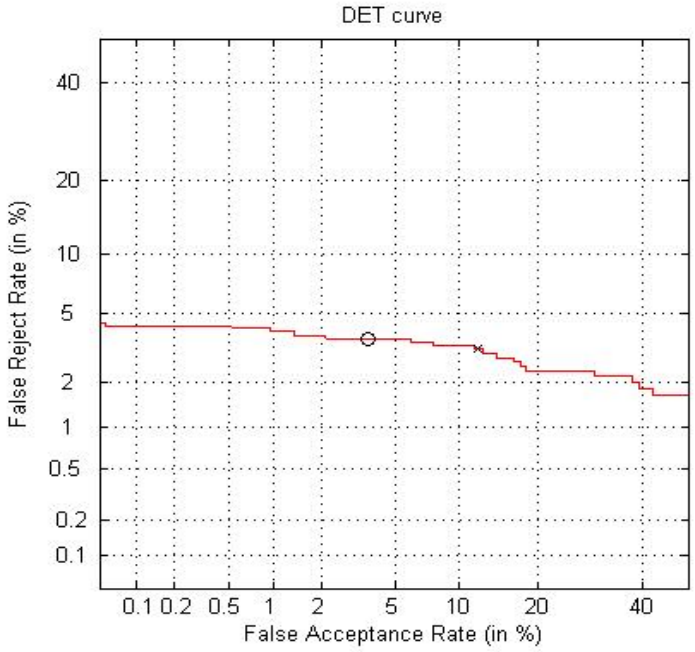

Figure 6.8: Plot of DET curve for CASIA.

6.5.2 For MMU

Genuine and Imposter Distribution

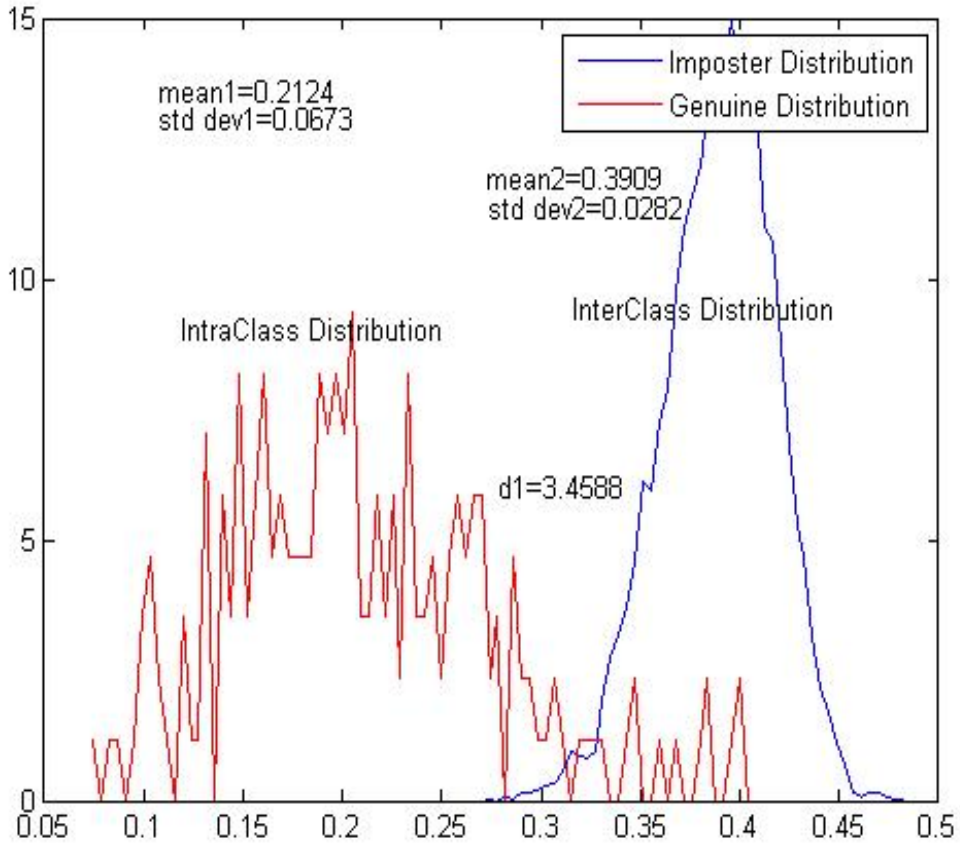

Figure 6.9: Genuine and imposter distribution using special gabor filter bank.

ROC and DET Curves

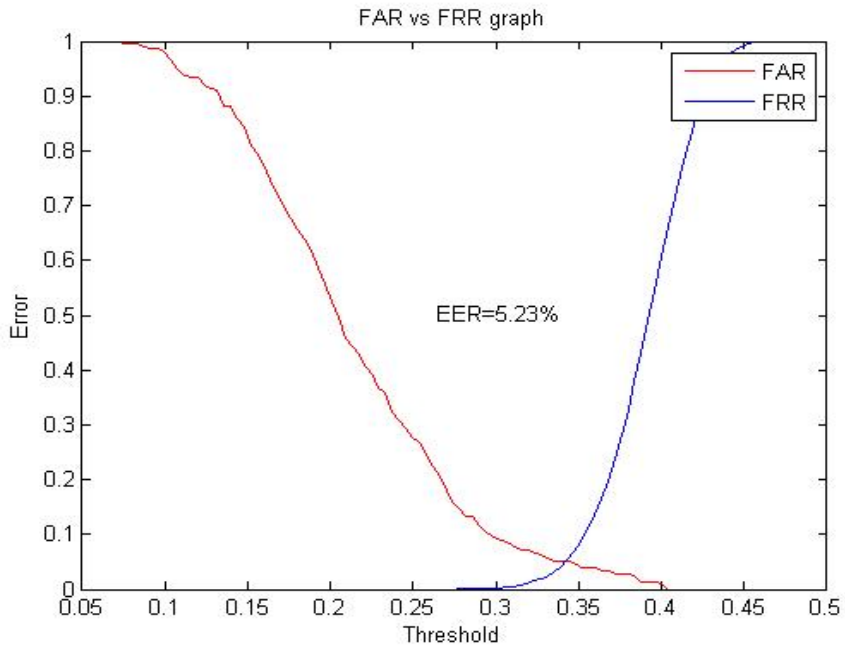

Figure 6.10: Plot of FAR versus FRR for MMU.

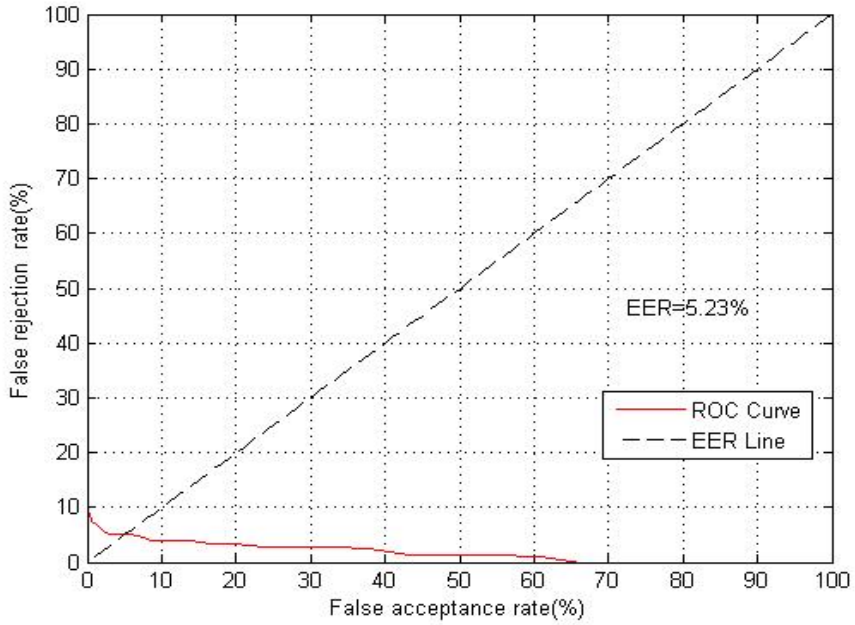

Figure 6.11: Plot of Receiver Operating Characteristic curve for MMU.

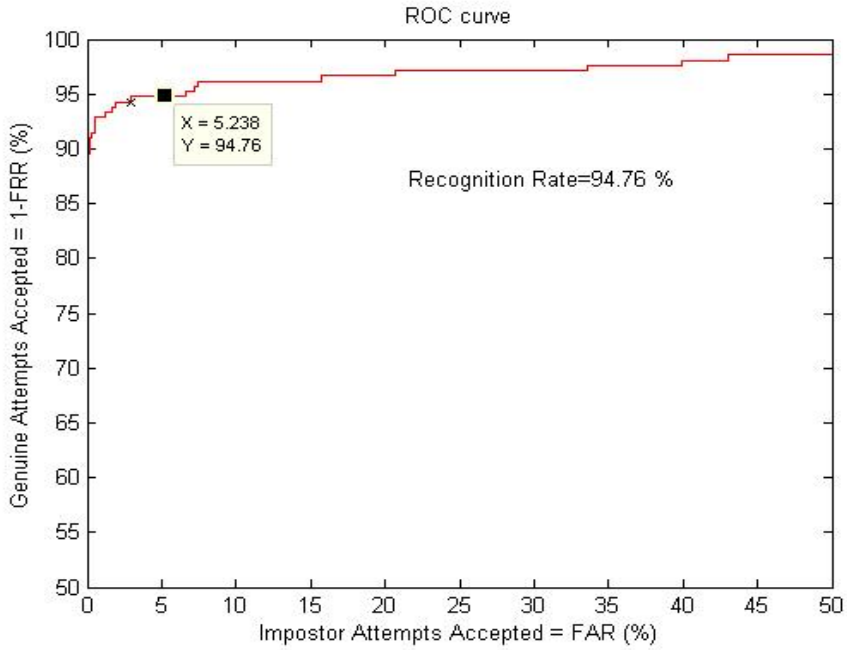

Figure 6.12: Plot of FAR versus GAR for MMU.

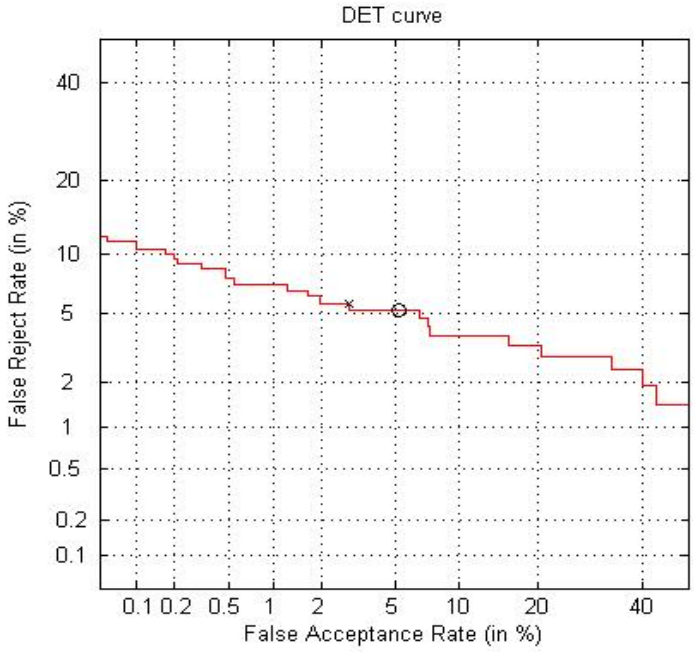

Figure 6.13: Plot of DET curve for MMU.

6.5.3 For IITD

Genuine and Imposter Distribution

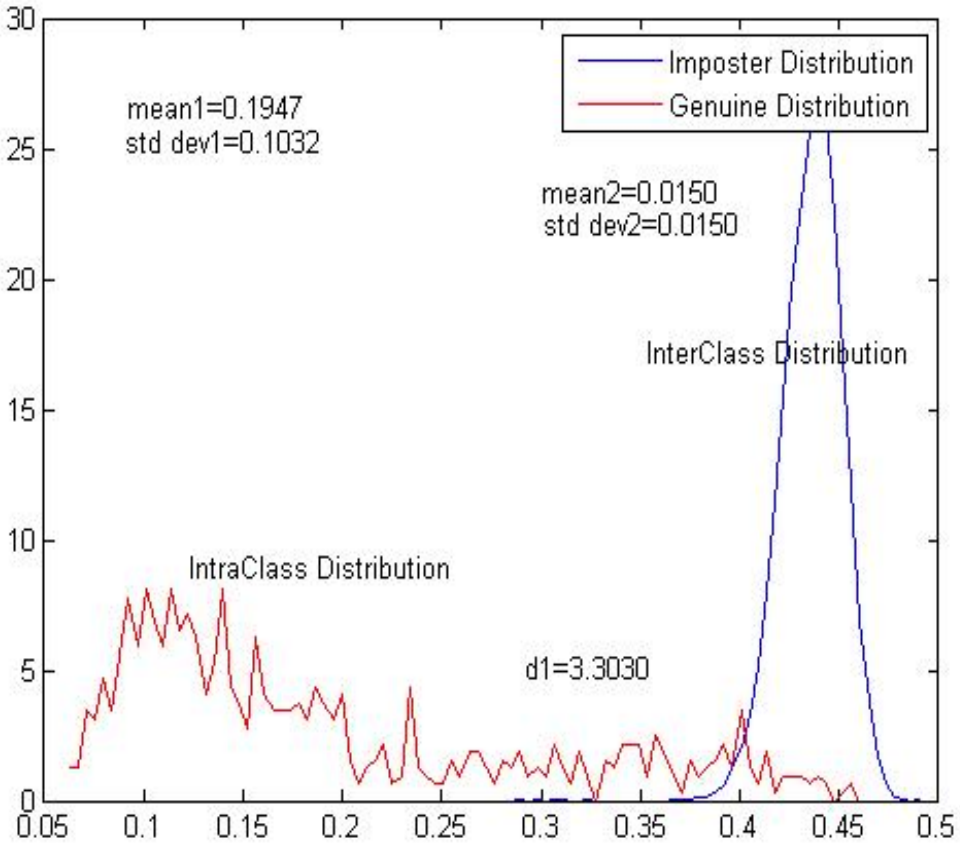

Figure 6.14: Genuine and imposter distribution using special gabor filter bank .

ROC and DET Curves

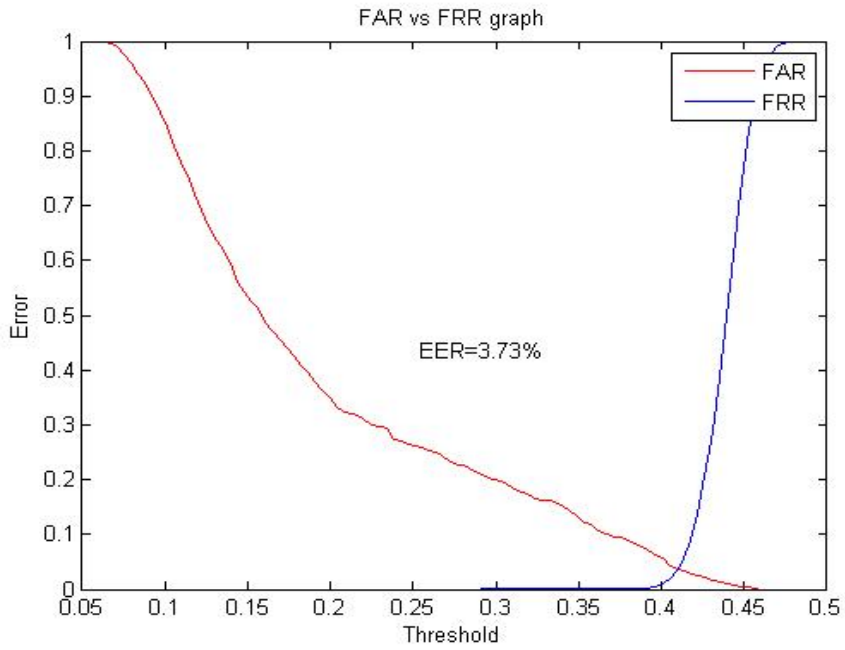

Figure 6.15: Plot of FAR versus FRR for IITD.

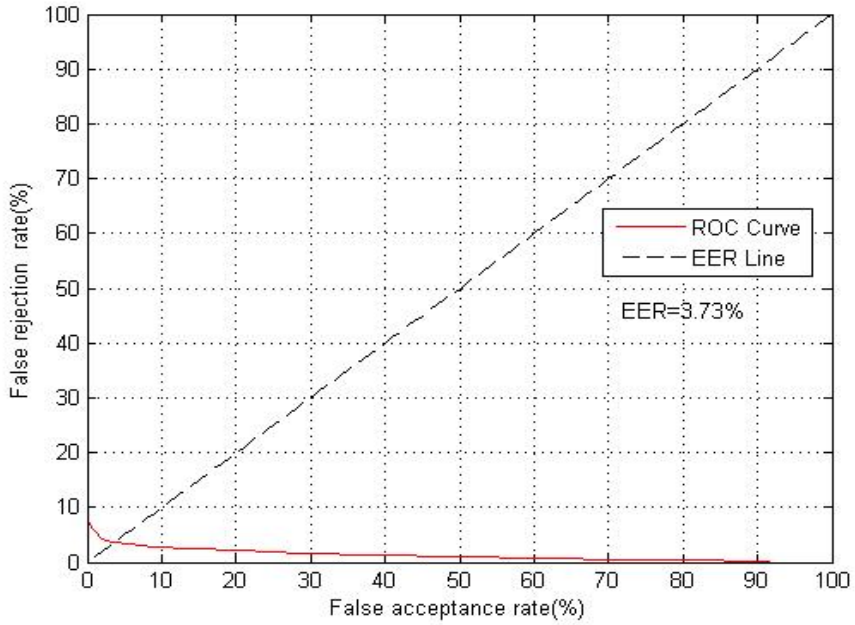

Figure 6.16: Plot of Receiver Operating Characteristic curve for IITD.

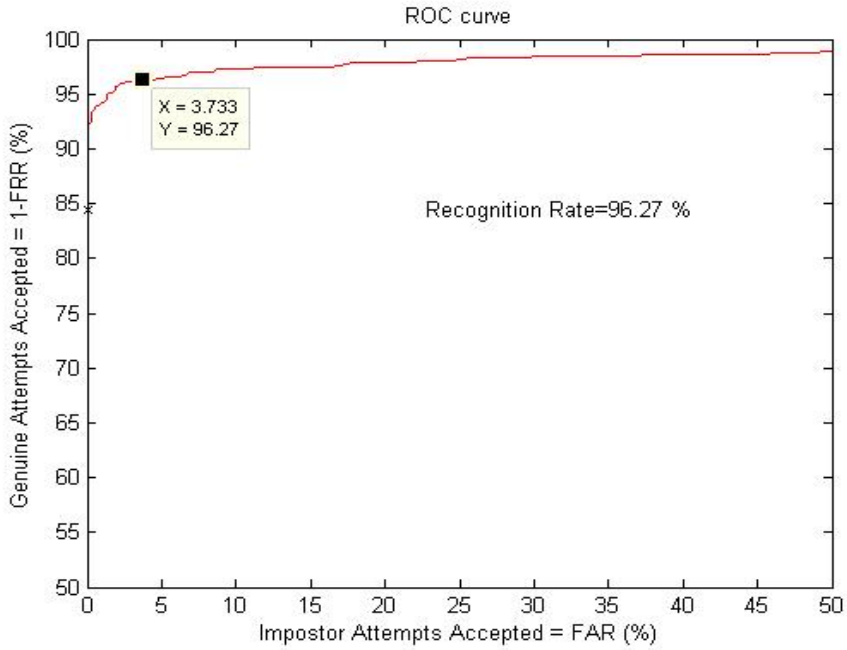

Figure 6.17: Plot of FAR versus GAR for IITD.

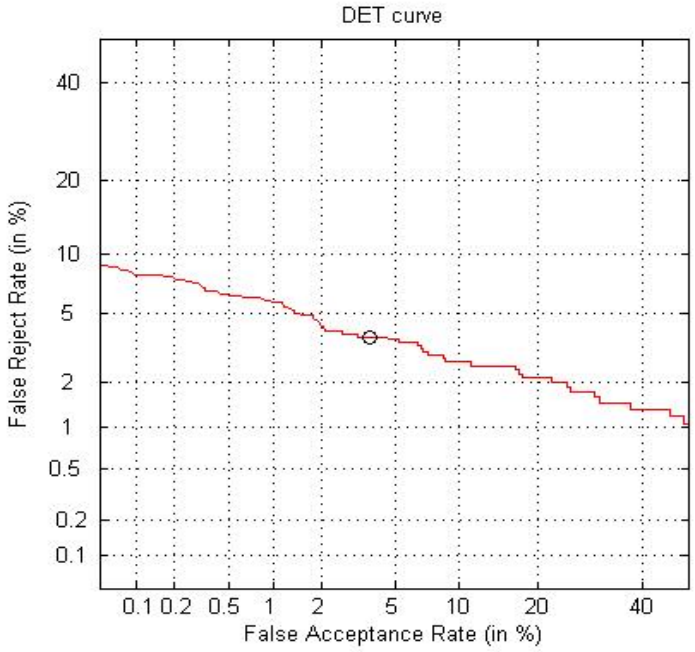

Figure 6.18: Plot of DET curve for IITD.

6.6 Results for Performance Analysis using Special Gabor Filters with Two Scales.

6.6.1 For CASIA

Genuine and Imposter Distribution

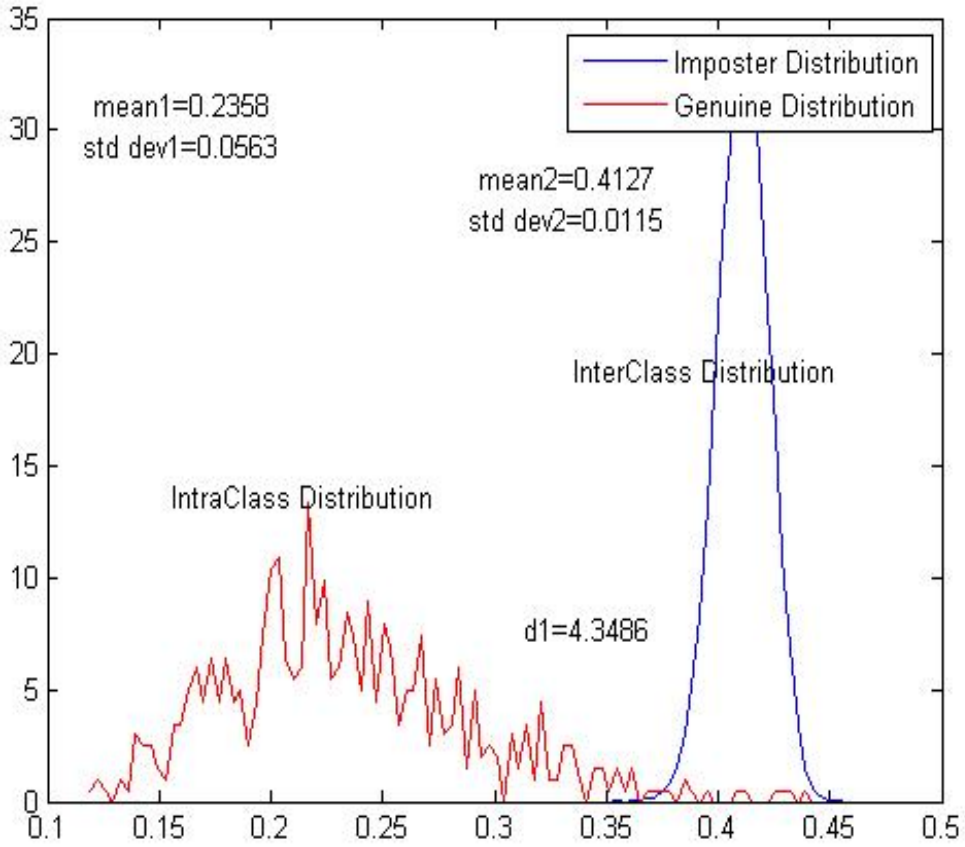

Figure 6.19: Genuine and imposter distribution using special gabor filter bank.

ROC and DET Curves

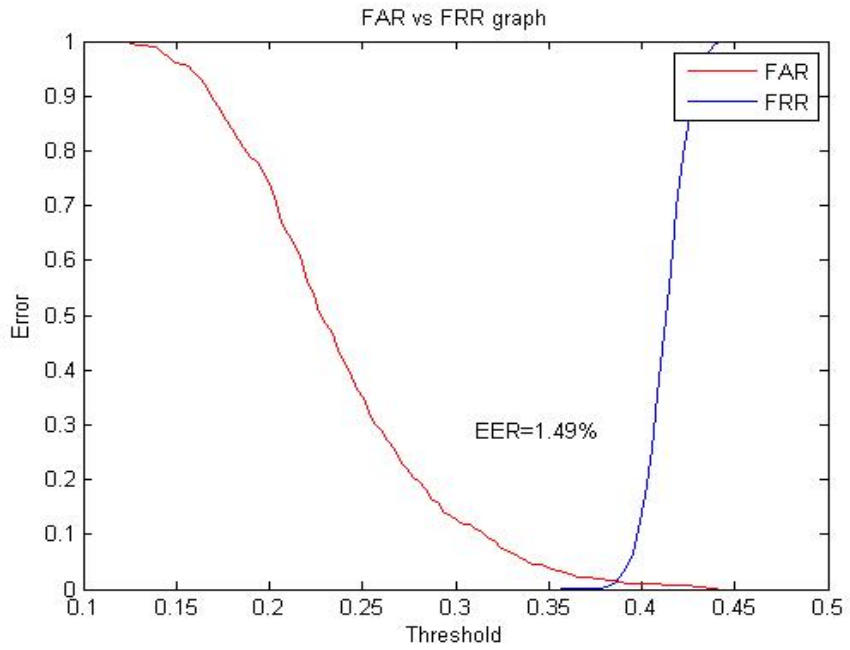

Figure 6.20: Plot of FAR versus FRR for CASIA.

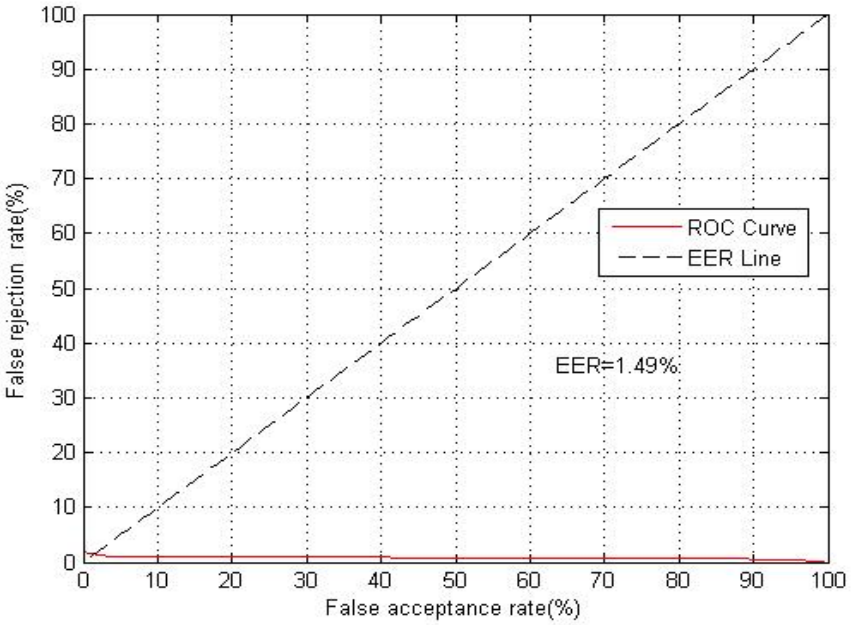

Figure 6.21: Plot of Receiver Operating Characteristic curve for CASIA.

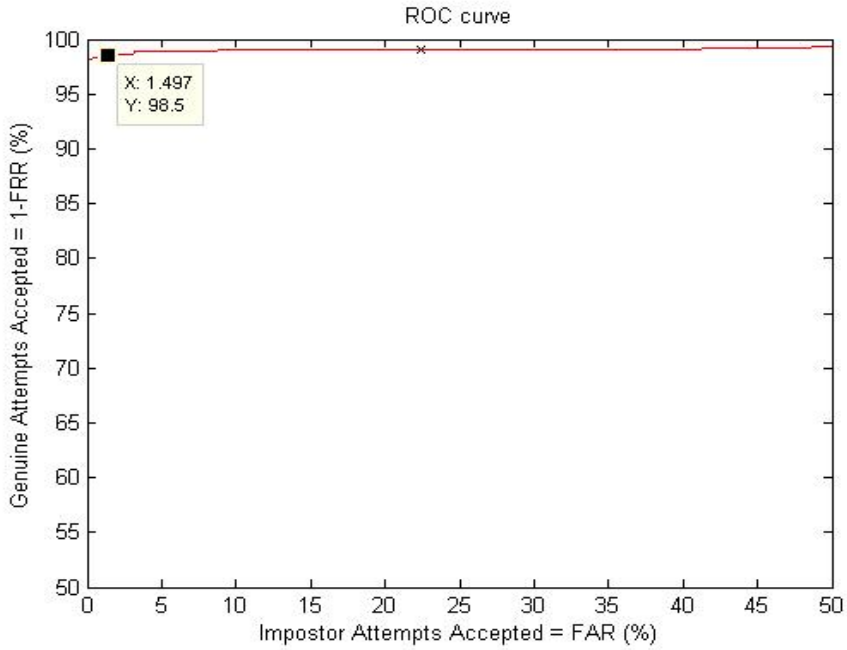

Figure 6.22: Plot of FAR versus GAR for CASIA.

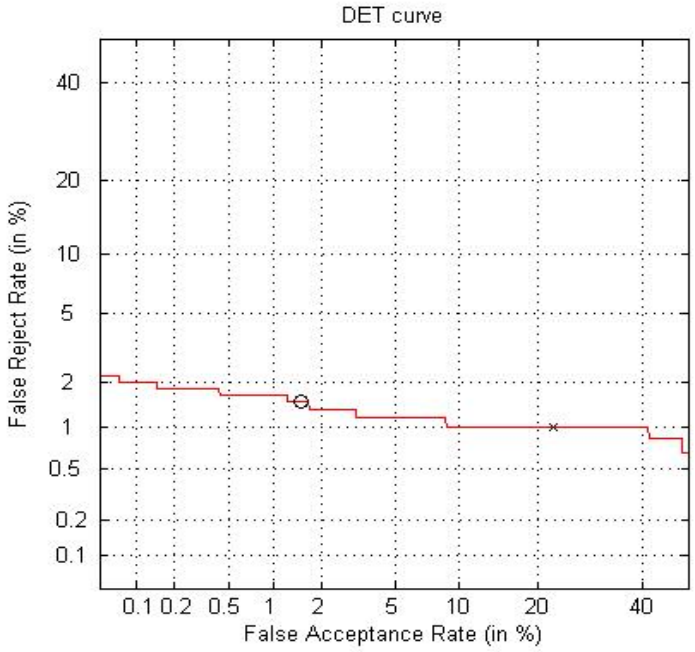

Figure 6.23: Plot of DET curve for CASIA.

6.6.2 For MMU

Genuine and Imposter Distribution

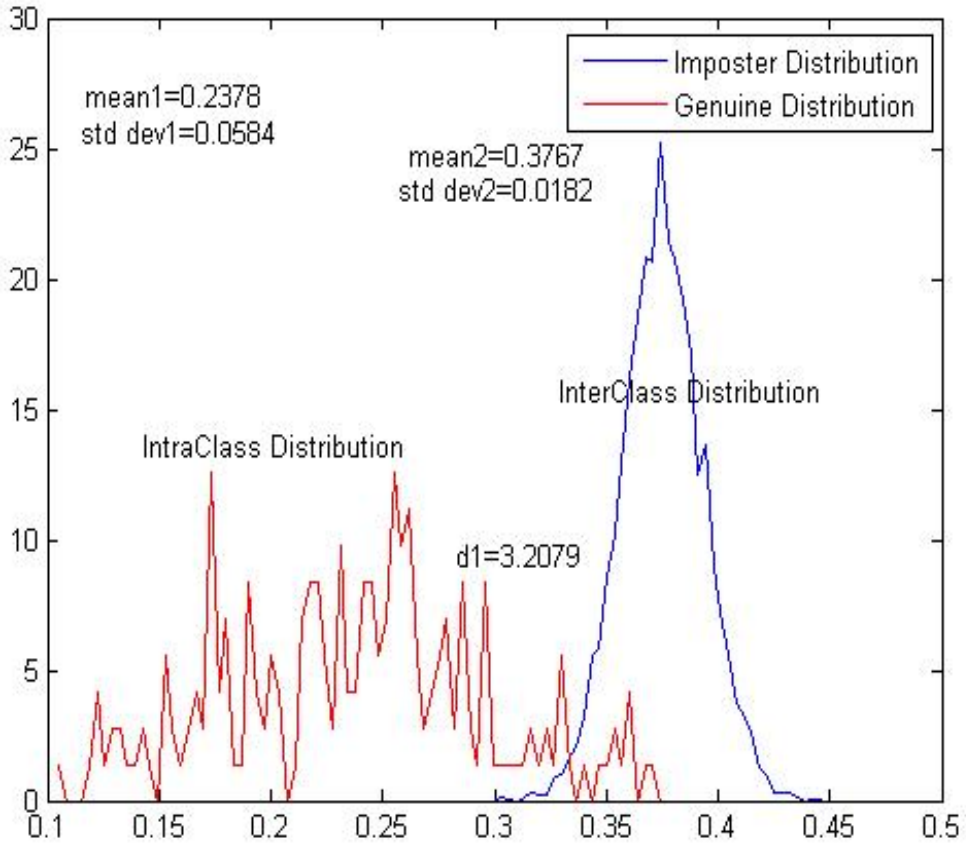

Figure 6.24: Genuine and imposter distribution using special gabor filter bank.

ROC and DET Curves

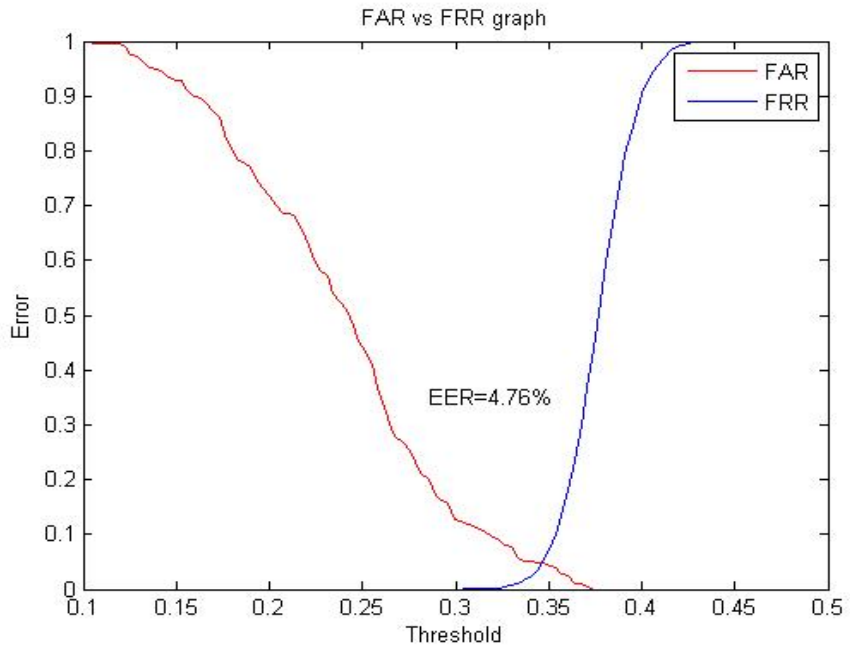

Figure 6.25: Plot of FAR versus FRR for MMU.

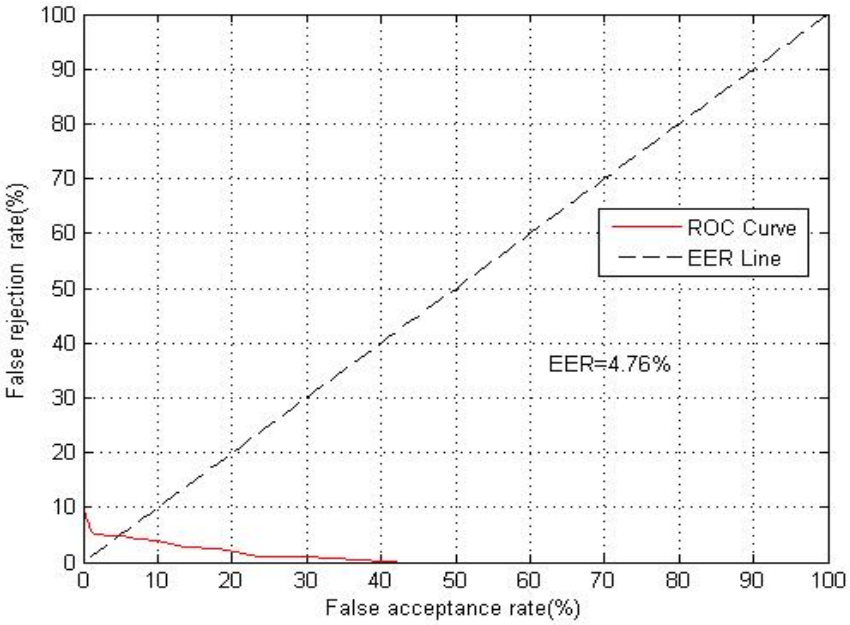

Figure 6.26: Plot of Receiver Operating Characteristic curve for MMU.

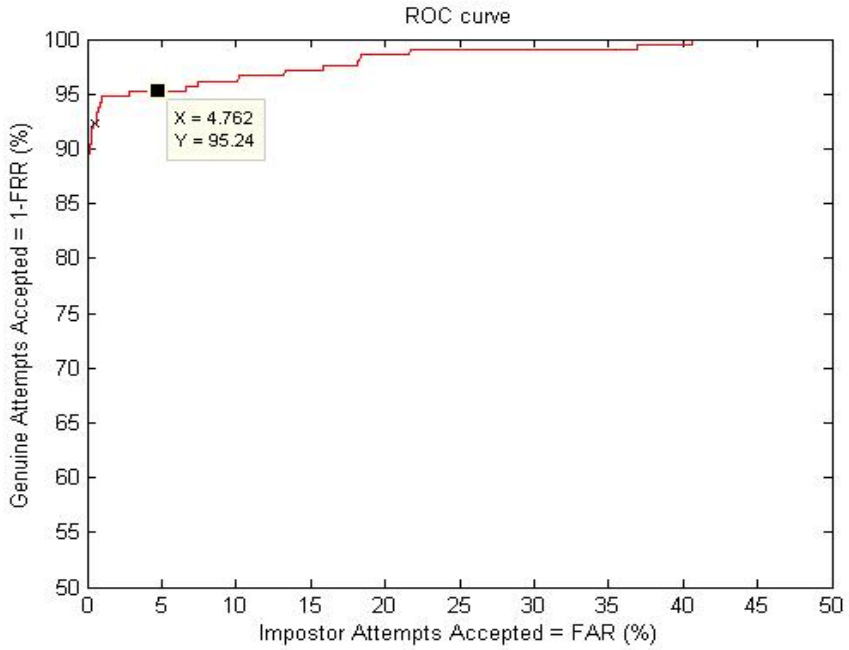

Figure 6.27: Plot of FAR versus GAR for MMU.

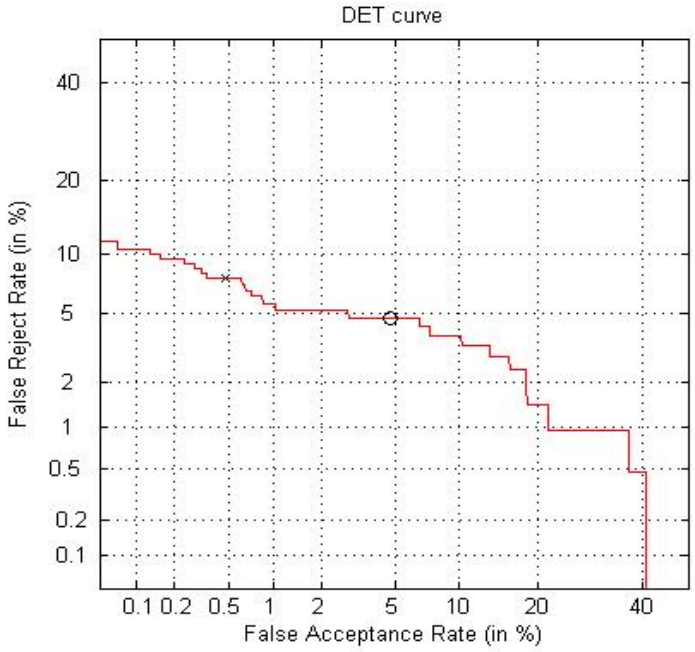

Figure 6.28: Plot of DET curve for MMU.

6.6.3 For IITD

Genuine and Imposter Distribution

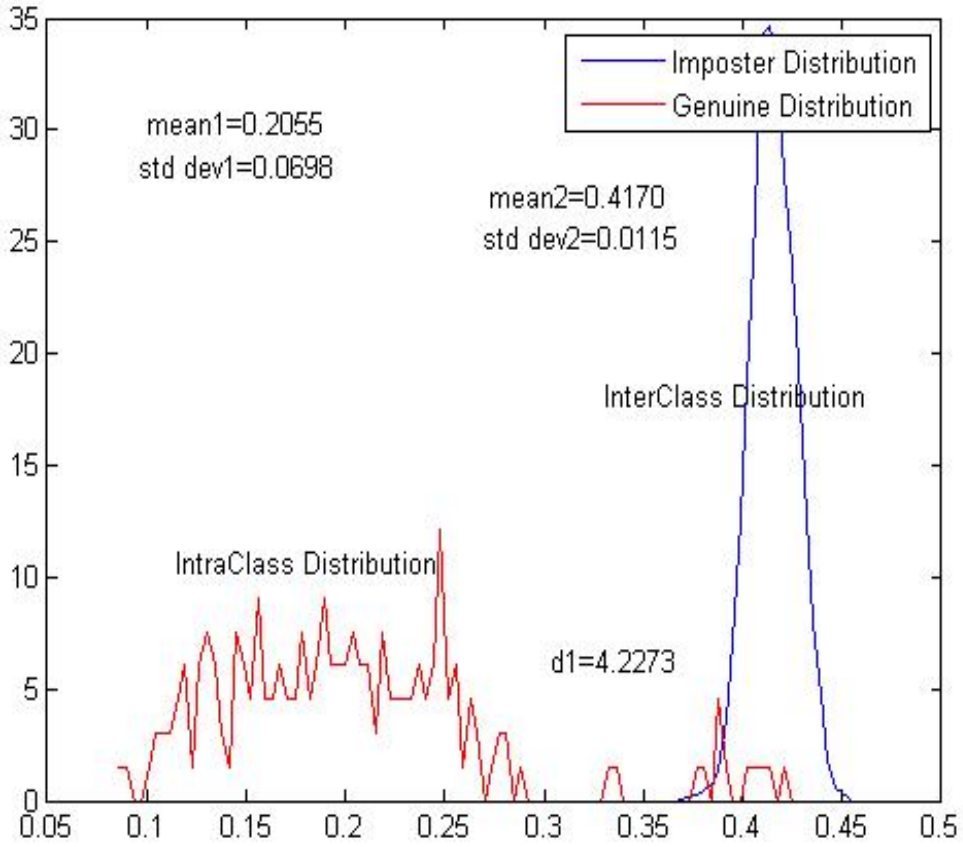

Figure 6.29: Genuine and imposter distribution using special gabor filter bank.

ROC and DET Curves

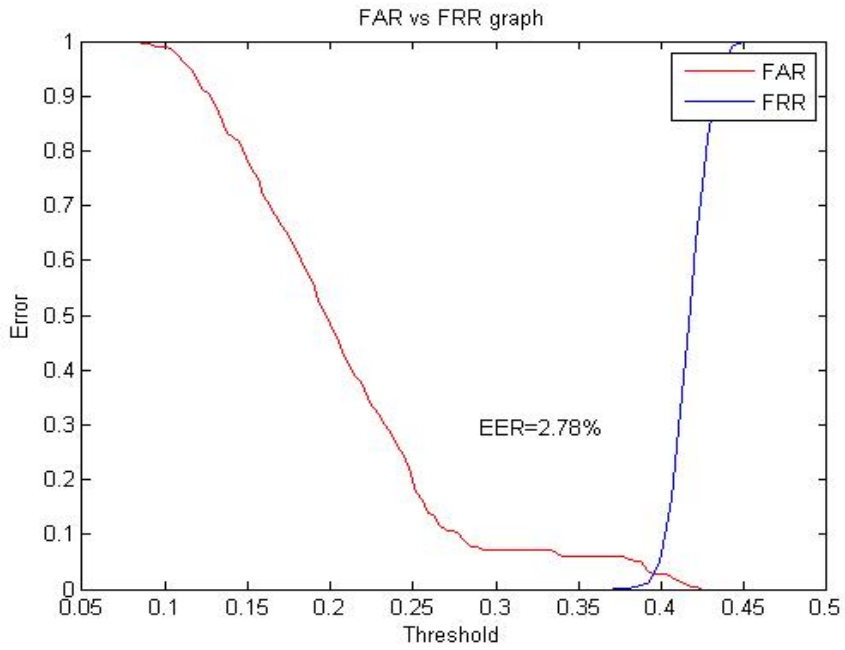

Figure 6.30: Plot of FAR versus FRR for IITD.

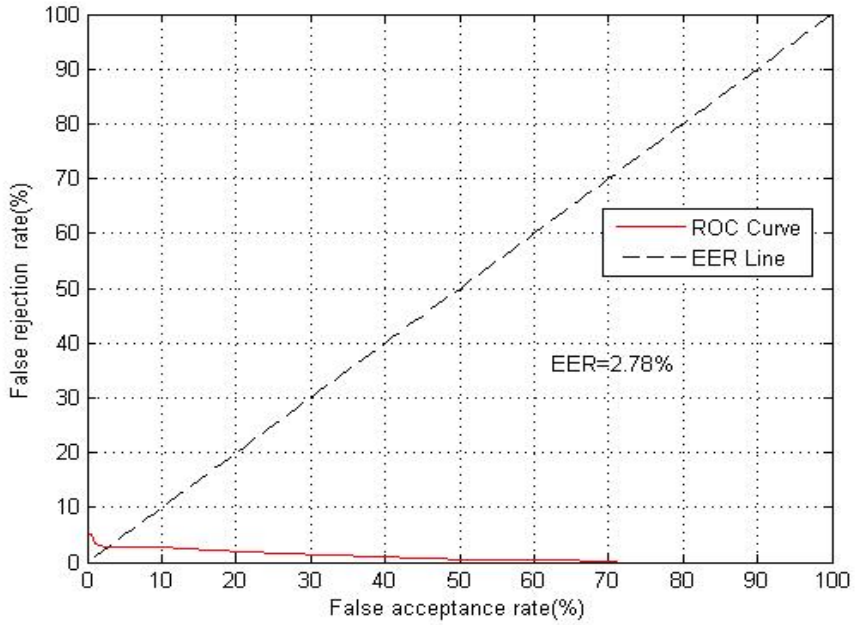

Figure 6.31: Plot of Receiver Operating Characteristic curve for IITD.

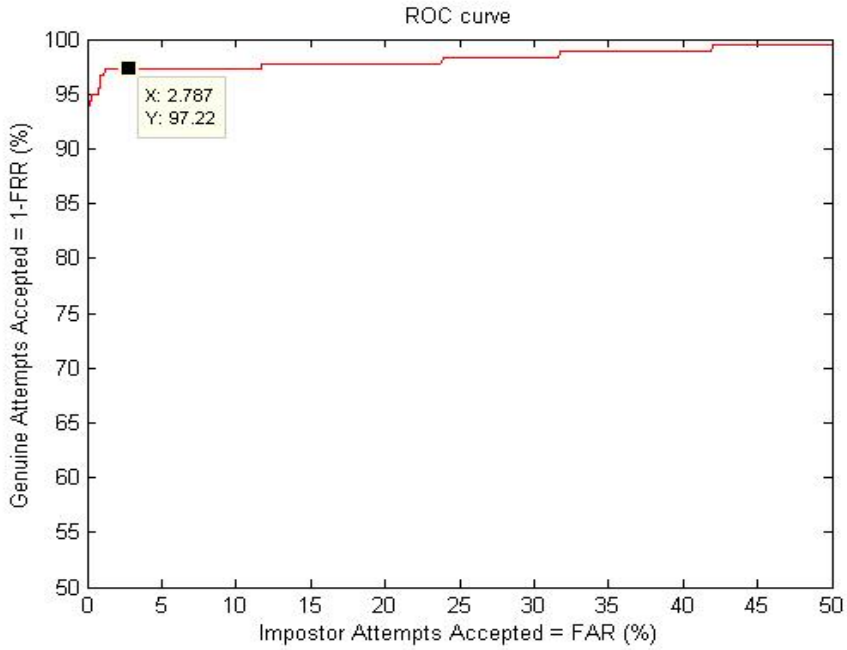

Figure 6.32: Plot of FAR versus GAR for IITD.

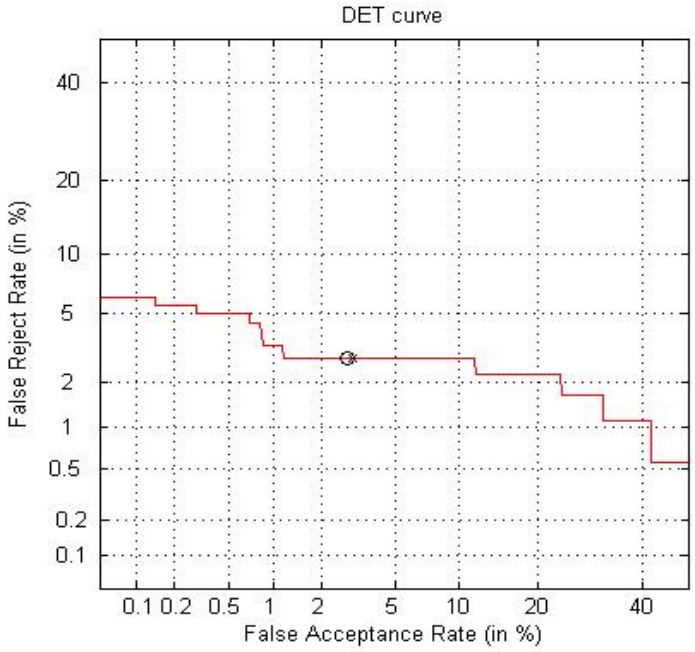

Figure 6.33: Plot of DET curve for IITD.

6.7 Results for Performance Analysis using LOG Gabor Filters

6.7.1 For CASIA

Genuine and Imposter Distribution

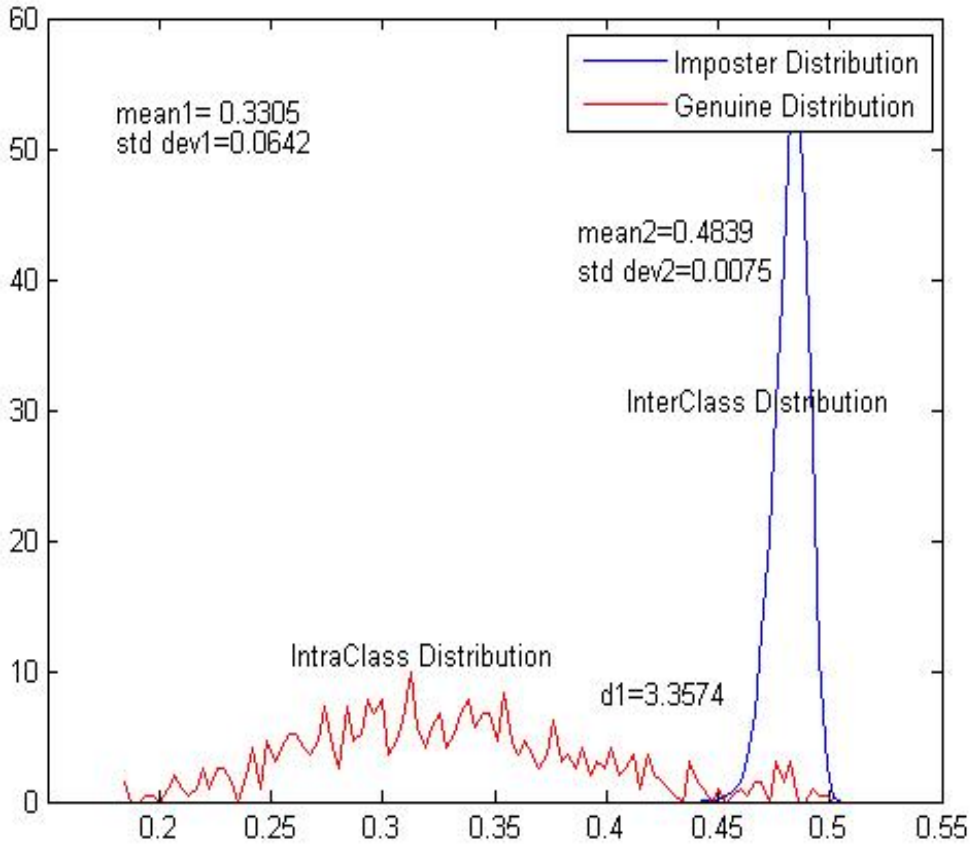

Figure 6.34: Genuine and imposter distribution using Log gabor filter bank.

ROC and DET Curves

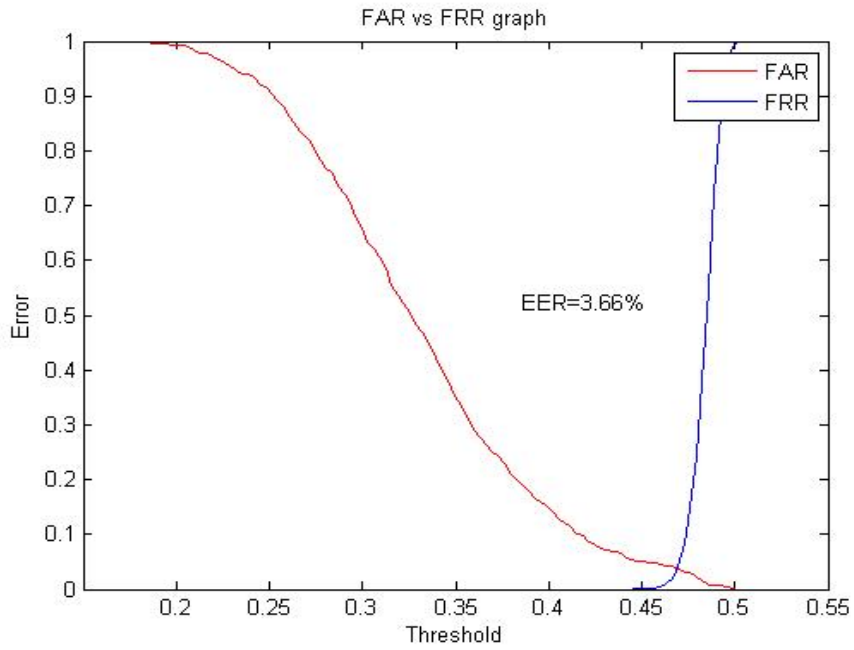

Figure 6.35: Plot of FAR versus FRR for CASIA.

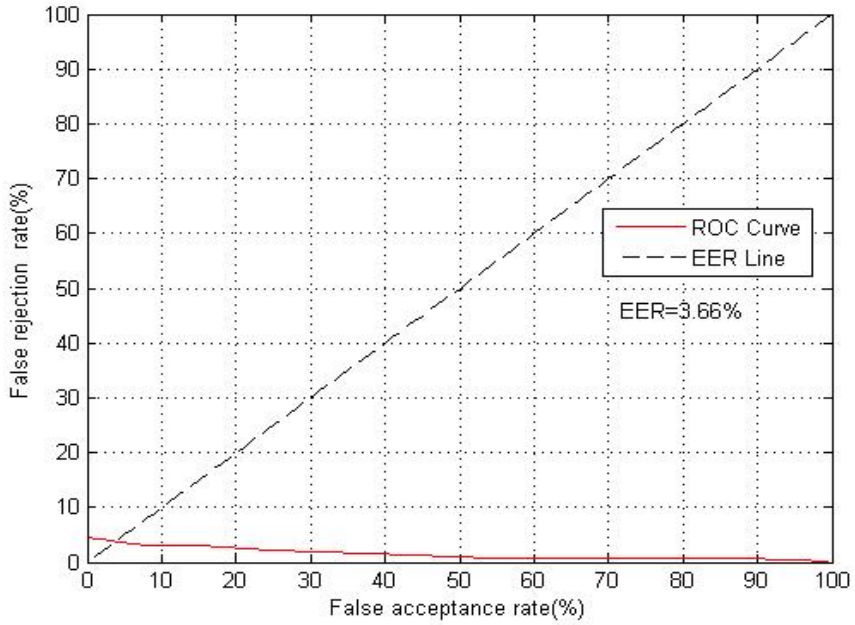

Figure 6.36: Plot of Receiver Operating Characteristic curve for CASIA.

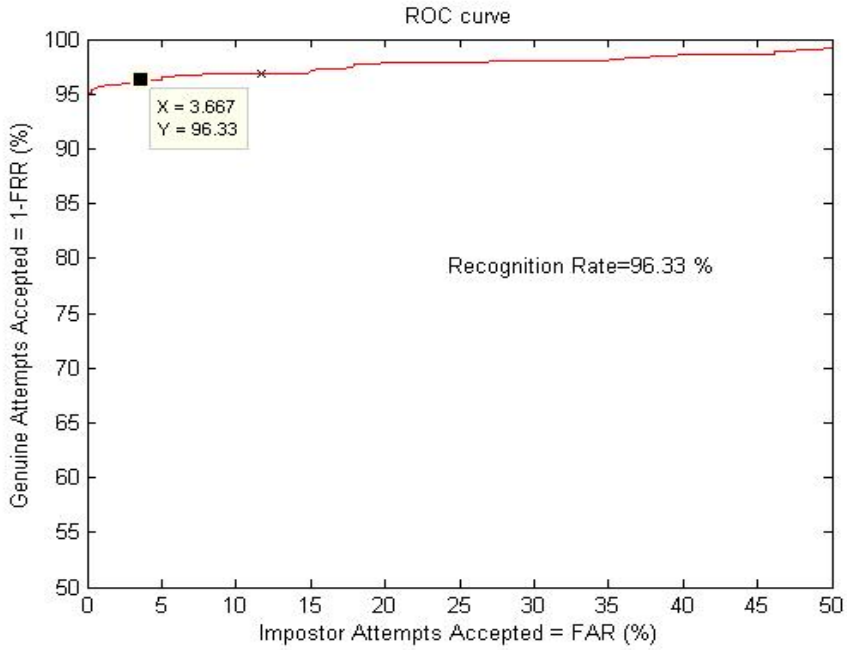

Figure 6.37: Plot of FAR versus GAR for CASIA.

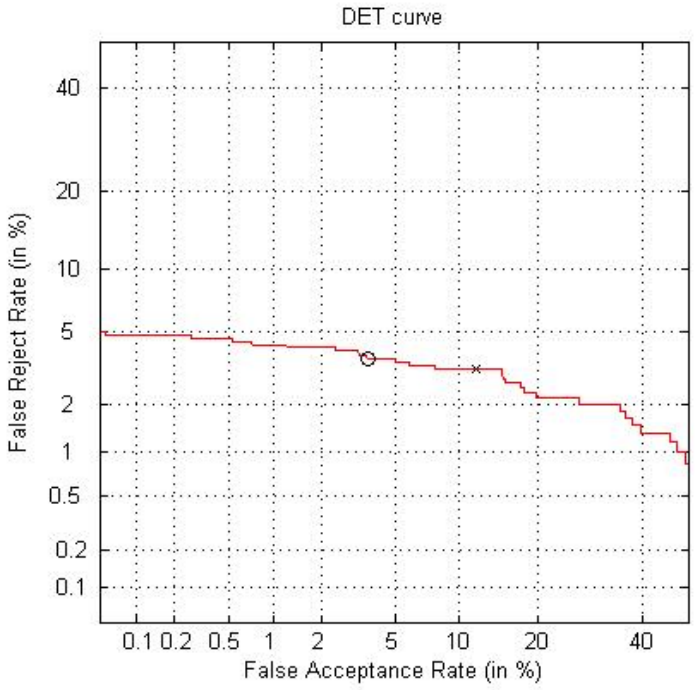

Figure 6.38: Plot of DET curve for CASIA.

6.7.2 For MMU

Genuine and Imposter Distribution

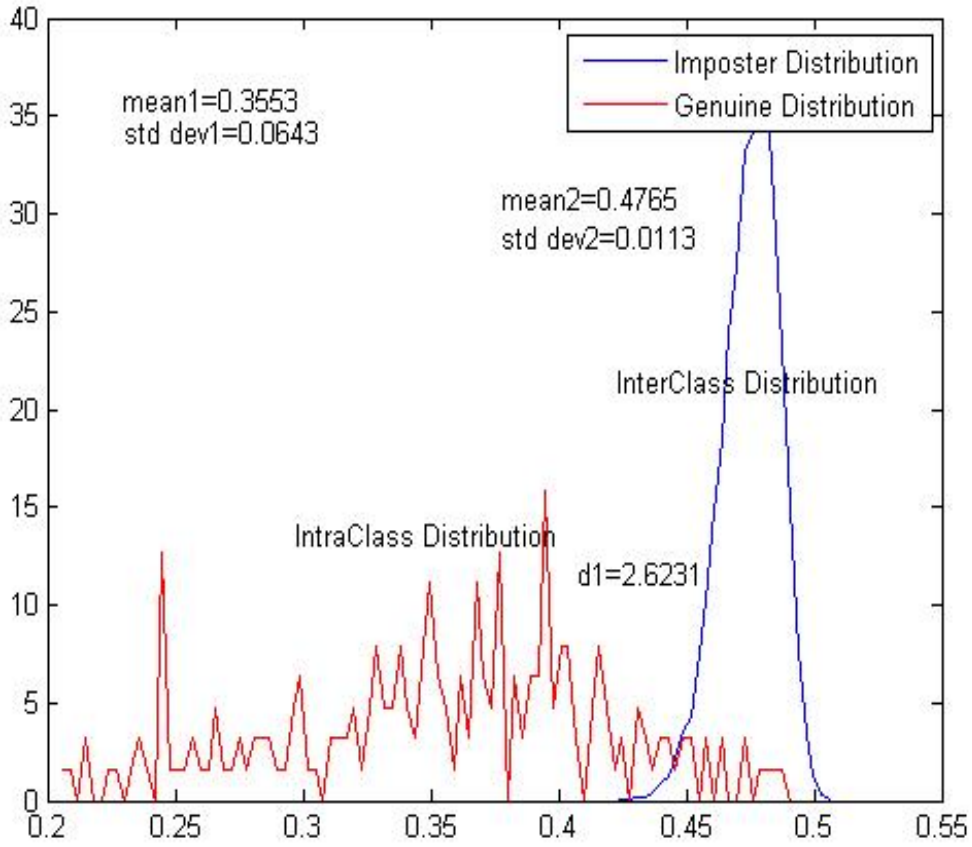

Figure 6.39: Genuine and imposter distribution using special gabor filter bank.

ROC and DET Curves

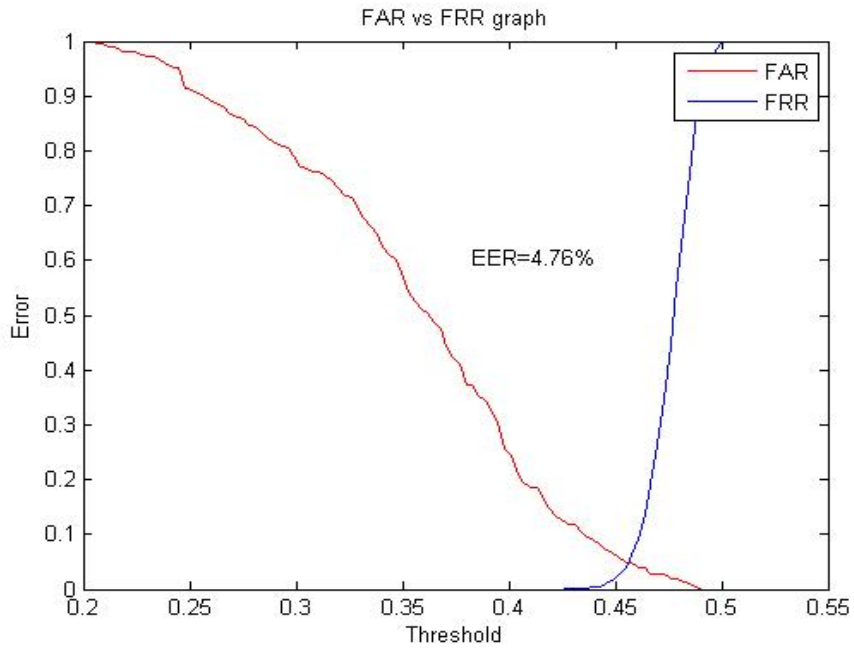

Figure 6.40: Plot of FAR versus FRR for MMU.

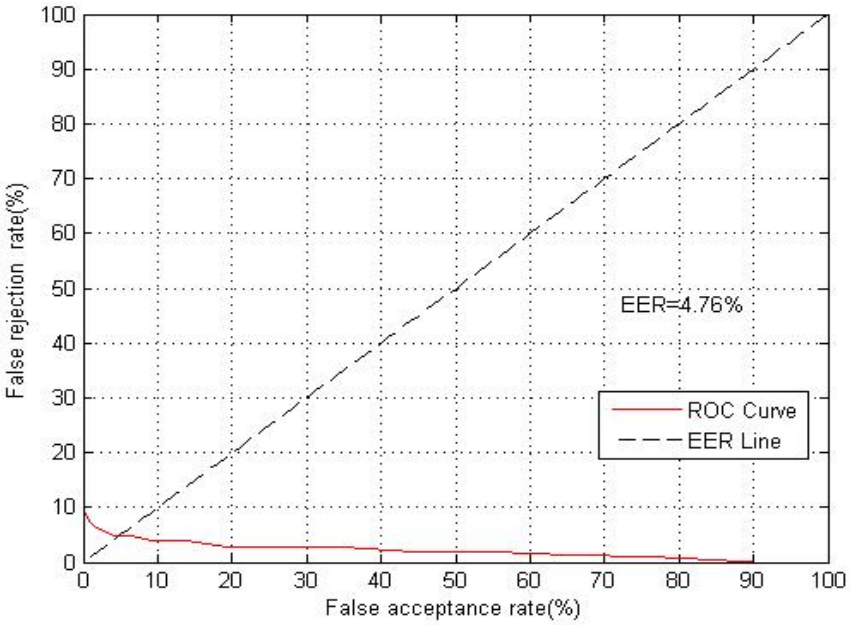

Figure 6.41: Plot of Receiver Operating Characteristic curve for MMU.

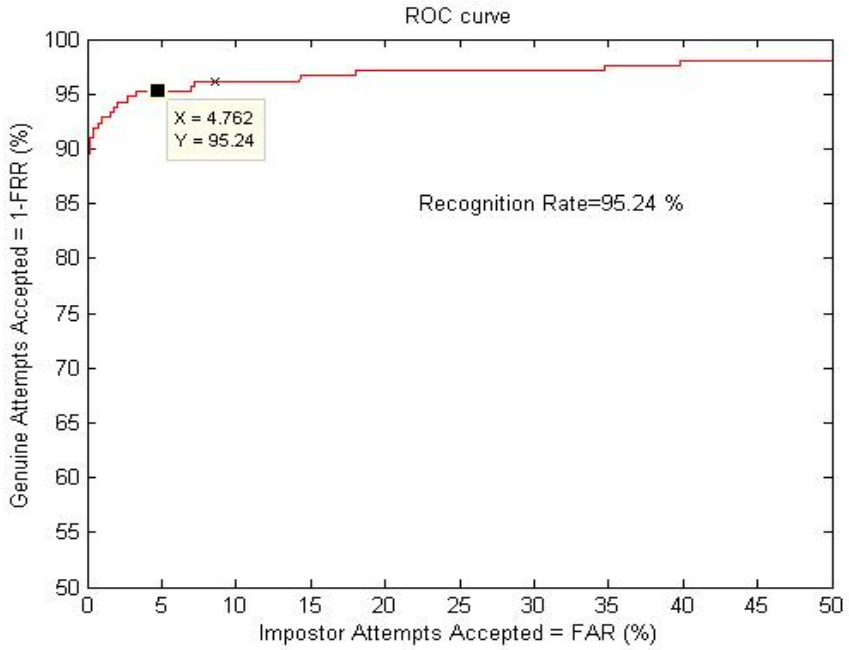

Figure 6.42: Plot of FAR versus GAR for MMU.

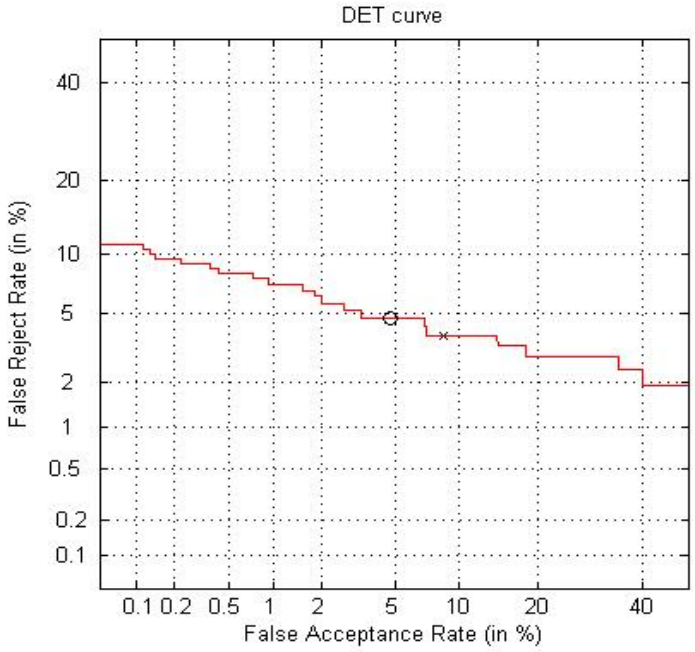

Figure 6.43: Plot of DET curve for MMU.

6.7.3 For IITD

Genuine and Imposter Distribution

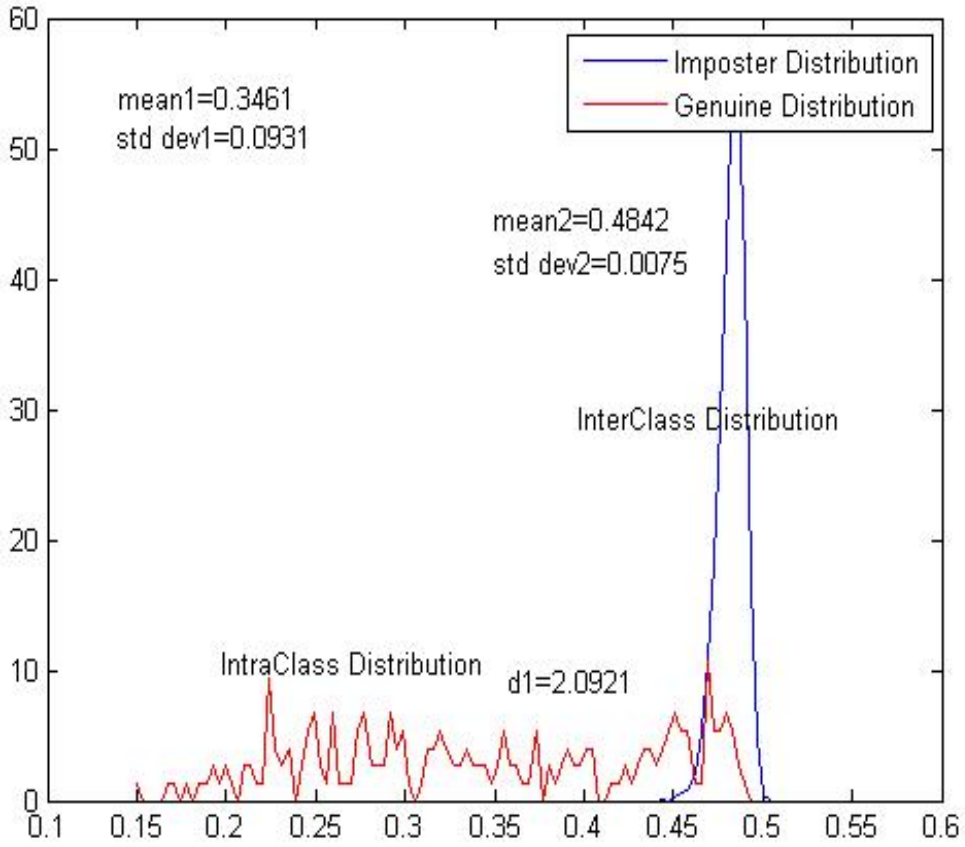

Figure 6.44: Genuine and imposter distribution using special gabor filter bank.

ROC and DET Curves

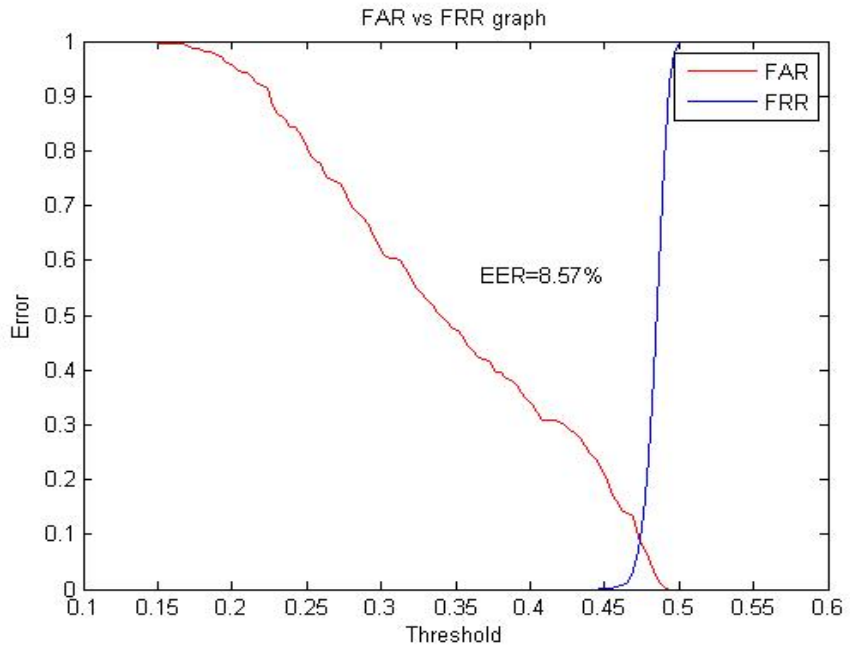

Figure 6.45: Plot of FAR versus FRR for IITD.

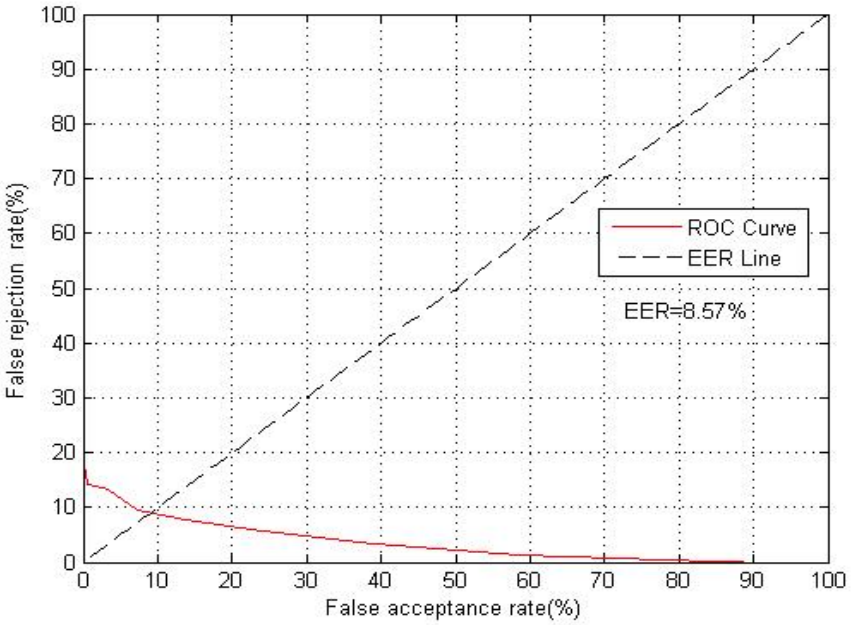

Figure 6.46: Plot of Receiver Operating Characteristic curve for IITD.

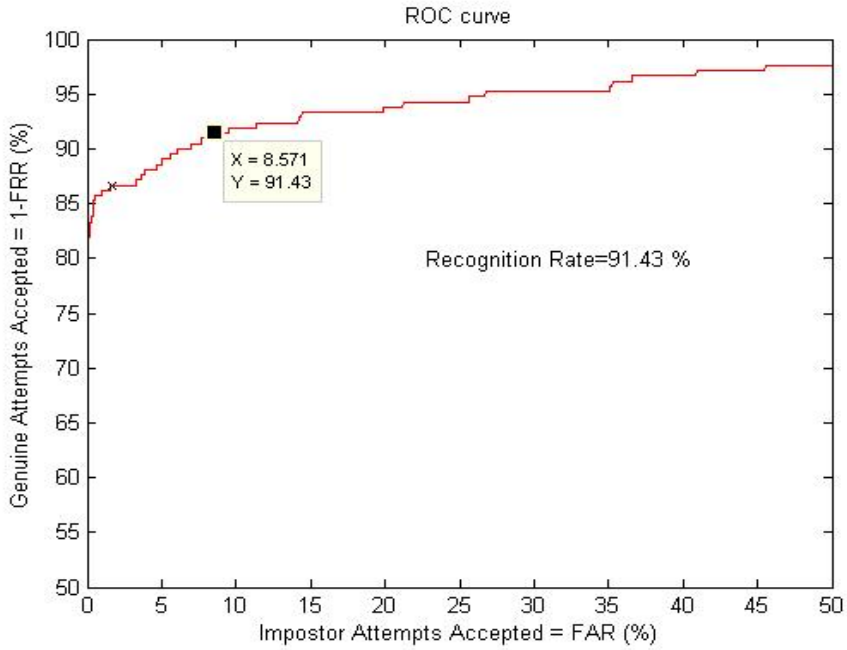

Figure 6.47: Plot of FAR versus GAR for IITD.

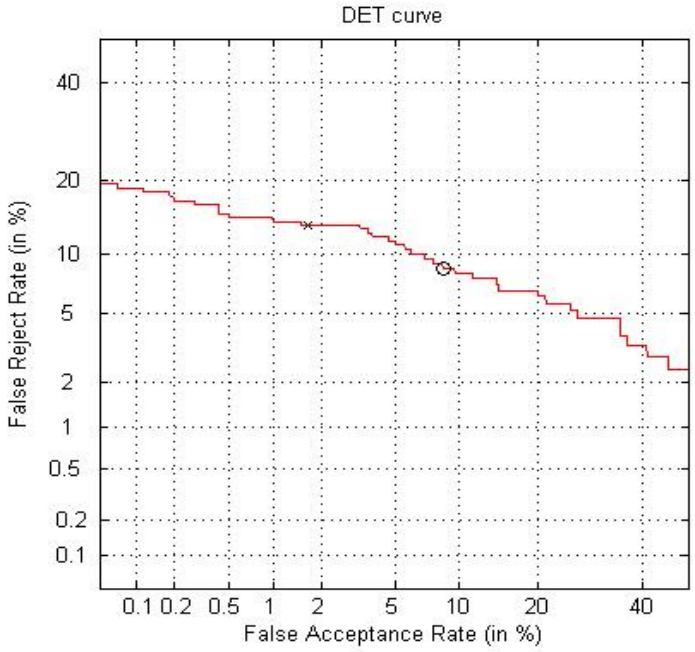

Figure 6.48: Plot of DET curve for IITD.

6.7.4 Effect of Number of Shifts on Performance

For analysis of rotational inconsistencies, we have performed experiments on MMU database, the results are as shown

Genuine and Imposter Distribution

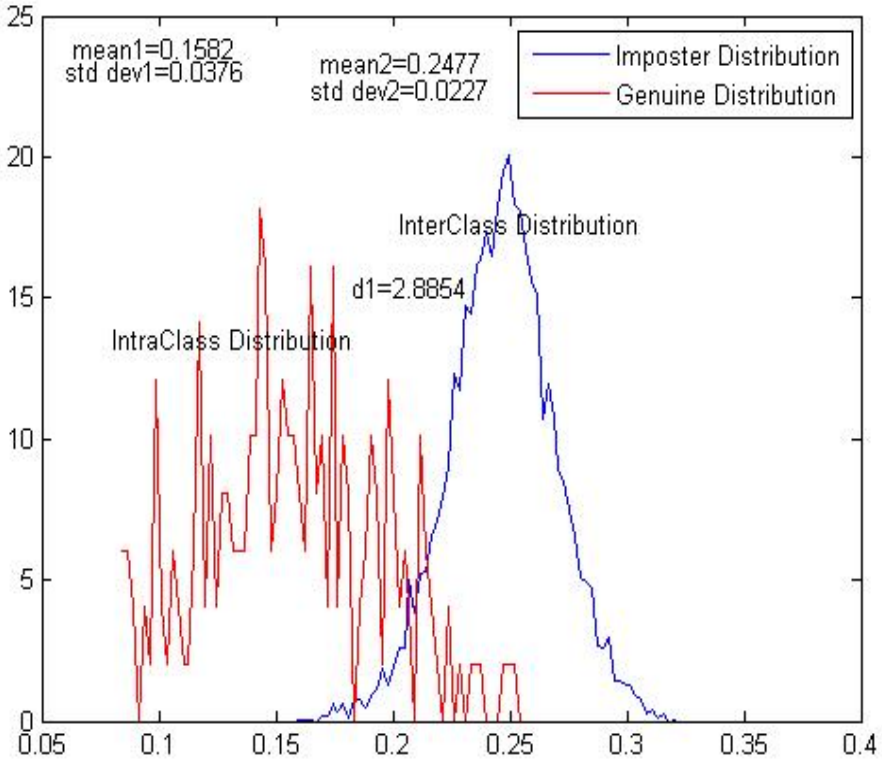

Figure 6.49: Genuine and imposter distribution using special gabor filter bank for 4shifts.

ROC and DET Curves

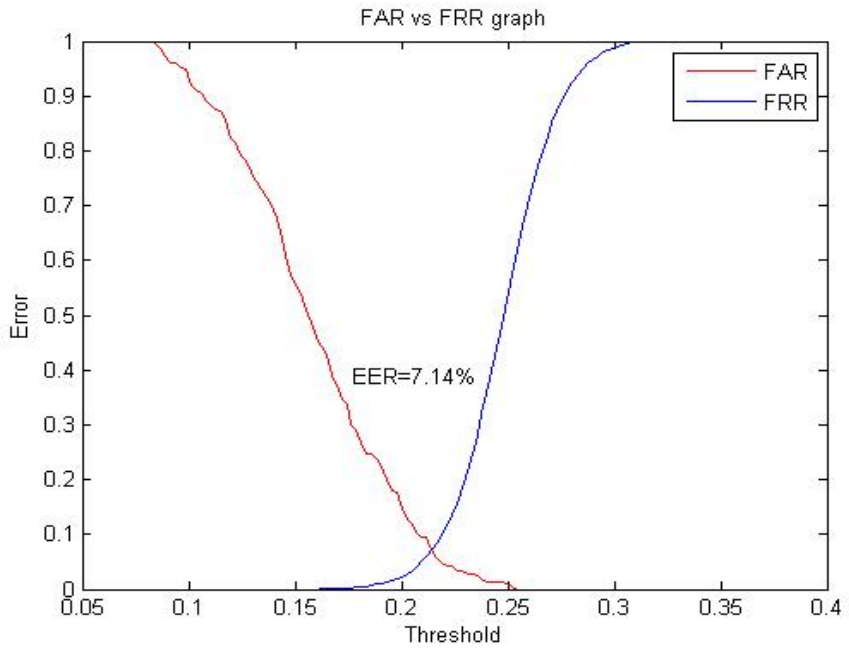

Figure 6.50: Plot of FAR versus FRR for MMU for 4shifts..

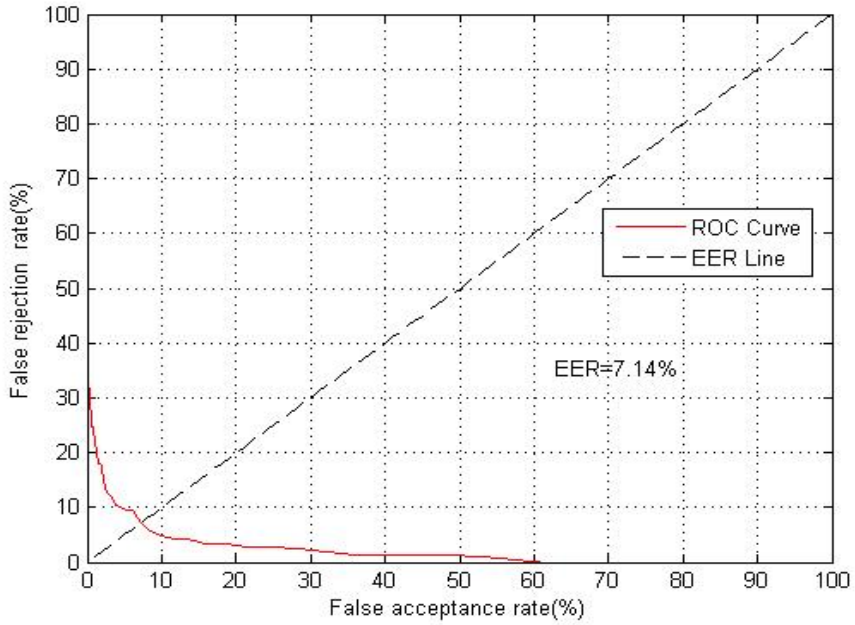

Figure 6.51: Plot of Receiver Operating Characteristic curve for MMU for 4shifts.

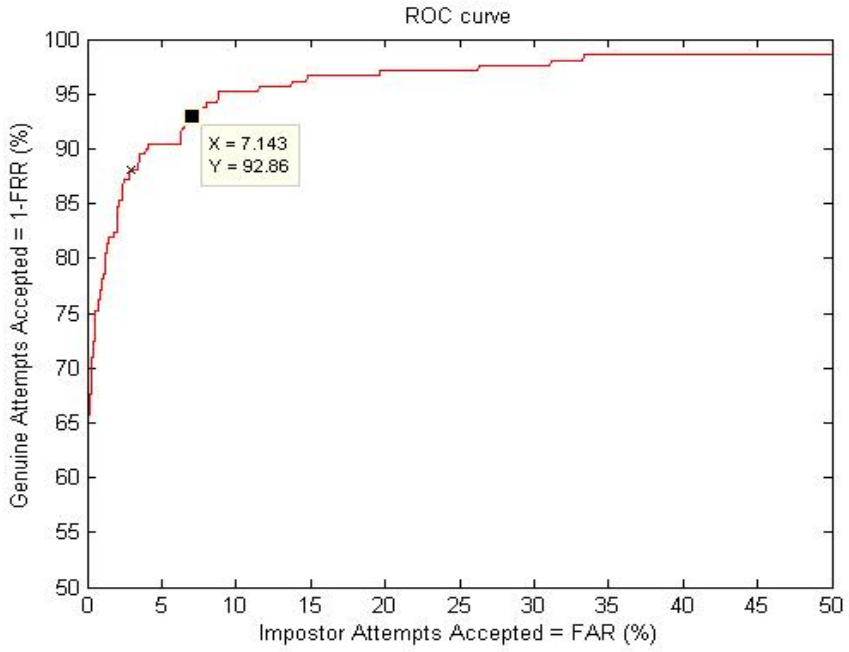

Figure 6.52: Plot of FAR versus GAR for MMU for 4shifts.

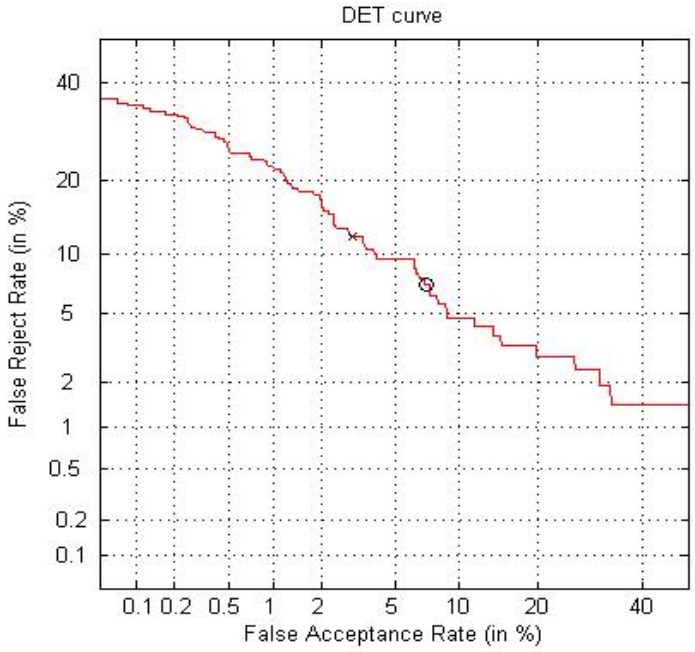

Figure 6.53: Plot of DET curve for MMU for 4shifts.

6.8 Summary of Results

From the above results it is clear that increasing number of scales of gabor filters results in increased recognition accuracy and better class separation between genuine and imposter distribution. We have found two scales of gabor filter provided optimal recognition with EER of 1.49% for CASIA database. For three and four scales of gabor filter the EER was 1.66% each for CASIA database. Similar results were obtained for MMU and IITD database. For three and four scales of gabor filter the number of feature vectors are more and also computation time is high. For the two scales of gabor filters we can find frequency bandwidth in octaves as-

$$\alpha = log_2 \left(\frac{f_{max}}{f_{min}} \right) \tag{6.1}$$

for two scales $f_{max} = 0.1667$, $f_{min} = 0.05$, So $\alpha = 1.73$ octaves. for four scales $f_{max} = 0.4$, $f_{min} = 0.05$, So $\alpha = 3$ octaves.

We have got better results for gabor filters than log-gabor for same frequency bandwidth. The only disadvantage of gabor filters is that it needs multiscale representation, while for log-gabor filters can have arbitrary frequency bandwidths for one scale.

For CASIA, MMU, and IITD minimum of 8 shifts were found to give accurate results since all rotational inconsistencies are removed. For MMU with 4 shifts in template bits results in low recognition and poor class separation between genuine and imposter distribution.

Tables 6.2, 6.3, 6.4 summarize the performance analysis of our implemented iris recognition system on CASIA version 1, MMU, IITD databses respectively. In table 6.5, comparison of our implemented system with some standard iris recognition systems is given.

Feature Extracion	Threshold	FAR %	FRR %	d'	Verification %
Gabor filter(1 scale)	0.40	3.67	3.66	4.41	96.34
Gabor filter(2 scales)	0.38	1.49	1.50	4.34	98.51
Log gabor filter	0.46	3.67	3.66	3.35	96.33

Table 6.2: Summary of performance analysis for CASIA.

Feature Extracion	Threshold	FAR %	FRR %	d'	Verification %
Gabor filter(1 scale)	0.34	5.26	5.23	3.45	94.77
Gabor filters(2 scales)	0.34	4.76	4.76	3.20	95.24
Log gabor filter	0.45	4.71	4.76	2.62	95.24

Table 6.3: Summary of performance analysis for MMU.

Feature Extracion	Threshold	FAR %	FRR %	EER	Verification %
Gabor filter(1 scale)	0.41	3.75	3.73	3.30	96.27
Gabor filter(2 scale)	0.39	2.78	2.77	4.22	97.22
Log gabor filter	0.47	8.55	8.57	2.09	91.43

Table 6.4: Summary of performance analysis for IITD.

6.9 Comparison with existing methods

Systems	Recognition rate %	Equal error rate %
Daugman [1]	100	0.08
Li Ma [19]	100	0.07
Tan [18]	99.19	0.57
Wildes [11]	-	1.76
Our implementation	98.51	1.49

Table 6.5: Comparisons of our implemented system with existing methods.

The values in the above table are taken from [20].

Chapter 7

Conclusion

7.1 Summary of Work

This thesis has presented an iris recognition system, which was tested using three publicly available iris image databases in order to verify the claimed performance of iris recognition technology.

Firstly, Two automatic segmentation algorithms were presented, which would localize the iris region from an eye image and isolate noisy areas. First Automatic segmentation algorithm uses the Integro-differential operator for localizing the iris boundary and using binary morphology for pupil region segmentation, and the Integro-differential operator for localizing occluding eyelids. In Second algorithm Circular Hough Transform is used for localization of iris boundary and binary morphology for pupil region segmentation is used.

Next, the segmented iris region was normalized to eliminate dimensional inconsistencies between iris regions. This was achieved by implementing a version of Daugmans rubber sheet model, where the iris is modeled as a flexible rubber sheet, which is unwrapped into a rectangular block with constant polar dimensions.

Finally, features of the iris were encoded by convolving the normalized iris region with special gabor filterbank and phase quantizing the output in order to produce a bit-wise biometric template. The Hamming distance was chosen as a matching metric, which gave a measure of how many bits disagreed between two templates. A failure of statistical independence between two templates would result in a match, that is, the two templates were seemed to have been generated from the same iris if the Hamming distance produced was lower than a set Hamming distance. For comparison we also tested our system using 1D Log-Gabor filters for feature extraction to verify our system performance.

7.2 Summary of Findings

Analysis of the developed iris recognition system has revealed a number of interesting conclusions. It can be stated that segmentation is the critical stage of iris recognition, since areas that are wrongly identified as iris regions will corrupt biometric templates resulting in very poor recognition. The results presented in Chapter 3 have also shown that segmentation can be the most difficult stage of iris recognition because its success is dependent on the imaging quality of eye images. With the CASIA database only 95% of the images managed to segment successfully due to poor imaging conditions, while 97% of the MMU database images segmented correctly, while 92% of the MMU database images segmented correctly. (The above results are not calculated on entire database, they were obtained on the databases taken for performance evaluation.)

Another interesting finding was that the encoding process required two scales of Gabor filter that provided optimal accurate recognition, since the open literature mentions the use of multi-scale representation in the encoding process. The two scales of gabor filter provided frequency bandwidth of 1.73 octaves.

For CASIA and IITD databases gabor filter with two scales, and template resolution of 64 pixels by 1024 pixels was found to provided optimum encoding. For MMU template resolution of 30 pixels by 720 pixels was used.

Good recognition rate was achieved with the CASIA data set, with a separation point of 0.38, a false accept rate of 1.49 % and false reject rate of 1.50 % was possible,with equal error rate of 1.49 %, claiming the correct verification rate of 98.51 %.

For MMU data set, with a separation point of 0.34, a false accept rate of 4.76 % and false reject rate of 4.76 % was possible,with equal error rate of 4.76 %, claiming the correct verification rate of 95.24 %.

For IITD data set, with a separation point of 0.39, a false accept rate of 2.78 % and false reject rate of 2.77 % was possible,with equal error rate of 2.78 %, claiming the correct verification rate of 96.27 %.

These results confirm that iris recognition is a reliable and accurate biometric technology.

Bibliography

[1] Daugman, J. G., "How iris recognition works," *IEEE Transactions on Circuits and Systems for Video Technology*, Vol. 14, No. 1, January 2004, pp. 21–30.

[2] Daugman, J. G., "High confidence visual recognition of persons by a test of statistical independence," *IEEE Transactions on Pattern Analysis and Machine Intelligence*, Vol. 25, No. 11, November 1993, pp. 1148–1161.

[3] Jain, A. K., *Handbook of Biometrics*, Springer, New York, USA, 2007.

[4] Proenca, H., *Towards Non-Cooperative Biometric Iris Recognition*, Ph.D. thesis, University of Beira Interior, Department of Computer Science, october 2006.

[5] Bellis, M., "Inventors: Police technology and forensic science http:// inventors.about.com/library/inventors/blforensic.htm." .

[6] Jain, A. K., Hong, L., and Pankanti, S., "Biometric identification," *Communications of the ACM*, Vol. 43, No. 2, 2000, pp. 91–98.

[7] Anil K. Jain, R. B. and Pankanti, S., *Personal Identification in networked society*, Kluwer Academic Publisher, E.U.A, 1999.

[8] A. K. Jain, S. L., *Encyclopedia of Biometrics*, Springer, New York, USA, 2009.

[9] Daugman, J. G., "Iris recognition. http://www.cl.cam.ac.uk/jgd1000/." 2006.

[10] Boles, W. W. and Boshash, B., "A human identification technique using images of the iris and wavelet transform," *IEEE Transactions on Signal Processing*, Vol. 46, No. 4, April 1998, pp. 1185–1188.

[11] Wildes, R. P., "Iris recognition: an emerging biometric technology," *Proceedings of the IEEE*, Vol. 85, No. 9, September 1997, pp. 1348–1363.

[12] Nishino, K. and Nayar, S. K., "Eyes for relighting," *ACM Trans. Graph*, Vol. 23, No. 3, 2004, pp. 704–711.

[13] Camus, T. and Wildes, R., "Reliable and fast eye finding in close-up images," *Proceedings of the IEEE 16th International Conference on Pattern Recognition*, August 2002, pp. 389–394.

[14] D. Martin-Roche, C. S.-A. and R.Sanchez-Reillo, "Iris recognition for biometric identification using dyadic wavelet transform zero-crossing," *IEEE Aerospace and Electronic Systems Magazine*, Vol. 17, No. 10, 2002, pp. 3–6.

[15] Jiali Cui, Yunhong Wang, T. T. L. M. and Sun, Z., "A fast and robust iris localization method based on texture segmentation," *Proceedings of the SPIE Defense and Security Symposium*, Vol. 5404, August 2004, pp. 401–408.

[16] Junzhou Huang, Yunhong Wang, T. T. and Cui, J., "A new iris segmentation method for recognition," *Proceedings of the 17th International Conference on Pattern Recognition (ICPR04)*, Vol. 3, August 2004, pp. 23–26.

[17] Kong, W. K. and Zhang, D., "Accurate iris segmentation method based on novel reflection and eyelash detection model," *Proceedings of the 2001 International Symposium on Inteligent Multimedia, Video and Speech Processing*, May 2001, pp. 263–266.

[18] Li Ma, Y. W. and Tan, T., "Iris recognition using circular symmetric filters," *Proceedings of the 25th International Conference on Pattern Recognition (ICPR02)*, August 2002, pp. 414–417.

[19] Li Ma, Tieniu Tan, Y. W. and Zhang, D., "Personal identification based on iris texture analysis," *IEEE Transactions on Pattern Analysis and Machine Intelligence*, Vol. 25, No. 12, December 2004, pp. 2519–2533.

[20] Li Ma, Y. W. and Zhang, D., "Efficient iris recognition by characterizing key local variations," *IEEE Transactions on Image Processing*, Vol. 13, No. 6, June 2004, pp. 739–750.

[21] Mira, J. and Mayer, J., "Image feature extraction for application of biometric identification of iris - a morphological approach," *Proceedings of the 16th Brazilian Symposium on Computer Graphics and Image Processing (SIBGRAPI 2003)*, October 2003, pp. 391–398.

[22] Li Ma, Y. W. and Tan, T., "Iris recognition based on multichannel gabor filtering," *Proceedings of the 5th Asian Conference on Computer Vision ACCV2002*, January 2002, pp. 279–283.

[23] Ali, J. and Hassanien, A., "An iris recognition system to enhance e-security environment based on wavelet theory," *AMO - Advanced Modeling and Optimization*, Vol. 5, No. 2, 2003, pp. 93–104.

[24] Christel Tisse, Lionel Martin, L. T. and Robert, M., "Person identification technique using human iris recognition," *Proceedings of the 25th International Conference on Vision Interface*, 2002, pp. 294–299.

[25] Ya Huang, S. L. and Chen, E., "An efficient iris recognition system," *Proceedings of the First International Conference on Machine Learning and Cybernetics*, China, November 2002, pp. 450–454.

[26] Yong Zhu, T. T. and Wang, Y., "Biometric personal identification based on iris patterns," *Proceedings of the 13th International Conference on Pattern Recognition (ICPR00)*, Barcelona, September 2000, pp. 2801–2804.

[27] "CASIA iris image database. http://www.sinobiometrics.com/casiairis.htm." .

[28] Masek, L., *Recognition of Human Iris Patterns for Biometric Identification*, Master's thesis, The University of Western Australia,department of computer science and software engineering, 2003.

[29] Abhyankar, A. and schuckers, S., "Active shape models for efficient iris segmentation," *Proceedings of the SPIE Conference on Biometric technology for human identification*, Vol. 6202, Orlando, April 2006.

[30] Monro, D. M. and Rakshit, S., "DCT based iris recognition," *IEEE Transactions on Pattern Analysis and Machine Intelligence*, Vol. 29, No. 4, April 2007, pp. 586–595.

[31] "University of Bath.University of Bath iris image database. http://www.bath.ac.uk/elec-eng/pages/sipg/." 2004.

[32] "National Institute of Standards and Technology. Iris challenge evaluation. http://iris.nist.gov/ICE/." 2004.

[33] "Multimedia University. MMU iris image database. http://pesona.mmu.edu.my/ccteo." 2004.

[34] "Michal Dobes and Libor Machala. UPOL iris image database. http://phoenix.inf.upol.cz/iris/.." 2004.

[35] Ritter, N., "Location of the pupil-iris border in slit-lamp images of the cornea." *Proceedings of the International Conference on Image Analysis and Processing*, 1999.

[36] "John G. Daugman, U.S. Patent No 5291560 Biometric personal identification system based on iris analysis ." 1994.

[37] "Charles O' Neill, Cubic Spline Interpolation ." 2002.

[38] Burt, P. and Adelson, E., "The Laplacian Pyramid as a Compact Image Code," *IEEE Transactions on Image Processing*, Vol. 31, No. 4, 1983, pp. 532–540.

[39] Field, D. J., "Relations between the statistics of natural images and the response properties of cortical cells," *Journal of the Optical Society of America*, Vol. 4, No. 12, December 1987, pp. 2379–2394.

[40] Manjunath, B. and Ma, W., "Texture Features for Browsing and Retrieval of Image Data," *IEEE Transactions on Pattern Analysis And Machine Intelligence*, Vol. 18, No. 8, 1996, pp. 837–842.

[41] A. Martin, G. Doddington, T. K. M. O. and Przybocki, M., "The DET Curve in Assessment of Detection Task Performance," *Proceedings of the Fifth European Conference on Speech Communication and Technology*, Rhodes, Greece, September 1997, pp. 1895–1898.